Aus dem Institut für Medizinische Psychologie der
Ludwig-Maximilians-Universität München
Lehrstuhl: Medizinische Psychologie
Vorstand: Prof. Martha Merrow, Ph.D

Circadian Entrainment and Molecular Mechanisms of Protein Aggregation

Dissertation
zum Erwerb des Doktorgrades der Naturwissenschaften (Dr. rer. nat.)
an der Medizinischen Fakultät
der Ludwig-Maximilians-Universität München

vorgelegt von

Bala Subrahmanya Chakravarthy Koritala
aus
Penumuli, India

2016

Gedruckt mit Genehmigung der Medizinischen Fakultät der Ludwig-Maximilians-Universität München

Betreuerin:	Prof. Martha Merrow, Ph.D
Zweitgutachterin:	Prof. Dr. Regina Fluhrer
Dekan:	Prof. Dr. med. dent. Reinhard Hickel

Tag der mündlichen Prüfung: 24th November 2016

Eidesstattliche Versicherung

Koritala, Bala Subrahmanya Chakravarthy

Name, Vorname

Ich erkläre hiermit an Eides statt,

dass ich die vorliegende Dissertation mit dem Thema

Circadian Entrainment and Molecular Mechanisms of Protein Aggregation

selbständig verfasst, mich außer der angegebenen keiner weiteren Hilfsmittel bedient und alle Erkenntnisse, die aus dem Schrifttum ganz oder annähernd übernommen sind, als solche kenntlich gemacht und nach ihrer Herkunft unter Bezeichnung der Fundstelle einzeln nachgewiesen habe.

Ich erkläre des Weiteren, dass die hier vorgelegte Dissertation nicht in gleicher oder in ähnlicher Form bei einer anderen Stelle zur Erlangung eines akademischen Grades eingereicht wurde.

Munich, 29.11.16

Ort, Datum

Unterschrift Doktorandin/Doktorand

Table of Contents

Page. No

1. Summary

Living organisms used zeitgebers to synchronize/entrain their biological clocks (Pittendrigh, 1993). This synchronization specifies expression of genes and proteins to specific times of a day. Disruption of circadian entrainment has been reported to increase susceptibility to several diseases including cardiovascular diseases, cancer, dementia-associated disorders, metabolic disorders, etc. (Ferrell and Chiang, 2015; Musiek, 2015; Stevens et al., 2014), possibly due to disruption of phase specific molecular expression patterns.

In the present study, we investigated how temperature, a zeitgeber of the circadian clock, impacts a model of poly glutamine aggregation diseases. Clinical studies showed that patients with these diseases have a lower amplitude endogenous temperature rhythm (Pierangeli et al., 1997). Furthermore, endogenous temperature rhythms in healthy mice are sufficient to localize Heat Shock Factor-1 (HSF-1), a transcription factor that regulates expression of numerous heat shock genes, in the nucleus (Reinke et al., 2008). Heat shock proteins are suppressors of protein aggregation.

We hypothesized that temperature entrainment might directly impact protein aggregation via heat shock protein expression. To test this hypothesis, a *C. elegans* strain carrying a transgene expression of 35 glutamines (polyQ) was incubated in either constant temperature or 24 h temperature cycles. The aggregation of polyQ was significantly reduced in temperature cycles compared to constant conditions. We further investigated the composition of protein aggregates in the two temperature conditions, revealing greater complexity of aggregates formed in temperature cycles. We also investigated the expression of a subset of genes encoding heat shock proteins. We found that heat shock genes encoding proteins that have chaperone function are rhythmically expressed in temperature cycles.

Neurodegenerative pathologies can invoke metabolic stress. Unpublished data (Olmedo, Geibel, Merrow) shows that metabolic stress impedes development. We investigated the rate of development in poly glutamine transgenic worms. Our data

suggests that developmental timing is delayed in polyQ worms at all temperature conditions.

The major finding of this work is that zeitgebers of circadian clock can decrease the load of protein aggregates in poly-glutamine model, apparently by structuring the expression of their suppressors.

2. Zusammenfassung

Lebende Organismen brauchen Zeitgeber, um ihre innere Uhr zu synchronisieren (Pittendrigh, 1993). Diese Synchronisation konzentriert die Expression von Genen und Proteinen auf bestimmte Tageszeiten. Eine Störung des zirkadianen Entrainments erhöht die Anfälligkeit für etliche Krankheiten, unter anderem Herz-Kreislauferkrankungen, Krebs, Demenz-assoziierte Störungen, Stoffwechselkrankheiten und viele weitere (Ferrell and Chiang, 2015; Musiek, 2015; Stevens et al., 2014). Ursache hierfür ist möglicherweise eine Störung des phasenspezifischen molekularen Expressionsmusters.

Einer der bekannten Zeitgeber für die innere Uhr ist Temperatur. In der vorliegenden Studie haben wir untersucht, welchen Einfluss diese auf ein Modell für Polyglutamin-Aggregationserkrankungen hat. Klinische Studien haben gezeigt, dass der zirkadiane Körpertemperaturrhythmus von Patienten mit solchen Krankheiten eine niedrigere Amplitude hat (Pierangeli et al., 1997). Bei gesunden Mäusen reichen endogene Temperaturzyklen aus, um Hitzeschock-Faktor 1 (HSF-1) in den Zellkern zu lokalisieren (Reinke et al., 2008). HSF-1 ist ein Transkriptionsfaktor, der eine Vielzahl von Hitzeschockgenen reguliert. Diese sind wiederum Suppressoren der Proteinaggregation.

Wir nehmen an, dass das Entrainment mit Temperaturzyklen durch die Expression von Hitzeschockproteinen einen direkten Einfluss auf die Proteinaggregation hat. Um diese Hypothese zu untersuchen, wurde ein transgener Stamm des Fadenwurms *C. elegans* verwendet, welcher eine Mutation aufweist, die zur Expression von 35 Glutaminresten (PolyQ) führt. Die Würmer wurden entweder in konstanter Temperatur oder in Temperaturzyklen gehalten. Die PolyQ-Aggregation in Temperaturzyklen war im Vergleich zu konstanten Bedingungen signifikant geringer. Ferner untersuchten wir die Zusammensetzung der Aggregate in den beiden Temperaturregimes, wobei sich bei den Aggregaten aus den Temperaturzyklen eine deutlich größere Komplexität zeigte. Als Nächstes wurde die Expression einiger ausgewählter Gene untersucht, welche für Hitzeschockproteine kodieren. Dabei haben

wir herausgefunden, dass die Hitzeschockgene, die für Proteine mit Chaperon-Funktion kodieren, in Temperaturzyklen rhythmisch exprimiert werden.

Neurodegenerative Erkrankungen können zu metabolischer Belastung führen. Noch nicht veröffentlichte Daten aus unserem Labor (Olmedo, Geibel, Merrow) zeigen, dass dieser Stoffwechselstress die Entwicklung behindern kann. Wir haben daher die Geschwindigkeit der Entwicklung in transgenen PolyQ-Würmern untersucht. Unsere Daten deuten darauf hin, dass die Entwicklung dieser Tiere bei allen bisher untersuchten Temperaturen verzögert ist.

Die Haupterkenntnis der vorliegenden Arbeit ist, dass physiologische Zeitgeberzyklen - scheinbar durch die zeitlich strukturierte Expression von Suppressoren - die Menge an Proteinaggregaten in einem Polyglutamin-Modell verringern können.

3. Introduction

3.1. Biological Rhythms

In nature, all living organisms have evolved to anticipate predictable cyclic environmental changes by using their biological clocks, which are endogenous and regulate biological rhythms from the molecular level to the behavioral level. Biological clocks are categorized based on their period length. A period of rhythm length of less than 24-hours is called ultradian; a rhythm length of approximately 24-hours (earth rotation period) is circadian; one greater than 24-hours is infradian; and an approximate period of 1-year is circannual (Aschoff, 1981). In natural conditions, circadian rhythms are entrained by zeitgebers (environmental cues) and they also persist in constant conditions, thus confirming that the biological clock is endogenous (Aschoff, 1960; Merrow et al., 2005; Roenneberg and Merrow, 2005). There are many zeitgebers in the environment, but in chronobiology research the most commonly used zeitgebers are light-dark cycles and temperature cycles.

In the field of chronobiology (chrono = time, bios = life, logos = study), circadian rhythms (circa = approximately, dies = day) are studied in subjects varying from the acquatic cyanobacteria and gut microbes (Paulose et al., 2016) to humans. In the 17th century, de Mairan observed the first circadian rhythms in plants. His studies revealed the periodic leaf movements of a sensitive plant or Mimosa pudica in constant conditions (constant dark and putatively constant temperature) irrespective of natural light-dark cycles (de Marian, 1729). Researchers in the 19th century proposed that these periodic movements in free-running conditions were due to inherited rhythms regulated by the alternation of zeitgebers (de Candolle, 1835; Dutrochet, 1835; Hofmeister, 1867; Sachs, 1857). By the end of the 19th century, circadian rhythms had been observed in animals. Arthropods showed a periodic pigmentation cycle in constant free-running conditions (Kiesel, 1894).

The 20th century is considered the era of modern circadian biology, and Colin Pittendrigh and Jurgen Aschoff are considered the founders. In this period, circadian rhythms were observed in a range of subjects, from molecules to cells to organs to

physiological behavior in all six kingdoms of life. Richter first reported circadian rhythms in mammals by showing a circadian regulation of activity in rats (Richter, 1922). In the 1960's, Aschoff's first experiments on humans showed the circadian regulation of rectal temperatures, sleep-wake cycles and urine excretion(Aschoff, 1965). In addition to mammals, circadian rhythms have been identified in several genetic model organisms; for example, eclosion rhythms in *Drosophila melanogaster* (Bunning, 1935; Kalmus, 1935); release of fungal spores in *Neurospora crassa* (Pittendrigh et al., 1959); rhythmic leaf movement, photosynthesis, and the elongation of hypocotyl in *Arabidopsis thaliana* (Bunning, 1967; Dowson-Day and Millar, 1999) locomotion and olfaction behavior in *C. elegans* (Olmedo et al., 2012; Simonetta et al., 2009); locomotion activity in *Danio rerio* (Hurd et al., 1998); exogenous pH rhythms in *Saccharomyces cerevisiae* (Eelderink-Chen et al., 2010); and nitrogen fixation and photosynthesis in *Synechococcus elongatus* (Kondo and Ishiura, 2000). In addition to commonly used genetic models, cellular aggregation, bioluminescence and photosynthetic rhythms have also been shown in the unicellular *Gonyaulax polyedra* (Hastings et al., 1961; Roenneberg and Morse, 1993).

3.2. General Characteristics of Circadian Rhythm

Circadian rhythms are characterized based on the shared features observed in the circadian systems of different organisms. These characteristics were initially defined by Aschoff, Bünning and Pittendrigh and have been revisited in subsequent years (Aschoff, 1960; Merrow et al., 2005; Pittendrigh, 1960; Roenneberg and Merrow, 1998). These properties include:

- The period of a circadian rhythm is approximately that of the earth's rotation (24 hours).
- Circadian rhythms are endogenous and self sustained.
- Circadian rhythms are entrained to zeitgebers (light, temperature, feeding, etc…).
- Circadian rhythms are temperature compensated (The period of the free-running rhythm is not significantly changed over a range of 10 °C or more).

- The phases of free-running rhythms are the result of zeitgeber strength and structure.

3.3. Mechanism of the Circadian Clock

Any circadian system has three important components, including input pathway (entrainment pathway), rhythm generator (oscillator) and output pathway (circadian rhythms). The rhythm generator receives time signals through the input pathway and synchronizes its phase and period to the frequency of environmental cycles (zeitgebers), a process referred to as circadian entrainment (Eskin, 1979; Roenneberg et al., 2003). In nature, all organisms entrain their biological clocks to zeitgebers, but when exposed to free-running conditions they gradually desynchronize their biological clocks from natural environmental cycles. Thus, entrainment is essential in order for organisms to maintain their phase and period relationship with natural cycles. The zeitgebers that entrain biological clocks can be divided into photic and non-photic zeitgebers. Photic zeitgebers are light-dark cycles; non-photic zeitgebers are temperature cycles, feeding cycles, socialization, life style, etc.

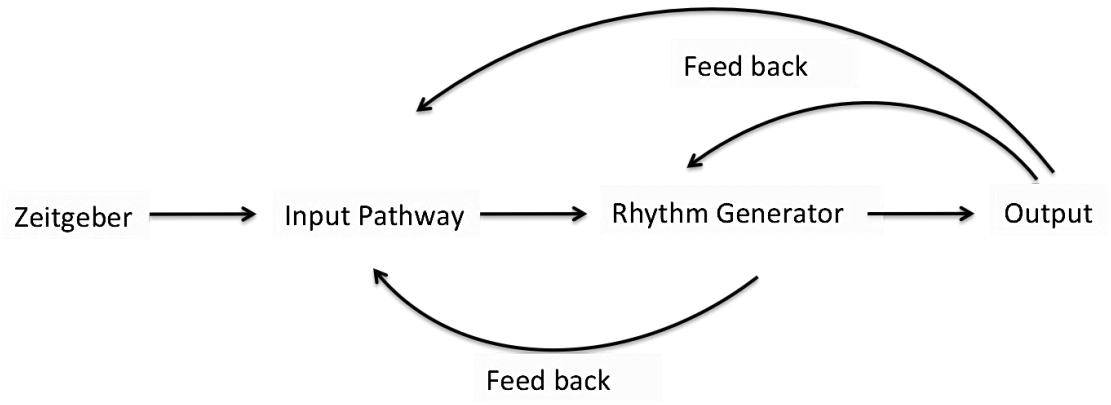

Figure 3-1: An outline of the circadian system. Zeitgeber (light, temperature, etc.) signals are transferred to the rhythm generator through the input pathway. The rhythm generator produces the circadian rhythms and regulates the output pathways. The rhythm generator may give feedback to the input pathways, and the output pathway may also give feedback to the input pathway and rhythm generator. Modified from (Eskin, 1979; Golombek and Rosenstein, 2010; Roenneberg and Merrow, 2000).

A clear example of how the entrainment pathway (input pathway) connects to the rhythm generator in mammals is the intrinsically photoreceptive retinal ganglion cells (ipRGCs), which express melanopsin and transmit light signals (For e.g. light-dark cycle) to the suprachiasmatic nucleus (Mohawk et al., 2012). The components involved in input pathways vary between organisms. For example, phytochromes and cryptochromes are involved in light sensing in *Arabidopsis thaliana* (Millar, 2004), WC-1, WC-2 and supposedly also cryptochromes in *Neurospora crassa* (Froehlich et al., 2010; Lee et al., 2000; Merrow et al., 2001), cryptochrome and the neurotransmitters such as possibly histamine, dopamine and serotonin in *Drosophila Melanogaster* (Yoshii et al., 2016) and CikA in *Synechococcus elongatus* (Dong and Golden, 2008).

An example of a cellular rhythm generator (oscillator) in mammals is the suprachiasmatic nucleus (SCN), the central pacemaker of the circadian system. The SCN is resistant to non-photic signals and largely entrained by photic zeitgebers (Buhr et al., 2010; Mohawk et al., 2012). However, every cell has its own oscillator, including the neuronal cells of SCN. The SCN is composed of 20,000 neurons, with an oscillation periods ranging from 22 to 30 hours. Intercellular coupling of all the neuronal cells in the SCN leads to a precise circadian period of its own tissue and its own activity rhythms (Herzog et al., 2004). The SCN not only regulates the activity rhythms but also regulates core body temperature, feeding, hormones, etc. (Lehman et al., 1987; Mohawk et al., 2012). In addition to the central pacemaker, mammals possess peripheral oscillators that regulate rhythms in physiological processes (blood pressure, heart rate, lipid metabolism, renal plasma flow and xenobiotic detoxification) in tissues. Peripheral oscillators are cell-autonomous, entrained by non-photic zeitgebers and the output of the SCN (Brown and Azzi, 2013; Schibler et al., 2003).

At the molecular level, thousands of genes have shown circadian rhythms, thought to be regulated by a transcriptional and translational feedback oscillator (Buhr and Takahashi, 2013). A stepping-stone to the understanding of the molecular clock mechanism was the discovery of the *period* gene in *Drosophila melanogaster* by means of mutagenesis screens (Konopka and Benzer, 1971). The transcriptional feedback loop involves both positive and negative transcriptional regulatory elements.

The positive elements are mainly transcriptional activators of clock genes; the negative elements are inhibitors of positive elements. In mammals, transcriptional activators (BMAL1 and CLOCK/NPAS2) localize to the nucleus and promote the expression of Period (PER1, PER2) and Cryptochrome (CRY1, CRY2). The expressed PER and CRY proteins in the cytoplasm interact with each other, localize to the nucleus and inhibit the transcriptional activity of BMAL1 and CLOCK. The period of this transcriptional feedback loop is roughly 24 hours, and it plays an important role in the circadian behavior of mammals (Gekakis et al., 1998; Ko and Takahashi, 2006; Kume et al., 1999). Similar feedback loops have also been identified in other genetic models, despite the lack of conservation of their components at the sequence level. For example, in *A. thaliana*, TIMING OF CAB EXPRESSION 1 (TOC1) is a positive element and negative elements are LATE ELONGATED HYPOCOTYL (LHY) and CIRCADIAN CLOCK ASSOCIATED 1 (CCA1) (McWatters and Devlin, 2011) in *D. melanogaster,* CLOCK (CLK) and CYCLE (CYC) are positive elements and negative elements are PERIOD (PER and TIMELESS (TIM) (Hardin, 2011); in *N. crassa,* WHITE COLLAR-1 (WC-1) and WHITE COLLAR-2 (WC-2) are positive elements and negative elements are FREQUENCY (FRQ) and VIVID (VVD) (Baker et al., 2012).

The outputs of the circadian oscillator are circadian rhythms of molecules and physiological processes. These outputs can also feed back to the oscillator, as when melatonin secretion from the pineal gland is regulated by the SCN and eventually the pineal-released melatonin acts on the SCN (Kopp et al., 1997). Outputs can also become an input, called a zeitnehmer (Roenneberg and Merrow, 2000). In mammals, for example, the circadian rhythm of the core body temperature acts as zeitnehmer (input) to entrain the peripheral oscillators. Recent evidence from Schibler's lab indicates that the circadian rhythm of heat shock factor-1 (HSF-1) binding to heat shock elements (HSE) is correlated with maximal core body temperature and food intake (Reinke et al., 2008). This suggests that physiological temperature fluctuations are sufficient for binding of HSF-1 to HSE elements and for the induction of heat shock protein (HSP) expression (Brown et al., 2002; Buhr et al., 2010). The phase of heat shock protein expression is similar to that of the mammalian clock gene *Per2* (Kornmann et al., 2007). Interestingly, heat shock elements have been identified in the promoter region of *Per2*, and mutations of these specific heat shock elements in

the *Per2* promoter abolish circadian rhythms of *Per2*. Additionally, deficiency of HSF-1 affects the circadian expression of *Per2* and the period of free-running locomotor activity in mammals. HSF-1 was also found to be an essential component for the resetting of *Per2* rhythms through an interaction of HSF-1 and BMAL1:CLOCK (Tamaru et al., 2011). These observations suggest an association between the mammalian circadian clock and the heat shock response (HSR) system that includes heat shock factor-1 and heat shock proteins.

3.4. Heat Shock Factor-1 (HSF-1)

Some organisms, such as *C. elegans*, *Drosophila* and yeast, possess only one heat shock factor (HSF-1) (Akerfelt et al., 2007; Fujimoto et al., 2010). In vertebrates, HSF-1 is one of four different heat shock factors (HSF1 - 4). Among them, HSF-1 is a highly conserved transcription-binding factor that regulates cellular proteotoxicity by induction of heat shock proteins. HSF-1 is involved in both physiological and stress response pathways that include development, metabolism, aging and transcriptional regulation (Vihervaara and Sistonen, 2014). The localization of HSF-1 is associated with various cellular processes (e.g. transcriptional regulation, development, etc). Recent studies have shown that the amount of nuclear HSF-1 correlates with cancer prognoses (Mendillo et al., 2012; Santagata et al., 2011). There are several contradictory studies associated with thermal stress and nuclear localization of HSF-1 in *C. elegans, Drosophila* and in humans (Baler et al., 1993; Chiang et al., 2012; Zandi et al., 1997). One study (Morton and Lamitina, 2013) reported that HSF-1 is predominantly a nuclear protein in *C. elegans*. However, under physiological condition, HSF-1 is an inactive monomer and is bound to Hsp70 and Hsp90. Under stress, trimirized HSF-1 binds to heat shock elements to induce expression of heat shock proteins, which prevent protein misfolding or aggregation (Vihervaara and Sistonen, 2014). In contrast, a recent study has shown that the localization of HSF-1 and binding of HSF-1 to DNA is associated with diurnal activity and physiological temperature cycles (Reinke et al., 2008).

3.5. The Chaperome

The chaperome is the collection of all chaperones, the central components of the proteostasis network that help to fold nascent and misfolded proteins to prevent the formation of non-functional aggregates. The chaperome was initially characterized by molecular weight, but recently the chaperome has been redefined based on function (ATP dependent or independent). Heat shock proteins (small Hsps, Hsp40s, Hsp60s, Hsp70s, Hsp90s and Hsp100s) share major parts of the chaperome as compared to other protein families (Brehme et al., 2014). These heat shock proteins are ubiquitously expressed in all organisms and in addition to daily clock regulated expression, are induced upon heat or cellular stress (Morimoto, 2011). Heat shock proteins are associated with different cellular processes, including protein folding by interacting with unfolded substrates in ATP dependent or independent manner. The ATP independent chaperones are called holdases (prefoldins, small Hsps, Hsp10s and Hsp40s) that can directly interact with nascent or denatured proteins. ATP dependent chaperones are foldases and disaggregases (Hsp60s, Hsp70s, Hsp90s and Hsp100s), which are further involved in folding mechanisms through ATP hydrolysis. Protein folding can be achieved only by co-ordination of holdases, foldases and disaggregases (Diaz-Villanueva et al., 2015).

In the present study, we focused on small heat shock proteins called holdases. These proteins are highly conserved in organisms ranging form bacteria to higher vertebrates. High temperatures enhance the activation and binding of small heat shock proteins to unfolded or denatured protein substrates in ATP independent manner and is released for further processing by foldases and disaggregases (Zhang et al., 2015). Small Hsps possess N-terminal, C-terminal and α-crystalline domains. Their substrate binding efficiency is higher at the N-terminal domain than at the C-terminal and α-crystalline domains. The number of small Hsps varies in different organisms. In *C. elegans,* 18 small HSPs have been reported to be encoded in their genome. In humans 10 small Hsps have been identified (Aevermann and Waters, 2008; Kappe et al., 2003) and several are associated with several diseases, including protein aggregation diseases, Williams Syndrome, early cataract, Desmin-related myopathy,

Charcot-Marie Tooth disease, multiple sclerosis, hereditary motor neuropathies, tauopathies and cancer.

3.6. The *C. elegans* Small Heat Shock Proteins

Small HSPs in *C. elegans* are so named based on their molecular weight (HSP12s, HSP16s, HSP17, HSP25, HSP43 and SIP1). Among them, HSP12s, HSP25 and HSP43 were observed in lab conditions (20°C) throughout the development of the worm. HSP16s are thought to be expressed only upon thermal stress and are thus called stress inducible chaperones (Jones et al., 1989; Jones et al., 1996; Stringham et al., 1992). The expression and function of HSP17 and HSP43 is not thoroughly understood, although recently these heat shock proteins have been regarded as molecular chaperones.

3.6.1. HSP12s

Heat shock proteins of the HSP12 family (HSP-12.1, HSP-12.2, HSP-12.3 and HSP-12.6) have high similarity in their sequences. In general, both the N- and C- terminal regions of small heat shock proteins are involved in the substrate binding process. Interestingly, the family of HSP12 heat shock proteins possess a short N-terminal domain and lack the C-terminal domain. The overexpression of HSP-12.1 enhanced the cell survival rate in *E.* coli (Qin et al., 2007) and recent reports suggest that the aggregation of citrate synthase is reduced at high concentrations of HSP-12.1 (Krause, 2013). This confirms that HSP-12.1 has a chaperone activity that other family members lack. The α-crystalline domain of HSP-12.6 is closely related to other small HSP's, although this heat shock protein cannot prevent protein aggregation *in vitro*. The expression level of HSP-12.6 is unaltered by several stressors (heat shock, alcohol, cadmium chloride and capton), and it has been reported that the expression of HSP-12.6 is unaltered by stress (Leroux et al., 1997a). Recent reports suggest that HSP-12.6 expression is altered by oxidative and cold stress (Krause, 2013).

3.6.2. HSP16s

C. elegans HSP16 family members are homologues to human α-crystallin (Johnson et al., 2016). Mutations of α-crystallins in the human eye can cause early cataracts that lead to blindness (Brady et al., 1997; Datskevich et al., 2012). In contrast to HSP12.2, HSP12.3 and HSP12.6 heat shock proteins, HSP16s are effective in the prevention of chemically- and thermally-induced citrate synthase aggregation *in vitro*. In addition, HSP16s have been reported as molecular chaperones (Jones et al., 1989; Leroux et al., 1997b). Recent studies have shown that the overexpression of HSP-16.2 *in vivo* reduces the amyloid formation and the toxicity of a β-amyloid peptide (Fonte et al., 2008). HSP16s are strongly associated with an increase in life span and the thermal tolerance of *C. elegans* (Walker and Lithgow, 2003). HSP16s are also essential for maintaining *C. elegans* immunity (Singh and Aballay, 2006). The expression levels of HSP16s are not detectable under laboratory conditions using northern blot and staining methods (Ding and Candido, 2000a; Jones et al., 1989). The expression levels of HSP16 family members increase upon heat shock, confirming that HSP16 are associated with heat shock and HSF-1 (Kourtis et al., 2012; Morton and Lamitina, 2013; Seo et al., 2013; Stringham et al., 1992).

3.6.3. HSP25

HSP25 is a constitutively expressed heat shock protein in the *C. elegans* development process. The expression of HSP25 in *C. elegans* is observed primarily in the M-lines of the muscle fiber and pharynx. Previous observations suggest that the HSP25 protein is unaffected by heat shock (Ding and Candido, 2000b), and that mRNA expression of HSP25 is down-regulated upon different stressors such as heat, cold, heavy metal, oxidative,and osmotic stress. HSP25 was reported as not capable of preventing thermally induced protein aggregation (Merck et al., 1993). However, a recent study suggests that HSP25 acts as a molecular chaperone and reduces the citrate synthase aggregation *in vitro* (Krause, 2013).

3.6.4. HSP43

HSP43 is also a constitutively expressed small heat shock protein in *C. elegans.* Immuno staining suggests that HSP43 is localized in the cells of the vulva and spermatheca. The importance of HSP43 in *C. elegans* is not yet known. Previous literature suggests that a knockdown of this heat shock protein has no effect on cell division or the developmental process. The expression level of HSP43 is not altered by heat shocks (Ding and Candido, 2000c)

3.6.5. SIP-1

SIP-1 is a stress-induced protein also known as SEC-1 (small embryonic chaperone), which plays an important role in embryonic development of *C. elegans*. Surprisingly, this protein is expressed only in *C. elegans* embryos and egg laying adults (Fleckenstein et al., 2015; Linder et al., 1996). SIP-1 was found in the insoluble protein fraction of day 12 adult wild type worms (Walther et al., 2015). Although closely related to HSP16s, the expression level of SIP-1 is not regulated by heat shock. Interestingly, the chaperone activity and structural conformation of SIP-1 are associated with pH. At acidic pH, SIP-1 suppresses citrate synthase aggregation *in vitro.* Under normal lab conditions, HSP16s have been reported in *sip1* deletion worms (Fleckenstein et al., 2015). This further supports that the expression of HSP16s can be altered in physiological conditions.

3.7. Protein Folding

Protein folding is an essential cellular process. Once a polypeptide (a linear chain of amino acids) has been translated by the ribosome, it must acquire its three-dimensional native conformation through a folding process. The steps of protein folding are defined by different structural elements. A chain of newly synthesized polypeptides is referred to as the primary structure of a protein. The secondary structure of a protein consists mainly of α-helices and β-sheets. The three-dimensional organization of these secondary structure elements is referred to as the tertiary structure. Finally, the quaternary structure describes the formation of a

multimeric complex by association of three-dimensional complexes of several polypeptide chains.

For decades, the concept of protein folding in the cell remained a puzzle. In 1973, based on *in vitro* experiments, Anfinsen proposed in his thermodynamic hypothesis on protein folding that the lowest Gibbs free energy of the system facilitates the native conformation of protein in given environmental conditions (solvents, ionic strength, pH, metal ions, prosthetic groups, temperature and other components). His *in vitro* experiments were helpful in understanding native structures inside the test tube, that the folding of a protein should follow a specific path, and that the duration of protein folding differs from one protein to another. Initially, a polypeptide can fold randomly within seconds or minutes, but if the entire folding process were based on the random search for a specific three-dimensional conformation, then folding of the protein would take longer than the age of the universe to achieve a native structure (Levinthal, 1968; Levinthal et al., 1962; Zwanzig et al., 1992). In a living cell, protein folding obviously must happen within a biologically relevant time period. Several models have been proposed to describe the rapid protein folding *in vitro*, such as the the framework model (Ptitsyn, 1973), diffusion-collision model (Karplus and Weaver, 1976), hydrophobic collapse model (Go, 1984), and the nucleation condensation model (Fersht, 1997). Currently, the view of protein folding mechanisms has evolved based on an energy landscape perspective (folding funnel), which satisfies the hypothesis and paradox of Anfinsen and Levinthal (Bryngelson et al., 1995; Dill and Chan, 1997). This model represents different kinds of energy landscapes. Among these, the smooth surface energy landscape is used to describe the fast folding of proteins without complex barriers. However, often the polypeptide must pass through a rugged energy landscape with kinetic traps and energy barriers; so the process of folding is slow, and partially folded intermediates populate the kinetic traps (Brockwell and Radford, 2007; Dill and Chan, 1997). In a cell or organism these partially folded intermediates require the assistance of chaperones to reach the native state. Molecular crowding in the system can cause intermolecular aggregation that leads to the formation of amorphous aggregates, toxic oligomers and amyloid fibrils (Hartl et al., 2011).

3.8 Protein Misfolding and Aggregation

Misfolding of proteins is a common molecular phenomenon in the protein folding process. Several factors accelerate the misfolding of proteins in the cell, such as stress conditions (thermal stress, extreme changes of pH, oxidative agents, equilibrium interface, high glucose levels, etc.), age and disease (Herczenik and Gebbink, 2008). The proteostasis network responds to the accumulation of misfolded proteins through the unfolded protein response (UPR) and heat shock response (HSR) and guides them to chaperones in order to achieve a native conformational state. Misfolded proteins that cannot be folded properly are degraded by the ERAD (Endoplasmic reticulum associate degradation), the proteasome and autophagy pathways (Amm et al., 2014; Hartl et al., 2011; Powers et al., 2009; Valastyan and Lindquist, 2014).

The performance of the proteostasis network declines with age and disease, creating an imbalance between the quality control machinery and the amount of misfolded protein. A deficiency of the proteostasis network and crowding of misfolded proteins results in the formation of inclusion bodies or aggregates (Dobson, 2003; Hipp et al., 2014). In this scenario, the proteostasis network is overloaded by misfolded proteins and the accumulated aggregates are deposited at specific cellular sites. Sequestration of protein aggregates may even protect the cell from toxicity. In bacteria, aggregate deposition is localized at the poles; in yeast, aggregates are deposited in two compartments: the JUNQ (Juxtanuclear quality control compartment) and IPOD (Insoluble protein deposit). Aggregation deposit centers present in yeast are also found in mammalian cells. In addition, mammalian cells possess aggresomes, which are not permanent but appear in conjunction with several disease states. The disaggregation process can reverse the process of aggregation. Several molecular chaperones and proteases are involved in the disaggregation process of prokaryotes and eukaryotes, such as ClpB or Hsp104, Hsp70, sHSPs, 26s proteasome, AAA+ proteases and valosin containing protein (Tyedmers et al., 2010).

Several human diseases associated with protein misfolding and aggregation are listed in Table 1-1. The effect of one or more mutations in the polypeptide causes protein misfolding, improper degradation or improper localization, which leads to loss of

protein function, can subsequently cause disease (cancer, carbonic anhydrase II, cystic fibrosis, pulmonary emphysema, liver disease, etc.). In some diseases, mutations cause a gain of functional toxicity to the cell by forming complexes such as oligomers, amyloid fibrils or aggregates (Knowles et al., 2014; Valastyan and Lindquist, 2014; Winklhofer et al., 2008). Aberrant misfolded proteins in the cell have a high propensity to co-aggregate with similar proteins. In parallel, aggregated species have a tendency to influence the aggregation behavior of other proteins and co-aggregate with them, a process first observed with polyglutamine aggregates. Influencing and co-aggregating can be a possible reason for the association of toxicity with neurodegenerative disease (Gidalevitz et al., 2006; Tyedmers et al., 2010). Prevention of aberrant aggregates in the diseases is associated with the efficiency of protein quality control.

Table 1-1: Diseases Associated with Protein Misfolding and Aggregation (Adapted from (Knowles et al., 2014; Valastyan and Lindquist, 2014).

Human Disease	**Aggregated peptides or proteins**
Alzheimer's disease	β-amyloid; Tau
Amyotrophic lateral sclerosis	SOD-1; TDP-43
Amyloid light chain amyloidosis	Light chains of Immunoglobulin
Amyloid A amyloidosis	A1 serum amyloid protein fragments
Apolipoprotein A1 amyloidosis	Apo A-1 fragments
Cataract	Crystallins
Familial amyloidotic polyneuropathy	Transthyretin (Mutants)
Hemodialysis related amyloidosis	β_2 –macroglobulin(s)
Huntington's disease	Huntingtin with polyQ expansion
Injection localized amyloidosis	Insulin
Lysosome amyloidosis	Lysozyme (Mutants)
Parkinson's disease	α-synuclein
Senile systemic amyloidosis	Transthyretin (Wildtype)
Spongiform encephalopathy	Prion protein
Type II diabetes	Amylin

Neurodegenerative diseases such as Alzheimer's disease, Amyotropic lateral sclerosis, Huntington's disease, Parkinson's disease and Spongiform encephalopathies, etc. are the major protein misfolding and aggregation diseases. In this study, we address the impact of zeitgeber conditions on protein aggregation in polyglutamine expansion disorders and in Parkinson's diseases.

3.8.1. Polyglutamine Disorders

An abnormal repetition of glutamine (CAG) in the respective genes causes polyglutamine (polyQ) disorders, which includes mainly neurodegenerative diseases such as Huntington's, Machado-Joseph's, Kennedy's, Spinal bulbar muscular atrophy, dentatorubral pallidoluysian atrophy and six types of spinocerebellar ataxia diseases (Fan et al., 2014). These are age-associated diseases, and they share a common molecular pathology of protein aggregation. For example, abnormally expanded polyQ stretch on the first exon of the *huntingtin* gene causes protein misfolding and aggregation. Such propensity of polyQ aggregation is associated with the length of polyQ stretch. A length of polyQ stretch ≥35 residues leads to polyQ aggregation, a hallmark of Huntington's disease (MacDonald et al., 1993). Furthermore, six types of spinocerebellar ataxia are due to abnormal expansion of polyQ on their causative genes, including ataxins-1,2 and 7, CACNA1A and TBP (Holmberg et al., 1998; Huynh et al., 1999; Koide et al., 1997; Matilla-Duenas et al., 2008; Zhuchenko et al., 1997). An expanded polyQ stretch in ataxin-3 causes Machado-Joseph's disease (Bettencourt and Lima, 2011). In dentatorubral pallidoluysian atrophy, Atrophin-1 has an expanded poly-glutamine stretch (Sato et al., 2009) and in Spinal bulbar muscular atrophy the androgen receptor is similarly mutated (La Spada and Taylor, 2003).

3.8.2. Parkinson's Disease

The molecular pathology of Parkinson's disease is associated with a degeneration of dopaminergic neurons, which are essential for motor control. The loss of dopaminergic neurons was predicted as a consequence of genetic mutations, dysfunction of the ubiquitin proteome system, defects in autophagy pathways and

mitochondrial dysfunction, etc. (Jankovic, 2007; McNaught et al., 2006). The Lewy bodies (protein inclusions) at the cellular level have a high content of aggregated α-synuclein (α-syn), which occurs due to mutations in the encoding gene. Several more mutations have been identified and associated with the progression of familial Parkinson's disease. These mutations can occur in genes such as *LRRK2, PARK2, PINK1, DJ-1* and *ATP13A2*. In clinical diagnosis, the symptoms of Parkinson's disease are divided into non-motor and motor, which include sleep-wake cycles and behaviour (Dexter and Jenner, 2013; Markaki and Tavernarakis, 2010; Muzerengi et al., 2007).

3.9. Circadian Biology and Protein Aggregation Diseases

Several studies indicate an association of (protein aggregation) diseases and disrupted circadian rhythms, including cancer, type 2 diabetes, neurodegenerative diseases and many more (Hastings and Goedert, 2013; Knowles et al., 2014; Kurose et al., 2014; Musiek, 2015; Savvidis and Koutsilieris, 2012; Valastyan and Lindquist, 2014). P53 is an essential protein involved in the regulation of the cell cycle and the circadian clock. A genetic mutation of p53 in cancer causes prion-like P53 aggregates, which are involved in cancer pathology (Silva et al., 2014). In parallel, a deficiency of p53 has an effect on the circadian expression of *Per2* and locomotor behavior (Miki et al., 2013). One aspect of cancer pathology is a disrupted circadian clock through p53. Type 2 diabetes is also associated with protein aggregation and disruption of the circadian clock. High fat diets induce the amylin aggregate formation and β-cell dysfunction (Hull et al., 2003). Although the reason for the dysfunction of β-cells in type 2 diabetes remains unclear, recent studies have shown that chaperones improve β-cell function in type 2 diabetes, suggesting an association between aggregate formation and β-cell dysfunction (Cadavez et al., 2014). However, dysfunctional β-cells also affect the circadian behavior of insulin secretion in type 2 diabetes (Kurose et al., 2014). Additionally, core body temperature rhythms were also disrupted in streptozotocin-induced diabetes (Ramos-Lobo et al., 2015). Because the chaperone induction is associated with circadian behavior of HSF-1, one can hypothesize that entrainment may play a role in the prognosis of type 2 diabetes.

In neurodegenerative diseases, circadian rhythms are disrupted from the molecular to the behavioral level. In Alzheimer's, Huntington's and in Parkinson's diseases, daily rhythms of activity, melatonin secretion and sleep-wake cycles are commonly disrupted (Aziz et al., 2010; Breen et al., 2014; Coogan et al., 2013; Hu et al., 2009; Morton et al., 2005; Niwa et al., 2011; Skene and Swaab, 2003; Videnovic and Golombek, 2013; Witting et al., 1990; Wu et al., 2006). Additionally, the amplitudes of core body temperature rhythms are affected in several neurodegenerative diseases (Kudo et al., 2011b; Pierangeli et al., 1997; Zhong et al., 2013). The expression of vasoactive intestinal polypeptide (VIP), a protein essential for the circadian regulation of SCN, is disrupted in Alzheimer's and in Huntington's diseases (Aton et al., 2005; Zhou et al., 1995). At the molecular level, the amplitude of *Per2* expression is reduced in the SCN of APP-PS1 transgenic mice (Duncan et al., 2012). Furthermore, the circadian behavior of the electrical output of the SCN was disrupted in mouse models for Parkinson and Huntington's diseases (Kudo et al., 2011a; Kudo et al., 2011b). Although it can be concluded that the circadian clock is disrupted in neurodegenerative diseases, the effect of circadian dysfunction on neurodegenerative diseases remains unclear. Several studies have reported effects of improving the circadian functions on the prognosis of neurodegenerative diseases. Inducing rhythmic sleep in a R6/2 mouse model for Huntington's disease, for example, recovered *Per2* rhythms in the SCN followed by cognitive improvement. Similarly, light entrainment, periodic melatonin treatment and scheduled feeding restored the circadian behavior in R6/2 mice (Maywood et al., 2010; Pallier et al., 2007), suggesting that entrainment can recover circadian functions in neurodegenerative diseases.

3.10. *Caenorhabditis elegans (C. elegans)* as a Model

C. elegans is a microscopic and transparent nematode. In nature, these nematodes are found in organic rich soils, composts and rotting fruits, etc. The gender of *C. elegans* is either hermaphrodite or male. Hermaphrodites are self-fertile but can also breed with males. Each worm has around 1000 somatic cells, including 302 neuronal cells. Recently, a pair of additional neuronal cells was found in males, and have been termed MCMs (Sammut et al., 2015). In *C. elegans*, postembryonic development

starts with discrete larval stages (L1, L2, L3 and L4), separated by molts (M1, M2, M3 and M4) and followed by adult worms. During molts, worms display a quiescent behavior (lethargus) when the worms cannot eat food, and an increased arousal threshold (Cho and Sternberg, 2014; Raizen et al., 2008; Singh and Sulston, 1978). In the Merrow lab, Dr. Maria Olmedo has developed a high throughput method to detect larval stages and molts using bioluminescence tools (Olmedo et al., 2015).

Fifty years ago, *C. elegans* was first used as a model organism to address biological questions in developmental biology, genetics and neurobiology, etc. This model was later extended to address questions in molecular biology. Around 83% of the sequences in the *C. elegans* proteome are homologous to those in humans (Lai et al., 2000), leading scientists to recognize the utility of *C. elegans* in the study of age associated human disease, including cancer, diabetes and neurodegenerative diseases, etc.

In our research, we used *C. elegans* to study the impact of zeitgebers on chaperone expression and protein aggregation in neurodegenerative diseases. Several studies have shown that *C. elegans* has circadian behaviors such as in stress tolerance, locomotion, defecation, rate of pharyngeal pumping, food consumption, oxygen consumption and olfaction (Kippert et al., 2002; Migliori et al., 2011; Olmedo et al., 2012; Saigusa et al., 2002; Simonetta et al., 2008). At the molecular level, light and temperature entrained circadian transcripts have been found by genome-wide analysis (van der Linden et al., 2010). Circadian rhythms have been observed in the oxidative state of peroxiredoxins and RNA levels of GRK-2 protein in constant free-running conditions (Olmedo et al., 2012). These observations suggest that *C. elegans* possesses a circadian clock, although the molecular oscillators are still to be discovered. In parallel, *C. elegans* transgenic models were established to study protein aggregation in neurodegenerative diseases (Li and Le, 2013). Most of these models include a transgenically expressed disease-specific gene fused to a flourescence reporter.

To address the prognosis of molecular pathology in polyglutamine expansion disorders, Morimoto's lab generated transgenic *C. elegans* strains with the muscle and neuron specific expression of fluorescence tagged polyQ proteins with different

lengths (Q0, Q19, Q35, Q40, Q44, Q67 and Q86, etc.). In these models, length dependent polyQ aggregation and toxicity occurs at a threshold of 35-40 glutamine repeats. In muscle specific polyQ models, the rate of aggregation is inversely correlated with worm motility (Brignull et al., 2006; Morley et al., 2002). In addition to polyglutamine disorders, transgenic worms were generated for Alzheimer's, Amyotrophic lateral sclerosis and Parkinson's disease (Li and Le, 2013). Considering the chaperome network, the functional families are highly similar between *C. elegans* and humans (Brehme et al., 2014). Accordingly, *C. elegans* can be invoked as a model for understanding the impact of zeitgebers on chaperone expression and protein aggregation in neurodegenerative models.

4. Aim of this work

Circadian clock disruption (e.g. disrupted sleep, activity, core body temperature, hormone secretion, etc.) in neurodegenerative diseases suggests a link between mechanisms of pathology and this pervasive timing program. The causes and effects of such a disrupted clock for patients is not known. Pharmacologically induced sleep, melatonin treatments and scheduled feeding restored circadian behavior in the Huntington's disease model mice (R6/2) (Maywood et al., 2010; Pallier et al., 2007), and imposing high amplitude light entrainment on dementia patients slowed the decline in cognitive function (Riemersma-van der Lek et al., 2008). However, the molecular mechanisms associated with zeitgebers and neurodegeneration are unclear. One study has shown that endogenous temperature rhythms induce rhythmic binding of HSF-1 (Heat Shock Factor-1) to promoters with a heat shock element (Reinke et al., 2008). HSF-1 is a transcription factor that regulates expression of numerous heat shock genes, which are involved in prevention of protein misfolding/aggregation (molecular pathology) in neurodegenerative disease. Building on the literature, we found that endogenous temperature rhythms are associated with light entrainment, melatonin, sleep and feeding cycles. We hypothesize that endogenous temperature cycles may regulate the abundance of heat shock proteins and thus might impact protein folding and/or aggregate formation in neurodegenerative disease.

The objectives covered in this thesis are as follows:

- To establish novel methods to characterize polyQ aggregates both quantitatively and qualitatively.
- Determine if and how temperature cycles impact Q35::YFP aggregate formation.
- Characterise how temperature cycles impact proteostasis network components, primarily heat shock proteins or chaperones.
- Determine developmental timing in *C. elegans* polyQ transgenic models.

5. Materials and Methods

5.1. Chemical Reagents

Chemicals used for preparing media and buffers are listed in table 5-1.

Table 5-1 Chemicals

Chemical	**Supplier**	**Order No.**
3-morpholinopropane-1-sulfonic acid (MOPS)	Roth	G979.4
Acetic acid (CH_3COOH)	AppliChem	A2083
Acrylamide30% Bis-AA 29:1	Biorad	161-0156
Agarose QE	MP	AGAP0100
Ammonium persulfate (APS)	Sigma	A3678
Bacto Agar	BD	214010
Bacto Peptone	BD	211677
Bacto Tryptone	BD	211705
Bacto Yeast Extract	BD	212750
Bis-Tris	AppliChem	A1025
Blasticidin	AppliChem	150477
Bovine serum albumin (BSA)	Sigma	A7906
Bromophemol blue	USB	US12370
Calcium Chloride ($CaCl_2$)	AppliChem	A4689
Chloroform	Sigma-Aldrich	C2434
Cholesterol	Sigma	C3292
Coomassie Blue G-250	Roche	1.15444
Difco Agar, granulated	BD	214530
Dimethysulfoxide (DMSO)	Merck	109678.01
D-Luciferin	PJK	102111
Ethanol	AppliChem	A3678
Ethylenediaminetetraacetate (EDTA)	AppliChem	A3145
Formic acid	Sigma	399388

Fluoro (5)-2-deoxyuridine (FUDR)	Abcam	Ab141270
Glycerol 87%	Applichem	A3739
Hydrochloric acid Standard 1M	AppliChem	A1434
Igepal CA-630 Mol Bio	Sigma	I-8896
Isopropanol	AppliChem	A1008
Magnesium Sulfate ($MgSO_4$)	Sigma	230391
Methanol	Merck	1.06009.1000
Milk powder, non fat	AppliChem	A0830
Phenol	AppliChem	A1153
Ponasterone A	Sigma	P3490
Ponceau S	Fluka	81460
Potassium Chloride (KCl)	AppliChem	A3980
Potassium Dihydrogen Phosphate (KH_2PO_4)	Sigma	P0662
Potassium hydroxide (KOH)	Sigma	P1767
Potassium Phosphate (KPO_4)	Sigma	P-5379
Sodium Chloride (NaCl)	AppliChem	A2942
Sodium phosphate monobasic dihydrate (NaH_2PO_4)	Sigma	71505
Sodium dodecyl sulfate (SDS)	AppliChem	A1502
Sodium hydrogen carbonate ($NaHCO_3$)	MERCK	6329
Sodium hydroxide (NaOH)	Roth	G771.6
Sodium hypochlorite (NaClO)	Sigma	S1898
SYBR Safe	Invitrogen	S33102
Tetramethylethylenediamine (TEMED)	Sigma	T-928
Tris(hydroxymethyl)aminoethane (Tris) ultra pure	AppliChem	A1086
Triton® X-100	Sigma	T-8787
TRIzol®Reagent	Invitrogen	15596026
Tween®-20	AppliChem	A4974
β-Mercaptoethanol	Sigma	M-3148
di-sodium hydrogen phosphate dihydrate	AppliChem	A4732,1000

5.2. Consumables

Consumables include materials and reagents used for the experiments are listed in table 5-2.

Table 5-2 Consumables

Consumables	**Suppliers**
100bp DNA ladder	New England Bio Labs
2-Log ladder	New England Bio Labs
Antibody of mouse actin	Santa Cruz Biotechnology
Antibody of mouse Green Fluorescent Protein (α-mouse-GFP)	Roche
Antibody of mouse Horseradish peroxidase (α-mouse-HRP)	Bio-Rad
Cover Slips 18x18 mm	Waldemer Knitter
Cover Slips 24x60 mm	Waldemer Knitter
EDTA Free Protease inhibitor cocktail tablets	Roche
Gene loading dye	New England Bio Labs
Micro AMP™ Optical Adhesive Film	Applied Biosystems
MicroAMP R Optical 384 well Reaction Plates	Applied Biosystems
Nunclon Delta Surface 96-well plates	Thermo scientific
NuPAGE™ Novex™ 4-12%	Invitrogen
Precision Plus Protein™ All Blue Standards	Bio-Rad
Protran Nirocellulose membrane 0.2uM	Whatman
9cm, 6cm, 3.5cm Petri dish	Greiner bio one
TC Flask T75, Standard	Sarstedt
Transblot R turbo™ transfer pack	Biorad
Cell Scraper 25 cm	Sarstedt
Sterile bacterial spreader	VWR
0.5 mm dia Zirconia/Silica beads	Biospec
Low Protein binding eppendorf tubes	Eppendorf

5.3. Kits

Kits used for the experiments are listed in table 5-3.

Table 5-3 Kits

Kits	Supplier
Pierce™ BCA protein assay	Thermofisher scientific
TaqMan Reverse Transcription Reagents	Applied Biosystems
DnaseI amplification grade	Invitrogen
Page Silver ™ Silver Staining	Fermentas Life Sciences
SuperSignal R West Femto Maximum sensitivity Substrate	Thermo Scientific

5.4. Laboratory Equipment

Laboratory equipment used for the experiments are listed in table 5-4.

Table 5-4 Laboratory equipment

Equipment	Company
Autoclave	Varioklav
Bio fuge primo R Centrifuge	Heraeus
Bioruptor™ UCD-200	Diogenode
Centrifuge 5417 R	Eppendorf
Chemidoc™ MP imaging system	Bio-Rad
Discovery.V8 SteREO microscope	Zeiss
Electrophoresis Power Supply- EPS601	Amersham pharmacia biotech
Fluorescence microscope LEICA ICC50 HD	Leica
Freezer -20 °C	Liebherr Premium NoFrost
Freezer HFC 586 -80 °C	Heraeus
Incubator 37 °C	Memmert
Incubators MIR-153	Sanyo
Laminar air flow	Interflow
Centro LB 960 Luminometer	Berthold
Membra Pure	Astacus

Microwave Oven	Privileg
Mini bead beater oa60ap-22-1-WB	Biospec products
Mini rocker-shaker MR-1	Gkisker
Mini spin plus	Eppendorf
Multiskan^{TM} FC Microplate Photometer	Thermo Scientific
NanoDrop® 1000 Spectrophotometer	Peqlab, Erlangen
NuPAGE® Pre-cast system	Invitrogen
Optima MAX-XP Ultracentrifuge	Beckmancoulter
pH meter	Mettler Toledo
Pipettes (Reference autoclavable)	Eppendorf
Qik Spin QS7000	Edward Instrument Co.
Real-Time PCR System	Applied Biosystems
Refrigerator 4 °C	Bosch electronic no frost
Rotina 420 Centrifuge	Hettich
Thermocycler	Peqlab,Waldbuttelbrunn
Thermomixer Comfort	Eppendorf
Transblot turbo transfer system	Bio-Rad
Vortex mixer	VELP Scientifica
Weighing machine TE1502S	Sartorius
Worm Incubator	Liebherr

5.5. Primers

Primers used for quantitative RT-PCR are listed in table 5-5.

Table 5-5 Primers

Gene	**Forward Primer**	**Reverse Primer**
act-4	5′-GGCATCACACCTTCTACAACGA-3′	5′-TGGATTGAGTGGAGCCTCAGT-3′
ama-1	5′-CAATCAGCAGTTGCAGAGAAA-3′	5′-CAGGCCCGGAATACAATTG-3′
hsp-4	5′-TGCCGTCGAGAGAGCTATTGA-3′	5′-GTTCCTTCTTTTGCTCCTTGTTTT-3′

hsp-12.6	5′-ACGAAGGAACCAAGTGGG-3′	5′-GGGCTTCTAGGCCTACTT-3′
hsp-16.1	5′-CAGTTTGCAGAGGCTCTCCA T-3′	5′-TTGTTCTCCTTGAATTGATAA TGTAT GTC-3′
hsp-16.2	5′-GTTTTTGGTGATCTTATGAG AGATATGG-3′	5′-GATGGCAAACTTTTGATCATT GTT-3′
hsp-43	5′-GACCTGTGGCTCGACGAT TT-3′	5′-TGTCGACGTCACGGGAGAA-3′
unc-54	5′-GAAGGACCCAGGATGGCAA TA-3′	5′-CCAGACGTTCTTCTTGGAGT CA-3′

5.6. Strains

Strains used for the experiments are listed in table 5-6.

Table 5-6 Strains

Strain/Genotype	**Models**	**Supplier**
N2; Wild type	*C. elegans*	Caenorhabditis Genetics Center
AM140; rmIs132 [unc54p::Q35::YFP]	*C. elegans*	Caenorhabditis Genetics Center
AM141; rmls133 [unc-54p::Q40::YFP]	*C. elegans*	Caenorhabditis Genetics Center
AM134; rmls126 [unc-54p::Q0::YFP]	*C. elegans*	Caenorhabditis Genetics Center
OW40; zgIs15 [unc54p::α-syn::YFP]	*C. elegans*	Gift from Ellen A.A. Nollen, Netherlands
PE254; feIs4 [sur-5::luc+::gfp; rol-6(su1006)]	*C. elegans*	Cristina Lagido Lab
hsp-16.1::gfp	*C. elegans*	Gift from Dr. Juhno Lee, South Korea
PE254 X AM134	*C. elegans*	Strain of Cristina Lagido
PE254 X AM141	*C. elegans*	Strain of Cristina Lagido
OP-50	*E. coli*	Caenorhabditis Genetics Center

5.7. Culture Media

LB Medium

1% (w/v) bacto-tryptone

0.5% (w/v) bacto-yeast

1% (w/v) NaCl

pH to 7.0 using 10 N NaOH

LB-Agar

1.5% (w/v) agar

1% (w/v) bacto-tryptone

0.5% (w/v) bacto-yeast

1% (w/v) NaCl

pH to 7.0 using 10 N NaOH

NGM Agar

1.7% (w/v) agar

0.051 M NaCl

0.25% (w/v) peptone

- Autoclave solution
- Cool down to 70°C

0.0005 mM $CaCl_2$

0.001 M $MgSO_4$

0.005% (v/v) Cholesterol (solved in ethanol)

0.025 M KPO_4

NGM-FUDR Agar

1.7% (w/v) agar

0.051 M NaCl

0.25% (w/v) peptone

- Autoclave solution
- Cool down to 70°C

0.0005 M $CaCl_2$

0.001 M $MgSO_4$

0.005% (v/v) Cholesterol (solved in ethanol)

0.025 M KPO_4

0.012% (w/v) FUDR

5.8. Buffers and Solutions

S-Basal

0.585% (w/v) NaCl

0.1% (w/v) K_2HPO_4

0.6% (w/v) KH_2PO_4 and 1 ml/l of 5 mg/ml Cholesterol.

M9 Buffer

0.3% (w/v) KH_2PO_4

0.6% (w/v) Na2HPO4

0.5% (w/v) NaCl

0.001 M $MgSO_4$

4x Native Sample Buffer

0.0625 M Tris-Cl (pH 6.8)

10% (v/v) glycerol

0.1% (w/v) bromophenol blue

1x SDS Sample Buffer

0.06 M Tris (pH 6.8)

10% (v/v) SDS

10% (v/v) glycerol

1.25% (v/v) β-Mercaptoethanol

0.005% (w/v) bromophenol blue

2x SDS Sample Buffer

1.20 M Tris (pH 6.8)

20% (v/v) SDS

20% (v/v) glycerol

2.5% (v/v) β-Mercaptoethanol

0.01% (w/v) bromophenol blue

4x SDS Sample Buffer

2.40 M Tris-Cl (pH 6.8)

40% (v/v) glycerol

8% (v/v) SDS

5% β-Mercaptoethanol

0.04% (v/v) bromophenol blue

SDD-AGE Sample Buffer

2x TAE

8% (v/v) SDS

20% (v/v) glycerol

0.01% (w/v) bromophenol blue

NP40 Lysis Buffer-1

0.05 M Tris-Cl (pH 8.0)

0.5 M NaCl

0.004 M EDTA

1% (v/v) Igepal CA-630

Protease inhibitor tablet Roche 2x (1tablet/10ml)

NP40 Lysis Buffer-2

0.05 M Tris-Cl (pH 8.0)

1.5 M NaCl

1% (v/v) Igepal CA-630

Protease inhibitor tablet Roche 2x (1 tablet/10 ml)

PBS (Phosphate Buffered Saline)

1.37 M NaCl

0.0027 M KCl

0.01 M Na_2HPO_4

0.0018 M KH_2PO_4

SDD-AGE Lysis Buffer

0.1 M Tris-Cl (pH 7.5)

0.05 M NaCl

0.01 M β-Mercaptoethanol

one Protease inhibitor tablet /10ml

SDD-AGE Sample Buffer

2x TAE

8% (v/v) SDS

20% (v/v) glycerol

0.01% (w/v) bromophenol blue

SDD-AGE Gel Running Buffer

1x TAE

0.1% (v/v) SDS

2x TAE Buffer

0.08 M Tris acetate

0.002 M EDTA

pH to 8.2-8.4

1x Tris-Glycine Buffer

0.025 M Tris-Cl

0.19 M Glycine

pH to 8.3

TBS Buffer

0.05 M Tris-Cl

1.37 M NaCl

0.0027 mM KCl

TBS-T (TBST+ Tween20) Buffer

0.1% (v/v) Tween 20

TBS Buffer

Luciferin Solution-1

100 μM D-Luciferin

S-basal

Reverse Transcription Reaction Mixture

TaqMan reverse transcription reagents were used to prepare reaction mixture which contained 1x RT-Buffer, 5.5 mM $MgCl_2$, 500 μM dNTP, 2.5 μM Random Hexamers, 0.4 U/μl RNase inhibitors, 1.25 U/μl reverse transcriptase in RNase-free H_2O.

qPCR Reaction Mixture

Reaction mixture consisted of 1x of SYBR Select with 500 nM of each primer in RNase-free H_2O.

Luciferin Solution-1

100 μM D-Luciferin

S-basal.

Luciferin Solution-2

100 μM D-Luciferin

2% (w/v) *E. coli* OP50 (wet weight)

S-basal.

***C. elegans* Freezing Solution**

30% (v/v) Glycerin

S-basal

5.9. *C. elegans* Physiological Methods

The basic physiological methods for maintaining *C. elegans* in the current study was obtained from worm book (Eisenmann, 2005).

5.9.1. *C. elegans* Culturing

5.9.1.1. General Maintenance of *C. elegans*

Worms were cultured in an incubator at 18 °C on NGM agar plates with *E. coli* (OP50). Animals were chunked or transferred to new NGM agar plates for routine maintenance. To preserve stocks, L1 and L2 stage worms were frozen at -80 °C using Freezing Solution.

5.9.1.2. Synchronization of Worms

To synchronize the worms, mixed stage worms were grown on NGM agar plates until they were gravid adult stage. At the gravid adult stage, worms were collected from 4-5 NGM agar plates into falcon tubes using M9 buffer. Over 5 min, worms passively sedimented to the bottom of the tube and then supernatant was removed. 5 ml of hypochlorite solution was added to the sedimented worms, followed by vigorous shaking for 2 min. Worms were centrifuged at 5000 g for 1 minute and the supernatant was discarded. The worm pellet was then washed with 5 ml of M9 buffer and centrifuged at 5000 g for 1 minute. The supernatant was removed and 1 ml of M9 buffer and 4 ml of hypochlorite solution were added to the worm pellet, followed by vigorous shaking. Immediately after the worm cuticles are not visualized the tube was centrifuged again at 5000 g for 1 minute and the supernatant was removed. This step was repeated 2 more times to wash the eggs from the hypochlorite solution. Eggs were resuspended in 2-3 ml of M9 buffer. Eggs were counted in 10 µl of the suspended buffer using microscope, estimated the approximate amount of eggs in 2-3 ml solution. Incubated overnight at 18 °C to get synchronized L1 worms. For measurement of developmental timing, the eggs were resuspended at a concentration of 20 eggs/µl.

5.9.1.3. Culturing of Worms for the Analysis of PolyQ Aggregates

Approximately 2000 Synchronized L1 worms were placed on NGM agar plates with *E. coli* (OP50). Worms were then grown in incubators programmed with one of several conditions: constant temperature (16.5 °C); lower amplitude zeitgeber (temperature) cycle (12 h at 15 °C and 12 h at 18 °C); or higher amplitude zeitgeber (temperature) cycle (12 h at 13 °C and 12 h at 20 °C). All incubations were performed in constant darkness. HOBO data loggers monitored light and temperatures in the incubators. At the L4 stage (day 0 adult), worms were collected from NGM plates, transferred to NGM-FUDR plates with 10x concentrated *E. coli* (OP50) and incubated at the same temperature conditions until day 8 of adulthood.

5.9.1.4. Culturing of *C. elegans* for the Analysis of Gene and Protein Expression

Synchronized populations of an approximately 1000 L1 worms were grown on NGM agar plates in constant (16.5 °C) and temperature cycle (13 °C for 12 h and 20 °C for 12 h). To create 24 or 48-hour time courses in cycling temperatures, we used two incubators where the cycles were programmed in antiphase, allowing us to collect samples for 24 hours over only 12 hours of sampling. Once the worms reached the L4 stage, worms were harvested at 2 h intervals for 48 h, in a dark room.

5.9.1.5. Single Worm Culture for Real-time Measurement of Developmental Timing

Single arrested L1-stage animals were transfered to each well of a white, 96-well plate containing 100 µl of Luciferin solution-1. After pipetting nematodes into each of the wells, 100 µl of Luciferin solution-2 was added to each well. This procedure helped to provide the food supply to all the worms in the plate at same time, so that development was synchronously resumed. The plate was then sealed with an air permeable membrane from Breathe Easier™ Diversified Biotech™ and placed in a luminometer to measure bioluminescence over larval development (Olmedo et al., 2015).

5.9.2. Motility Assay

Motility was assayed by counting body bends of *C. elegans* (Morley et al., 2002; van Ham et al., 2010). For this assay, approximately 100 synchronized L4 worms were grown under different conditions on NGM-FUDR agar plates. On the day of the assay, 200 µl of M9 buffer was added on top of the worms to induce swimming. After 1 minute, the movement of the worms was recorded for 1 min using a CCD video camera module of the Discovery V8 SteREO microscope. Body bends were manually counted from the recorded movies, with the researcher blind to the experimental conditions.

5.9.3. Microscopy Methods

5.9.3.1. Fluorescence Microscopy

To prepare worms for fluorescence microscopy, approximately 100 synchronized L4 worms were grown on a NGM-FUDR agar plate. Worms were collected on specific days to an eppendorf tube using 1 ml of cold M9 buffer. After collecting the worms, eppendorf tubes were placed in ice for 1 minute to sediment the worms to the bottom of the tube. Approximately 50 worms from the eppendorf tube were placed on top of a 24x60 mm coverslip with a 3% agarose pad. Worms were immobilized by adding 10 µl of 100% ice-cold ethanol and a small coverslip was placed on top of the worms to seal the pad. Fluorescence pictures were taken for a minimum of 10 animals using a Leica ICC50 HD fluorescence microscope through a 10x/0.22 numerical aperture objective. Fluorescence intensity was measured using ImageJ, and validated by manual counting by researchers blind to the conditions. For these experiments, pictures of Q35::YFP worms were taken at an exposure time of 5 ns to reduce the background signal. Since exposure times of 5 ns didn´t allow us to see the non-aggregated protein in control worms, pictures of Q0::YFP worms were taken with an exposure time of 12 ns.

5.9.4. Harvesting Animals for Diverse Purposes

5.9.4.1. Worm Harvesting for the Analysis of Aggregation

To extract the proteins from PolyQ-expressing worms, approximately 2000 synchronized L4 worms were grown on two 9 cm NGM-FUDR agar plates. On specific days between day 0 (L4 worms) and day 8, worms were collected into an eppendorf tube using cold M9 buffer. Worms were sedimented by centrifugation at 2000 g for 60 sec at 4 °C using a 5417 R eppendorf centrifuge and the supernatant was removed. The worm pellet was washed with 1 ml of ddH_2O to remove leftover bacteria. After centrifugation at 2000 g for 60 sec at 4 °C, the supernatant was removed; the worm pellet was frozen in liquid nitrogen and stored at -80 °C.

5.9.4.2. Worm Harvesting for the Analysis of RNA and Protein expression

At each time point, approximately 750-1000 worms were collected into an eppendorf tube using 2 ml of ice-cold M9 buffer. Worms were then sedimented at 5000 rpm for 15 s using an Eppendorf™ MiniSpin™. The supernatant was subsequently removed from the worm pellet and 1 ml of M9 buffer was added to wash the bacteria from the surface of the worms. After washing, M9 buffer was removed by centrifugation at 5000 rpm for 15 s. The worm pellet was transferred to a sterile mini bead-beater tube, rapidly frozen in liquid nitrogen and preserved at -80°C.

5.10. Biochemistry Methods

5.10.1. RNA Methods

5.10.1.1. RNA Extraction from *C. elegans*

RNA extraction was done by a Trizol based method. Frozen worm samples with 0.5 mm diameter of Zirconia/Silica beads were transfered from -80 ºC to liquid nitrogen and then transferred to ice immediately before starting the extraction. 0.5 ml of Trizol was added to each sample and the worms were lysed by applying 2 pulses of 30 sec in

a mini bead beater, separated by 5 minutes of incubation on ice. Samples were then incubated for 5 min on ice. After incubation, the worm lysate was transferred to a clean RNase free eppendorf tube, leaving the beads in the mini bead-beater tube. 100 µl of chloroform was added to each sample and the tubes were shaken manually for 15 sec. The samples were then incubated at room temperature for 3 min and centrifuged at 12,000 g / 4 °C for 15 min to separate the DNA and RNA (top layer) from proteins (bottom layer). Approximately 300 µl of the top layer was collected from each sample and transferred to a new RNase free eppendorf tube. The addition of chloroform and the centrifugation steps was repeated to achieve a high-quality extraction. 150 µl of 2-propanol was then added to 300 µl of the DNA and RNA mixture followed by incubation at room temperature for 10 min. After incubation, samples were centrifuged at 7,600 g for 10 min at 4 °C to collect the DNA/RNA pellet. The supernatant was then discarded carefully, without touching the pellet, and the pellet was washed thrice by addition of 0.5 ml of 70% EtOH and centrifugation at 7,600 g for 10 min at 4 °C. The supernatant was discarded, the pellet was air-dried, and subsequently dissolved by adding 20 µl of RNase free H_2O. The purity of RNA relative to DNA was assessed by measurement of the ratio between the absorbance at 260 and 280 nm and the purity of RNA relative to solvent contaminants was assessed by measuring the ratio between the absorbance at 260 and 230 nm using a NanoDrop® 1000 Spectrophotometer.

5.10.1.2. DNase Treatment

A DNase treatment was performed to remove DNA from the RNA extracts. For this experiment, we used the DnaseI amplification grade Kit from Invitrogen and followed the manufacturer's protocol. For a 25 µl reaction, 2.5 µg of RNA, 2.5 µl of 10x DNase I buffer and 2.5 µl of DNase I was added to RNase free H_2O. The reaction mixture was incubated at room temperature for 15 min followed by the addition of 2.5 µl of 25 mM EDTA solution and heated for 10 min at 65°C using thermo cycler from PeqLab.

5.10.1.3. cDNA Synthesis

To prepare cDNA, we used the TaqMan reverse transcription reaction reagents from Applied Biosystems. 100 µl of reverse transcription reaction mixture can convert a maximum of 2 µg of RNA to cDNA. For this experiment, we used 19 µl of reaction reagent to convert 100 ng of RNA. RNA was mixed with TaqMan reaction reagents and incubated at 25 °C for 10 min then reverse transcribed at 48 °C for 30 min, enzymes were inactivated at 95 °C for 5 min and the samples were held at 4 °C using thermocycler of PeqLab.

5.10.1.4. Quantitative Real-Time Polymerase Chain Reaction (qPCR)

We used the SYBR Select Master Mix to perform quantitative PCR using a ViiA7 Real-Time PCR System from Applied Biosystems. For this experiment, 15 µl of q-PCR reaction mixture was added to 50 ng of cDNA in a MicroAMP™ Optical 384-well plate. The plate was then sealed with MicroAMP™ Optical adhesive film from Applied Biosystems and centrifuged for 30 sec at 500 g to make sure that the samples were settled in the wells. The plate was placed into the thermal cycler and amplification was carried out using the following conditions. Data was analyzed by the 2-ΔΔCT method (Livak and Schmittgen, 2001).

		PCR (40 cycles)	
Step	**Activation**	**Denature**	**Anneal/Extend**
Time	10 min	15 Sec	1 min
Temperature	95 °C	95 °C	60 °C

5.10.2. Protein Methods

5.10.2.1. Protein Extraction Using Bioruptor

To extract proteins from the harvested animals, NP 40 lysis buffer-1 was added to the worm pellet at a 1:1 ratio and worms were lysed for 8 min with pauses of 30 sec at high current setting (320W), at 4°C using Bioruptor™ UCD-200. After lysis, a

clarifying spin was performed at 2000 rpm for 2 min to remove worm debris. The supernatant was then transferred to new eppendorf tubes without touching the pelleted debris.

5.10.2.2. Protein Extraction Using Bead Beater

To extract the proteins for Blue native poly acrylamide gel electrophoresis (BN-PAGE) and Native agarose gel electrophoresis (NAGE) a 1:1 ratio of 1X PBS buffer and protease inhibitor cocktail was added to the worm pellet and the protein samples were obtained by applying 2 pulses of 30 sec in the mini bead beater, separated by incubation on ice for 5 minutes.

5.10.2.3. Protein Quantification

Proteins were quantified using the Pierce™ BCA protein assay kit (Product No: 23225) from Thermofisher scientific, following the microplate procedure in the manufacturer's protocol. Absorbance was measured at 562 nm using a Multiskan™ FC Microplate Photometer from Thermo Scientific.

5.10.2.4. Protein Separation by Ultracentrifugation

Ultracentrifugation was used to separate soluble proteins from high molecular weight aggregates and insoluble proteins. For this experiment, the protein concentration in the samples was quantified and adjusted to 1.0 µg/µl with NP40 lysis buffer-1 (Walther et al., 2015). A second protein quantification was performed to make sure that the protein concentrations were as expected and another adjustment was made when necessary. 100 µg of protein was loaded into polycarbonate centrifuge tubes (Order no: 343778) from Beckman Coulter and the volumes were adjusted precisely for all the samples with NP40 lysis buffer-1. Tubes were then centrifuged at 500,000 g for 25 min at 4 °C. After centrifugation, the supernatant was collected as a soluble protein and frozen at -80 °C. The pellet was washed adding 100 µl of NP40 lysis buffer-1 followed by centrifugation at 500,000 g for 25 min at 4 °C. The supernatant was then removed and the pellets were preserved at -80 °C

5.10.3. Agarose Gel Electrophoresis

5.10.3.1. Native Agarose Gel Electrophoresis (NAGE)

NAGE was tested as a method to separate proteins in their native state (monomers, oligomers and aggregates) from crude protein lysates (Kim, 2011; van Ham et al., 2010). To perform NAGE, an agarose gel was prepared from 1% of Agarose in 1x Tris-Glycine Buffer. After boiling, the agarose solution was poured into a casting tray and left at room temperature. Once the gel was solidified, the gel comb was removed carefully, and the gel was placed into an electrophoresis unit. The gel was rinsed with 1x Tris-Glycine Buffer and equilibrated at 50 V for 1 hr, at 4°C. 60 μg of protein lysates (from section 5.10.2.2) with 4x native sample buffer was loaded on the gel and electrophoresed at 50 V for 16 hr at 4°C. The YFP signal on the gel was imaged using the Cy3 emission filter of the Bio-rad ChemiDoc™ MP imaging system. ImageJ was used to perform quantify separated forms of proteins.

5.10.3.2. Semi Denaturing Detergent Agarose Gel Electrophoresis (SDD-AGE)

SDD-AGE was performed to separate the SDS resistant polymers and aggregates from the crude protein samples. For this experiment, an equal volume of SDD-lysis buffer was added to the sedimented worm pellets (from section 5.9.4.1). The worms were lysed in semi-denaturing conditions using a Bioruptor™. Worm debris was separated from protein lysates at 2,500 g for 5 minutes. The supernatant was then collected and the concentration of protein in the samples was quantified using the Bradford assay (Bio-Rad) (Bradford, 1976). A 1.5% agarose gel was prepared with SDD-AGE running buffer as described in section 5.8. After it solidified, the gel was placed in an electrophoresis unit and rinsed with ice-cold SDD-AGE running buffer and equilibrated at 60 V for 60 min at 4 °C. Protein samples were then prepared by adding 4x SDD-AGE sample buffer to 15 μg of crude protein and different treatments were applied to observe high molecular weight SDS-resistant polymers (or =aggregates) and low molecular weight monomers. To observe the high molecular weight proteins, samples were incubated at room temperature for 10 min. To generate the negative control (monomers), the same protein samples were incubated with

sample buffer at 95 °C for 10 min. This method also serves to confirm that the high molecular weight species are not due to covalent bond modifications. All protein samples were loaded into the gel and resolved at 60 V for 4 h, at 4°C. The gel was further processed for transferring proteins to nitrocellulose member through capillary action (Kryndushkin et al., 2003; Shemesh et al., 2013).

5.10.4. Poly Acrylamide Gel Electrophoresis (PAGE)

5.10.4.1. Blue Native Poly Acrylamide Gel Electrophoresis (BN-PAGE)

To separate native proteins with a high resolution, we performed Blue Native PAGE. For this experiment, we used pre-cast NativePAGE™ Novex™ 4 - 16% gradient Bis-Tris gel from Invitrogen. The experiments were performed using the manufacture's protocol with minor modifications. Briefly, protein lysates were prepared from worms using a mini bead-beater (Section 5.10.2.2). Proteins concentrations were quantified by a Bradford assay and 10 μg of crude protein sample was loaded onto a gel with 4X NativePAGE™ sample buffer. The gel was run according to manufacturer's recommendations. Fluorescent bands on the gel, revealing the signal from the YFP reporter was imaged using a Cy3 filter (Bio-rad ChemiDoc™ MP imaging system). The quantification of the bands was done using Bio-rad Image Lab™ software.

5.10.4.2. NuPAGE

5.10.4.2.1. NuPAGE for Insoluble Proteins

NuPAGE is the pre casted and discontinuous SDS-PAGE gel system, where the proteins can resolve with neutral pH (7.0) (Penna and Cahalan, 2007). To resolve insoluble proteins, 50 μl of 1x SDS sample buffer was added to the insoluble pellet (from section 5.9.4.1) and incubated at 37 °C for 10 min with 30 sec of vortexing every 5 min. After dissolving the pellet, the protein solution was transferred from the polycarbonate ultracentrifuge tubes to eppendorf tubes and boiled for 10 min in a boiling water bath. Samples were then loaded into the NuPAGE™ Novex™ 4-12% gradient gel (Order no: WG1401BX10) and electrophoresed using MES buffer.

Proteins were resolved in the gel at 200V constant with 262mA until 1/3rd run then changed to 162mA for the remaining run.

5.10.4.2.2. NuPAGE for Soluble Proteins

For soluble proteins, 4x SDS Sample buffer was added to the 25 µl of soluble protein. Boiling, gel loading and resolving steps were performed as described for NuPAGE for Insoluble proteins in 5.10.4.2.1.

5.10.4.2.3. NuPAGE for Total Proteins

For the total protein, 12.5 µg of protein was suspended in 15 µl using NP40 lysis buffer–y1 then added the equal amount of 1x SDS Sample buffer. Further steps were performed as described for NuPAGE for Insoluble proteins in 5.10.4.2.1.

5.10.5. Capillary Transfer

Capillary transfer was performed to transfer the proteins from an SDD agarose gel to a 0.2µm Whatman ProTran® nitrocellulose membrane. To perform the capillary transfer, 10 pieces of chromatographic paper (17 x 10 cm) from Roth were placed on top of the flat tray. 15 pieces of gel blotting paper (17 x 10 cm) were then placed on top of the chromatographic papers and a nitrocellulose membrane of the same size was placed on top of the blotting paper. The SDD-agarose gel was washed with ddH_2O and placed on top of the nitrocellulose membrane, removing any air bubbles that might have formed between them. Two blotting papers of 30 x 10 cm were equilibrated in 1X TBS buffer and placed on top of the agarose gel, with the ends immersed in a 1X TBS buffer tank, acting as a wick for the transfer. 15 Blotting and 10 chromatographic papers of 17 x 10 cm were placed on top of the wet blotting paper bridge. A ½ kg weight block was placed on top to make sure membranes were in contact without any air gaps. This setup was left at room temperature overnight. The following day, the nitrocellulose membrane was washed with 1X TBS and used for the detection of the tagged proteins with a α-GFP antibody by western blotting.

5.10.6. Quantification Methods

5.10.6.1. Commasie G250 Staining of the NuPAGE Gel

After electrophoresis, NuPAGE gradient gel (4-12%) was placed in a microwave resistant plastic box and the gel was washed three times with ddH_2O. After washing, the gel was placed with ddH_2O until properly rinsed and followed microwave at the high level for 30-60sec without boiling for three times. Commasie G-250 solution was then added to the membrane and microwaved for 30sec at the high level. The staining container was placed on an orbital shaker for gentle shaking at room temperature for 20min. After gentle shaking, the gel was washed three times as described before and rinsed the gel in ddH_2O for 60min to remove the background and pictures were taken using Bio-rad ChemiDoc™ using manufacture's instructions.

5.10.6.2. Silver Staining of the NuPAGE gel

Silver staining was performed to the NuPAGE gradient gel (4-12%) using Page Silver™ Silver Staining kit (Product no: #K0681) of Fermantas. For silver staining, we followed the manufacture's maximum sensitivity staining protocol. This protocol was slightly modulated at the developing step and the developing time was fixed to 2-3 min.

5.10.6.3. Western Blotting

Western blotting was performed to transfer proteins from poly acrylamide gel to nitrocellulose membrane (Burnette, 1981). The protein gel was transferred to a 0.2 μM nitrocellulose membrane of Transblot® turbo™ transfer pack at a constant electrical power of 25 V and 2.5 A for 7 min using the Bio-rad trans-blot turbo transfer system. The nitrocellulose membrane was washed with ddH_2O and stained with 0.2% Ponceau by agitating the membrane for 1 min at room temperature to confirm the protein transfer. The membrane was then washed with TBS-T buffer for 5 min and blocked for 60 min with blocking solution (5% non-fat dried milk powder in TBS-T). After blocking, the membrane was washed for 60 sec using TBS-T buffer

and incubated with mouse α-GFP (1:5,000 in blocking solution), overnight at 4°C. The membrane was then washed with TBS-T buffer for 15 min by changing the buffer every 5 min. The membrane was then incubated with HRP-conjugated α-mouse antibody (1:10,000 in blocking solution) for 60 min at room temperature. Incubation was followed by three washes of the membrane for 15 min in TBS-T buffer. Incubating 3 min with 2 ml of ECL reagents mixture then developed the membrane. The chemiluminescence signal was observed using the Bio-rad Chemidoc™. Pictures were taken at 5 sec intervals until the signal showed saturation.

5.10.6.4. Quantification of Protein Bands from Gel Pictures and Nitrocellulose Membrane

Protein bands were quantified using Image Lab Version 5.1 build 8. To quantify the proteins, on the gels and blots, pictures were taken using a Bio-rad ChemiDoc™ and uploaded to Image Lab. Protein bands were selected using the lane-band tool and quantified using the quantity tool, accordingly to the manufacturer´s instructions. Calculations were performed using Microsoft® Excel® for Mac 2011.

5.10.7. Proteomics

These protocols were performed by Dr. Maria Robles.

5.10.7.1 Sample Preparation for LC-MS

Insoluble pellets were processed for mass spectrometry analysis as in Hops et al. *in preparation*. Briefly, pellets from the ultracentrifugation were resuspended in 100 ul of 2% sodium dodecyl sulfate (SDS) and incubated at 95 °C for 10 min prior to centrifugation for 10 min at 16,000 g. Supernatants were discarded and pellets were washed twice in 2% SDS by shaking at 1,000 rpm for 5 min, prior to centrifugation at 16,000 g for 10 min. The pellets were again washed twice in PBS for 5 min with shaking at 1,000 rpm, centrifuged at 16,000 g for 10 min and the supernatant was discarded. Then, pellets were re-solubilized with 100 µl of 90% formic acid and incubated at 37 °C for 45 min under shaking at 1,000 rpm prior to snap-freezing of

samples in liquid nitrogen and then evaporating them in a speed-vac with a cold-trap overnight (RVC 2-25 Martin Chirst GmbH). The next day, 50 µl of denaturation buffer (6M urea/2M thiourea/10mM dithiothreitol (DTT)) was added to the samples and sonicated for 15 min in a water bath before adding 5 µl of 0.55M Iodoacetamide (IAA) and incubating in the dark at R/T for 10 min with shaking at 1,000 rpm. After that 1:100 (enzyme:protein) LysC was added and samples were incubated at R/T for at least 3 hours with shaking at 1,000 rpm. Samples were then diluted with 150 µl of ammonium bicarbonate prior to the addition of 1:100 (enzyme:protein) trypsin. Digestion was performed by incubating at R/T overnight with shaking at 1,000 rpm. The next day digestion was stopped by adding 10 µl of 10% TFA. Peptides were purified in styrenedivinylbenzene–reversed phase sulfonated (SDB-RPS; 3M Empore) StageTips.

5.10.7.2. LC-MS/MS Analysis and Data Processing

Prior to MS, peptide mixtures were separated on a 50 cm reversed phase column (diameter of 75 mm packed in-house-with ReproSil-Pur C18-AQ3-9 mm 1.9 µm resin (Dr. Maisch GmbH) over a 60 min gradient of 5% - 50% buffer B (0.1% formic 10 acid and 80% ACN) using the Proxeon EASY-nLC system with a flow rate of 300 nl/min. The nLC system was coupled to a Q Exactive HF mass spectrometer (Thermo Fisher Scientific), acquiring full scans (300–1,650 *m*/*z*, *R* = 60,000 at 200 *m*/*z*) at a target of 3^{e6} ions. The ten most intense ions were isolated to a target of 1^{e5} with maximum injection time 120 ms and fragmented with higher-energy collisional dissociation (HCD) (isolation window 1,4 m/z, normalized collision energy 27), underfill ratio 10%) and detected in the Orbitrap (R=15,000). Raw mass spectrometry files were processed within the MaxQuant environment (version 1.5.2.17) using the integrated Andromeda search engine with a false-discovery rate (FDR) is 0.1 at the protein, peptide and modification level. The search included variable modifications for oxidized methionine (M), acetylation (protein N-term) and phospho (STY) and fixed modifications for carbamidomethyl (C). Peptides with at least six amino acids were considered for identification, and “match between runs” was enabled with a matching time window of 0.7 min to transfer MS1 identifications between runs. Peptides and proteins were identified using a UniProt FASTA database from *C. elegans* (from 2012).

5.11.1. Fluorescence Signal Analysis

Fluorescence from microscopy was measured using the ImageJ open source program. To analyze aggregation, the pictures taken from the fluorescence microscope (from section 5.9.3.1) were converted into the 8-bit grey scale and the threshold was fixed to remove background signals. Afterwards, watershed image processing was performed for a pixel-based segmentation of nearby aggregates. In each worm, number and size of fluorescent aggregates were calculated using the particle analysis tool.

5.11.2. Data Analysis for Larval Development

To study developmental timing in Q0 and Q35 transgenic *C. elegans*, data was analyzed based on a published algorithm (Olmedo et al., 2015). The raw data acquired from the luminometer was analyzed using R software. To measure the duration of the molts and larval stages, raw data was trend-corrected by dividing with centered moving average. 75% of the moving average value was used as a threshold for generating a binary file to evaluate the molting time of the worm. The onset and offset of the molt was detected by the transition of values from 1 to 0 and 0 to 1 respectively. Stabilizing the transition of values in the binary file for an hour-prevented noise from the luminescence signal of the worm; molts and larval stages were then calculated and plotted using GraphPad PRISM v6.0c. The Student's *t*-test was used for statistical analysis.

6. Results

6.1 Analysis of Protein Aggregation in *C. elegans* Neurodegeneration Models at Different Zeitgeber Conditions

6.1.1. Optimization of Methods for the Analysis of Protein Aggregation in *C. elegans* Neurodegeneration Models

6.1.1.1. Analysis of Q35::YFP and α-synuclein::YFP in Blue Native Poly Acrylamide Gel Electrophoresis (BN-PAGE)

To study the impact of zeitgeber conditions on the aggregation of Q35::YFP and α-synuclein::YFP in *C. elegans*, the aggregation was quantified by biochemical methods and fluorescence microscopy.

In the process of establishing a robust biochemical method for the quantification of soluble and insoluble Q35::YFP and α-synuclein::YFP, protein lysates were resolved in blue native polyacrylamide gels (BN-PAGE) (Fiala et al., 2011; Nucifora et al., 2012) followed by fluorescence imaging. Interestingly, five different protein bands were observed from Day 2 to 6 in all Q35::YFP protein samples acquired from different zeitgeber conditions (Fig. 6-1a). We suspected that band-1 corresponded to high molecular weight insoluble aggregates of Q35::YFP, which remained unresolved on the gel. The signal of band-1 was not visualized at Day 0 samples and had very low signal at Day 2 samples.

As a control, we resolved crude proteins of α-synuclein::YFP in blue native gels followed by fluorescence imaging. A strong fluorescent band (Band-1) was observed in Day 2 and Day 4 samples compared to Day 0 and Day 6 samples in all conditions. Low intensity bands were also observed on the gel (Fig. 6-1b). However, identification of these protein bands from blue native gels of Q35::YFP and α-synuclein::YFP was not possible due to a lack of suitable protein markers. The

results suggest that the quantification of insoluble and soluble Q35::YFP and α-synuclein::YFP proteins may not be possible by BN-PAGE. However, the observation of Q35::YFP insoluble aggregates in the wells suggested another approach to analyze aggregation by using gels with larger pore size.

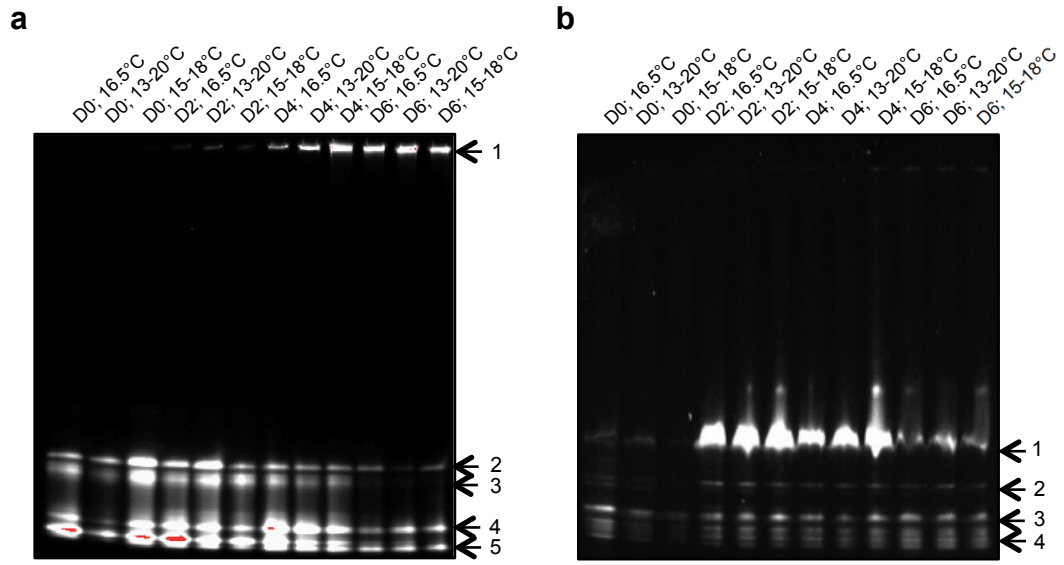

Fig. 6-1: Blue native polyacrylamide gel of Q35::YFP and α-synuclein::YFP. Samples were collected over time (Day 0-6) from worms held in constant temperature (16.5°C), lower amplitude temperature cycle (12 h at 15 °C and 12 h at 18 °C) and higher amplitude temperature cycle (12 h at 13 °C and 12 h at 20 °C). Bands are represented with numbers. a) Blue native gel of Q35::YFP protein samples. b) Blue native gel of α-synuclein::YFP samples.

6.1.1.2. Analysis of Q35::YFP by Native Agarose Gel Electrophoresis (NAGE)

Based on the observations from BN-PAGE, we hypothesized that high molecular weight native protein aggregates of Q35::YFP may enter into those agarose gels that have a larger pore size. Native agarose gel electrophoresis (NAGE) (Kim, 2011; van Ham et al., 2010) was used to resolve the crude proteins of Q35 worms under different zeitgeber conditions. Some protein species of Q35::YFP migrated into the gel and were visualized as a single fluorescent band (Band-2 of Fig. 6-2). Despite the larger pore size, fluorescent species were still found in the wells; these were suspected to be Q35::YFP aggregates (Band-1 of Fig. 6-2). The intensity of the fluorescent band on the gel was strong at Day 2 and Day 4 in all zeitgeber conditions, compared to Day 0 and Day 6, suggesting that these low molecular weight forms appear in adult worms

and then disappear again, possibly due to their aggregation. However, Q35 protein species in the wells and on the gel were difficult to quantify and identify due to the lack of loading controls and protein markers. Additionally, we identified that proteins resolve poorly in NAGE compared to Blue native PAGE. We conclude that Native Agarose Gel Electrophoresis (NAGE) may not be sufficient for the separation of totally insoluble species from soluble species of Q35::YFP.

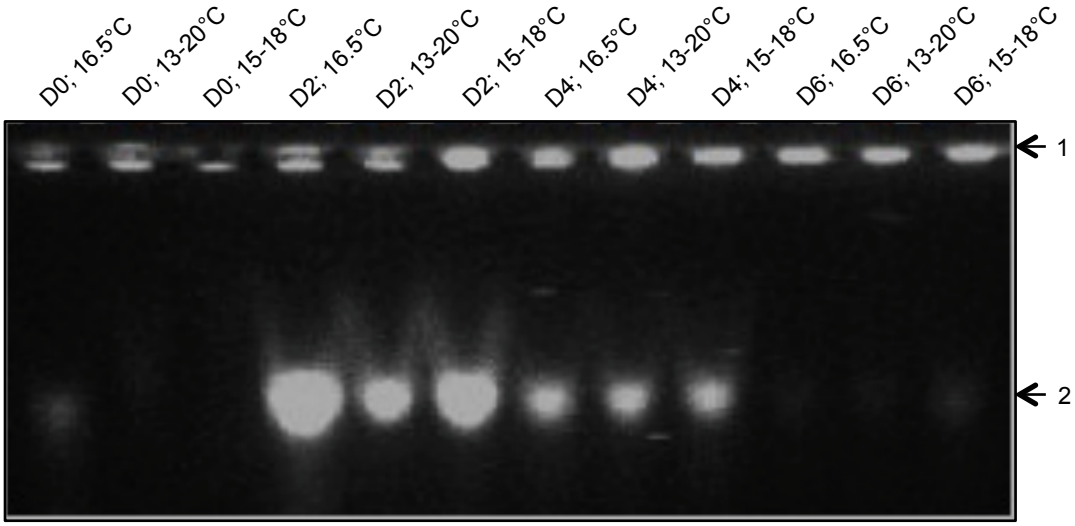

Fig. 6-2: Native agarose gel for analysis of Q35::YFP. Protein samples of Q35::YFP worms with age Day 0-6 in different zeitgeber conditions. Constant temperature is 16.5 °C; lower amplitude temperature cycle (12 h at 15°C and 12 h at 18°C) and higher amplitude temperature cycle (12 h at 13 °C and 12 h at 20 °C). Protein bands are indicated by numbers (1 and 2).

6.1.1.3. Analysis of Q35::YFP by Semi Denaturing Detergent Agarose Gel Electrophoresis (SDD-AGE)

Our previous experiments suggested that native aggregates cannot be resolved by BN-PAGE and NAGE. Further, we approached semi-denaturing methods (SDD-AGE) for protein lysates in order to visualize high molecular weight polymers and monomers (Kryndushkin et al., 2003; Shemesh et al., 2013). We resolved crude protein samples extracted over time from different zeitgeber conditions into SDD agarose gels with and without boiling. As per the literature, boiling treatment dissolves the polymers to Q35::YFP monomers. In our results, we observed two different bands from each protein sample, both with and without boiling treatment.

Band-1 from all protein samples were suspected to be high molecular weight polymers (intermediate aggregates) and band-2 as monomers (Fig. 6-3). The visualized signals of band-1 (high molecular weight polymer) at Day 2 and Day 4 from the higher amplitude temperature cycle were weaker than those from the constant conditions and lower amplitude temperature cycles. This suggests that the formation of high molecular weight polymers may be slower in higher amplitude temperature cycles compared to other conditions. However, because identification of Q35::YFP protein species is difficult without a suitable protein marker and because the quantification of proteins bands is a challenging process given a lack of loading controls, we conclude cautiously that SDD-AGE is not a robust method for precise quantification of protein aggregation.

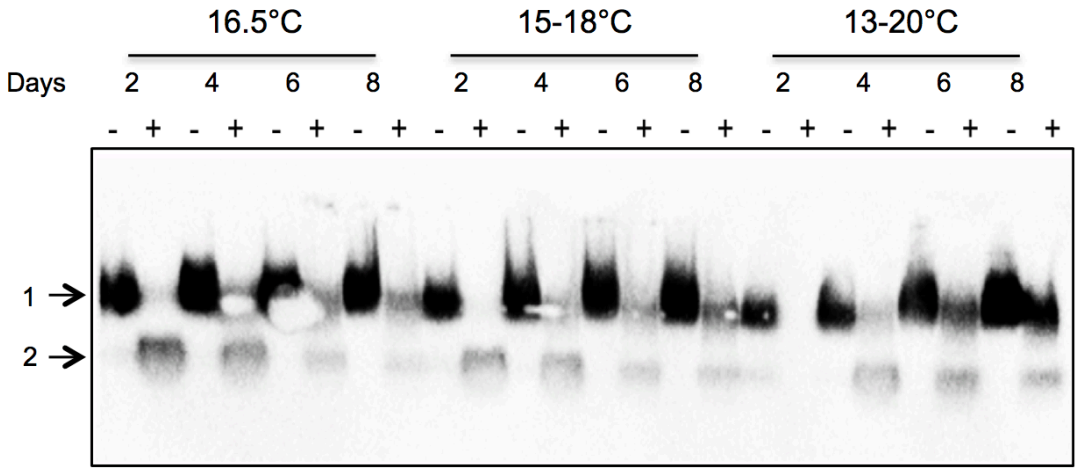

Fig. 6-3: Semi denaturing detergent agarose gel for analysis of Q35::YFP. Days represents age with respective zeitgeber conditions; Constant temperature (16.5 °C), lower amplitude temperature cycle (15 °C for 12 h and 18 °C for 12 h), higher amplitude temperature cycles (13 °C for 12 h and 20 °C for 12 h); - and + symbols represent absence or presence of heat treatment (at 95 °C). Numbers represent protein bands. Band-1 and Band-2 are YFP signals from heat-treated and non-heat treated samples, respectively.

6.1.1.4. Analysis of Q35::YFP and α-synuclein::YFP in Protein Lysates using SDS-PAGE and Western Blot

We further analyzed Q35::YFP and α-synuclein::YFP protein lysates using standard SDS-PAGE (Laemmli, 1970). We resolved denatured protein extracts that had been denatured using Laemmli buffer in a Bio-rad 4-15% Criterion™ TGX Stain-Free™ gradient gel. Western blotting (Burnette, 1981) was used for detection of YFP. A time

course experiment in different zeitgeber conditions for Q35::YFP and α-synuclein::YFP proteins is shown in figure 6-4. The Q35 western blot suggests that the YFP signal decreases with age in all zeitgeber conditions. We observed, however, that the amount of Q35::YFP is higher at all time points in a higher amplitude temperature cycle compared a lower one and also in comparison with constant conditions. Some high molecular-weight Q35::YFP species were observed in the wells, possibly corresponding to insoluble aggregates (Figs. 6-4 a, e).

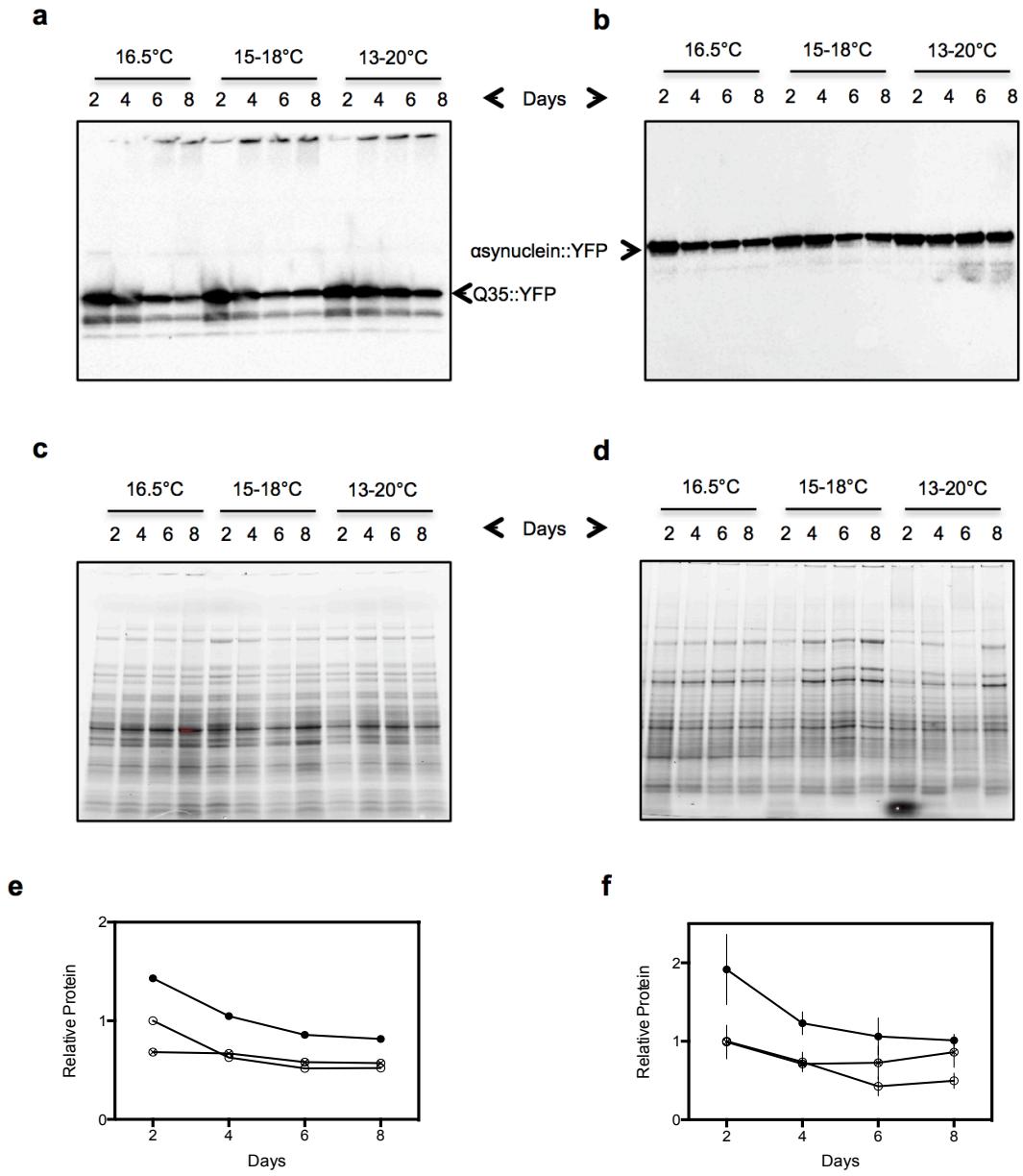

Fig. 6-4: Analysis of Q35::YFP and α-synuclein::YFP in crude protein extract by western blot. Constant temperature (16.5 °C; Open circles), lower amplitude temperature cycle (15 °C for 12 h and 18 °C for 12 h; Crossed circles) and higher amplitude temperature cycle (13 °C

for 12 h and 20 °C for 12 h; Closed circles). Protein samples were collected over time from the three-zeitgeber conditions. a) Immunoblotting of Q35::YFP; b) Immunoblotting of α-synuclein: YFP; c) Stain free gel of total proteins from Q35::YFP worms; d) Stain free gel of protein samples from α-synuclein::YFP worms; e) Quantitative analysis of Q35::YFP. The amount of protein decreases with age in all zeitgeber conditions of ± SEM of three experiments; f) Quantitative analysis of α-synuclein::YFP from three independent experiments. The amount of protein decreases with age in all zeitgeber conditions of ± SEM of three experiments.

After quantitation of α-synuclein::YFP signal from three independent experiments, we observed similar trends as for Q35::YFP, with higher amplitude temperature cycles having more α-synuclein::YFP at Day 2 and Day 4 compared to lower amplitude temperature cycles and constant conditions (Figs. 6-4 b, e). However, from this data it was difficult to predict the effect of higher amplitude temperature cycles on aggregation of Q35::YFP and α-synuclein::YFP.

We suspect that the specific bands observed in SDS-PAGE may be a mixture of SDS-soluble components (coming from native SDS-soluble polymers and intermediate aggregates), which are involved in the formation of high molecular weight compact insoluble aggregates. In this experiment, we observed more SDS-soluble forms in higher amplitude temperature cycles. We hypothesize that higher amplitude temperature cycles have less aggregation compared to other conditions. However, this method was unable to provide enough information on insoluble and soluble proteins.

6.1.1.5. Summarized Results of BN-PAGE, NAGE, SDD-AGE and SDS-PAGE for Quantifying Q35::YFP and α-synuclein::YFP aggregation

The biochemical methods tested to quantify insoluble and soluble proteins from native or denatured crude protein samples did not provide sufficient information on insoluble and soluble protein species from Q35::YFP and α-synuclein::YFP. BN-PAGE is a good method to separate different protein species in a high-resolution manner, but it does not identify those species because it lacks a suitable protein marker because proteins do not run true to their molecular weight in native gels. Based on the published papers from van Ham et al., 2010 and Shemesh et al., 2013, we experimented with NAGE and SDD-AGE methods. Even though we found that some protein species do enter these gels, the protein nevertheless cannot be reliably characterised due to the lack of loading controls and suitable protein markers.

Furthermore, characteristic pattern of protein bands were not observed using these methods. We further performed SDS-PAGE (Laemmli, 1970), a protocol calling for rigorous denaturation of protein extracts. Treatment of extracts for SDS-PAGE dissolves the SDS soluble forms that include native monomers, polymers and intermediate aggregates, leading to a Q35::YFP band of a precise molecular weight. The SDS-resistant aggregates do not enter on the gel due to their high molecular weight. Although these results were inconclusive due to the limited tools available, they help to show the trend of SDS-resistant aggregation. We eventually seperated native soluble protein species from insoluble proteins by ultracentrifugation followed by an SDS-treatment of insoluble species for the quantification of SDS-solubilized insoluble forms (see below, section 6.1.2.2).

6.1.2. Analysis of Q35::YFP Protein Aggregation using Optimized Methods

6.1.2.1. Analysis of Q35::YFP using Fluorescence Microscopy

The results of SDD-AGE and SDS-PAGE suggest that higher amplitude temperature cycles enable interesting conditions that may influence aggregate formation, which is a key aspect of our working hypothesis. We analyzed Q35::YFP aggregation in worms held at constant temperature (16.5 °C) and at temperature cycle (13 °C for 12 h and 20 °C for 12 h) using fluorescence microscopy.

Fluorescent signals from Q35::YFP aggregates were captured by fluorescence microscopy and then quantified using imageJ (Fig. 6-5c). PolyQ proteins were soluble/non-aggregated in the muscle cells of Q35 worms until they reached adulthood. The aggregation started in adults and increased with age. We did not identify fluorescent aggregates using microscopy at Day 0 (L4) adults in any of the zeitgeber conditions. The onset of aggregation was observed in Day 2 adults; thereafter, aggregation increased with age in both constant and cyclic conditions. Interestingly, at Day 2 and Day 4 the number of aggregates was significantly lower in cyclic conditions than in constant conditions. In older worms, at Day 6 and 8 of adulthood, the number of aggregates was not significantly different between the two

zeitgeber conditions. However, the experimental replicates at Day 8 showed a trend that worms have a lower number of aggregates in cyclic compared to constant conditions (Figs. 6-5 a, d). The control Q0::YFP, did not form aggregates with aging, at least until Day 8, and in either constant or cyclic conditions (Fig. 6-5b). Thus, fluorescence microscopy of Q35::YFP worms in zeitgeber conditions suggests that temperature cycles impact the formation of aggregates.

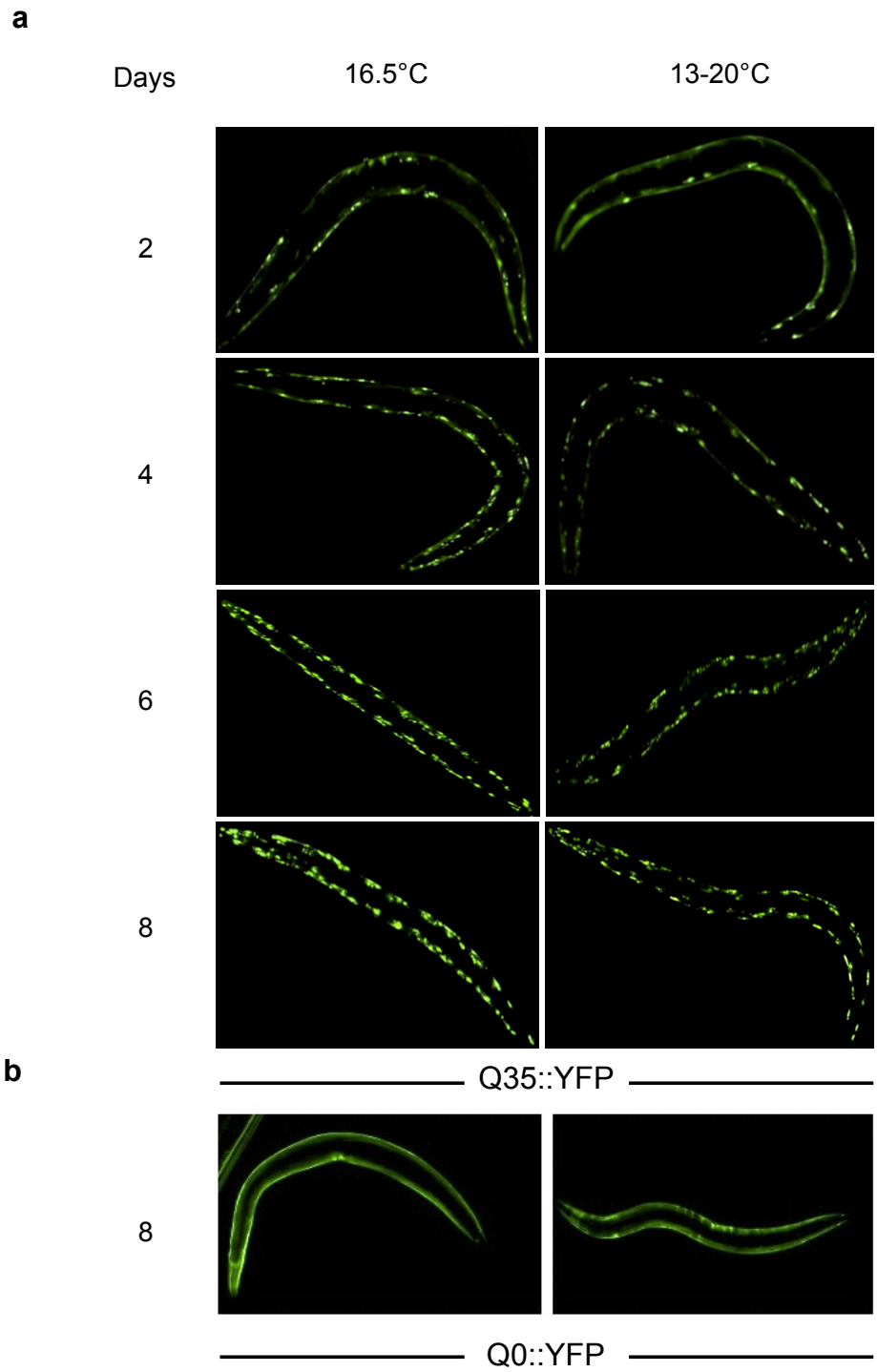

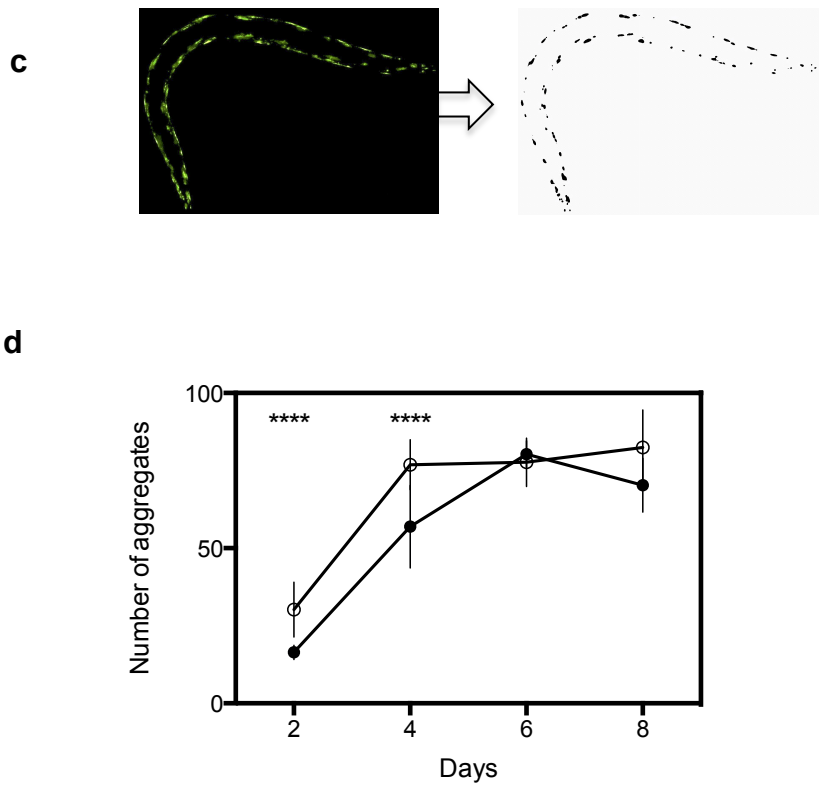

Fig. 6-5: Microscopic analysis of number of aggregates in Q35::YFP and Q0::YFP worms in zeitgeber conditions with age (Day 2-8 adults). a) The right and left panels show the visualization of fluorescent aggregates in Q35::YFP worms at constant (16.5 °C) and cyclic conditions (13 °C for 12 h and 20 °C for 12 h) respectively; b) Day 8 adults of Q0::YFP worms in constant and cyclic conditions show no aggregates; c) Left panel is an example of the fluorescence aggregates of Q35::YFP worms. Right panel represents the aggregates from the same worm using imageJ; d) Quantification of the number of aggregates by age in constant and cyclic conditions of Q35::YFP worms. Open and closed circles represent constant and cyclic conditions, respectively. Each data point represents the ± SEM of three independent experiments. Aggregates were analyzed from ≥ 10 worms from each experiment. The number of Q35 aggregates from cyclic temperatures is significantly lower compared to constant temperature at Day 2 and 4 adults when comparing three independent experiments *(Mann-Whitney U-Test, ****p< 0.001).*

6.1.2.2. Analysis of Q35::YFP using Ultracentrifugation, NuPAGE and Western Blot

The results of BN-PAGE, NAGE, SDD-AGE and SDS-PAGE with crude proteins did not enable identification and quantification of the insoluble and soluble Q35::YFP protein species. We used ultracentrifugation to separate soluble and insoluble species (pelleted proetins) and subjected the samples to NuPAGE 4-12% Bis-Tris gel in MES running buffer (Penna and Cahalan, 2007) and western blot (Burnette, 1981) analysis. Q35::YFP was detected using an α-GFP antibody. The amount of soluble and SDS-

soluble Q35::YFP aggregates were quantified by age in constant and cyclic conditions. The western blot suggests that SDS soluble aggregates from the protein pellet were resolved on the gel with some polyQ species. SDS-reisistant polyQ aggregates were still found in the wells (Fig. 6-6a). The YFP Signal from the blot was normalized to total protein (Fig. 6-6e). We found that the amount of soluble Q35::YFP decreased with age by increasing insoluble Q35::YFP (Fig. 6-6a-d). Furthermore, we observed that the age-dependent increase of SDS soluble Q35::YFP proteins from the insoluble proteins is quantitatively different in extracts from animals held in constant conditions versus temperature cycles. We observed that the amount of insoluble Q35::YFP is lower at Day 6 and Day 8 of the samples acquired from temperature cycles compared to the constant conditions.

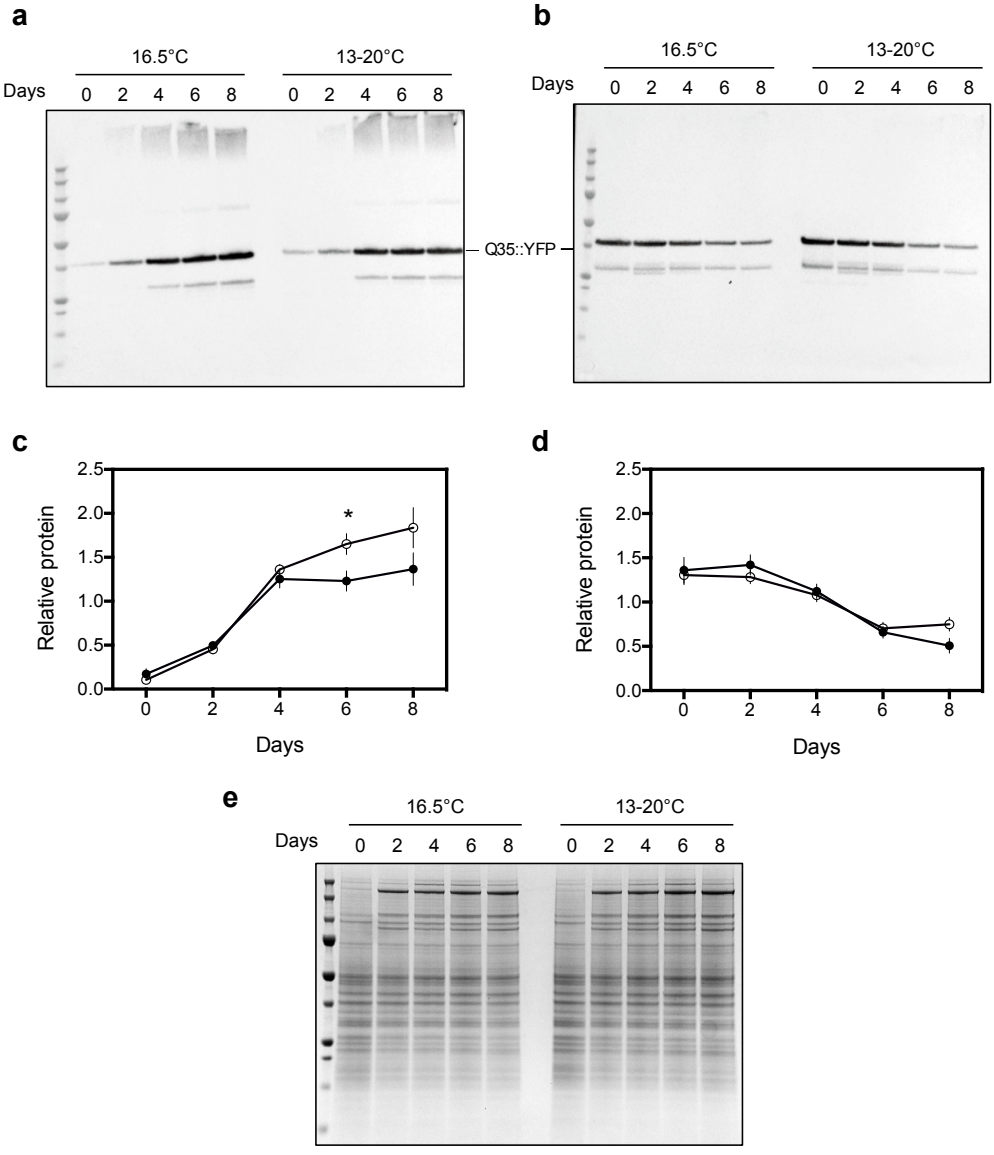

Fig. 6-6: Quantification of insoluble and soluble Q35::YFP by age (Day 0-8) from constant (16.5 °C) and cyclic temperatures (13 °C for 12 h and 20 °C for 12 h) of three independent experiments. a) Representative western blot of solubilized Q35::YFP from pelleted proteins. Age at harvest is indicated for the samples from worms held in constant (left) or 24 h temperature cycles (right). b) Western blot of soluble Q35::YFP from animals held in constant (left) and 24h temperature cycles (right). c) Quantitation of Q35::YFP from pelleted proteins from animals cultivated in constant (open circles) and temperature cycles (closed circles) The amount of pelleted YFP was significantly different between the cultivation conditions on day 6 *(Mann-Whitney U-Test, $p< 0.05$)*. d) Quantitation of soluble Q35::YFP from supernatants. Constant conditions are graphed as open circles and temperature cycles as closed circles. Soluble YFP decreases with age in both constant and cyclic temperatures. e) An example of the gels used for quantitation of total protein: coomassie stained NuPAGE gradient gel (4-12%). Data for panel b and d are from three independent experiments.

Particularly at Day 6, we observed that insoluble Q35::YFP is significantly lower in the three independent experiments (Fig. 6-6b). Following the observation of the significant difference at Day 6, we became interested in understanding the composition of proteins in Q35 aggregate formation in animals held in either at constant conditions or 24h temperature cycles.

This is a highly robust method for the quantification of both insoluble and soluble Q35::YFP from protein lysates. The results support the hypothesis that age-dependent aggregate formation is delayed in temperature cycles compared to constant conditions. The results obtained with this method show the same trend as those obtained from the analysis of the number of aggregates by fluorescence microscopy.

6.1.2.3. Analysis of Cellular Proteins in Q35::YFP Aggregates by NuPAGE and Silver Staining

Based on the observations from Figure 4-6, I hypothesized that the protein composition of Q35::YFP aggregates would also show differences. We collected samples from Day 6 and 8 from the worms held in constant conditions and temperature cycles. After ultracentrifugation, retention of the pellets (the soluble fraction was not used here) and SDS treatment of the pellets, the solubilized proteins were resolved on a gradient gel and visualized with silver staining. We compared lanes of these gels to understand the gross differences in the pelleted proteins. In general, protein bands were observed as very compact and closely spaced on the gel. There was a strong band closed to 37 kDa, which may correspond to be Q35::YFP. Furthermore, we used the silver stained gels to estimate the collection of proteins

involved in Q35 aggregation, but no significant differences were observed in the amount of insoluble protein between zeitgeber conditions at Day 6 and Day 8 (Fig. 6-7 a, b). We also report here that the quantity of the band that runs at the same molecular weight as Q35::YFP is low in cycling conditions compared to constant conditions at Day 6 and Day 8 (Figs. 6-7 a, c). Our silver staining results suggest that highly sensitive protein analysis tools such as proteomics may be required in order to identify the quantitative changes of cellular proteins involved in polyQ aggregation.

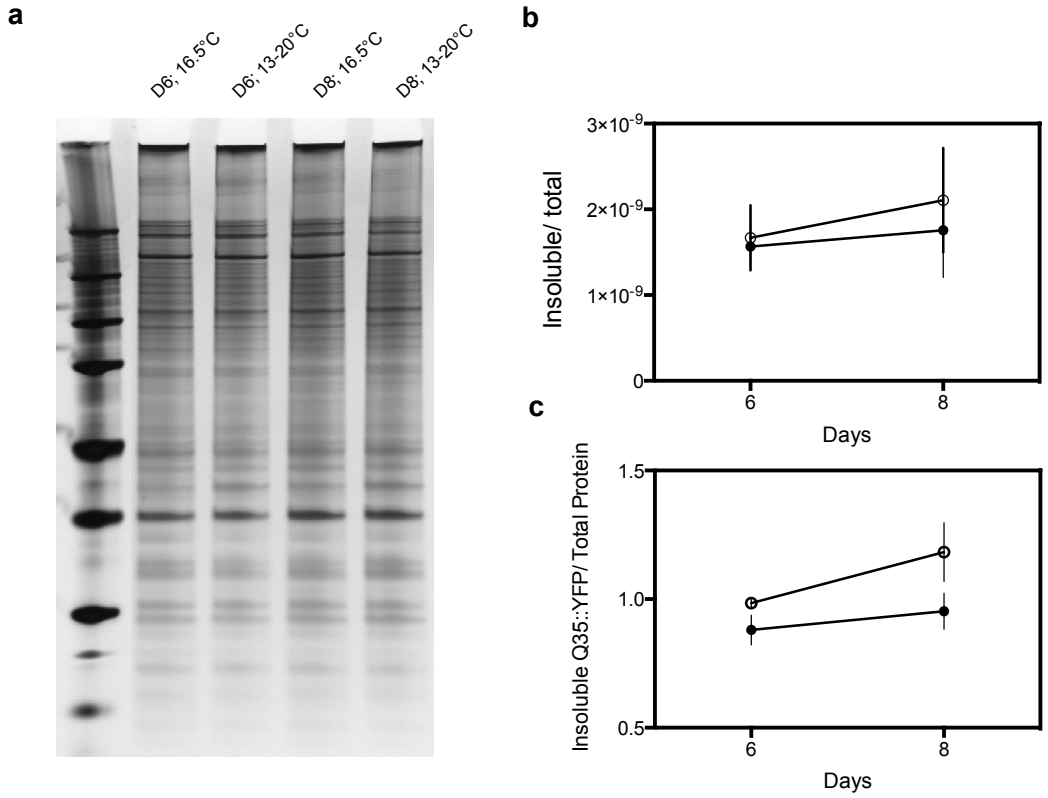

Fig. 6-7: Silver staining for analysis of cellular proteins in Q35 aggregates with age in Zeitgeber conditions of three independent experiments. Open circles represent constant condition (16.5 °C). Closed circles represent cyclic condition (13 °C for 12 h and 20 °C for 12 h). a) Silver stained NuPAGE gel of insoluble proteins samples were collected from Day 6 and Day 8; b) Quantitative analysis of insoluble proteins from constant and cyclic conditions. No significant differences in the amount of insoluble proteins between the zeitgeber conditions; c) Quantitative analysis of the bands running at the same molecular weight consistent with Q35::YFP is less dense in cyclic compared to constant conditions.

6.1.2.4. Analysis of Cellular Proteins in Q35::YFP aggregates using LC-MS

To better understand the impact of temperature cycles on Q35::YFP aggregation, we further analyzed the proteins involved with polyQ aggregation using LC-MS (Peng et

al., 2003). We focused on Day 6 samples and compared the proteins present in samples from constant conditions with those from temperature cycles. We found around 60 proteins are significantly more abundant in cyclic conditions compared to constant conditions. Interestingly, RME-8, RAN-1, CCT-6 and RPL-1 are more abundant in cyclic conditions. RNAi screens by Ellen Nollen suggest that these candidate proteins are suppressors of polyQ aggregation (Nollen et al., 2004).

In addition to aggregation suppressors, we identified proteins involved in proteostasis mechanisms (CYN-7 and RPL-41). CYN-7, also known as CYP-7, is involved in the protein folding process (Page et al., 1996). We were also able to identify a small number of proteins that were significantly more abundant in constant conditions (16.5 °C). Among this sub-group, the only protein has been reported as a polyQ aggregation suppressor (Nollen et al., 2004), is RPS-26 (Fig. 6-8).

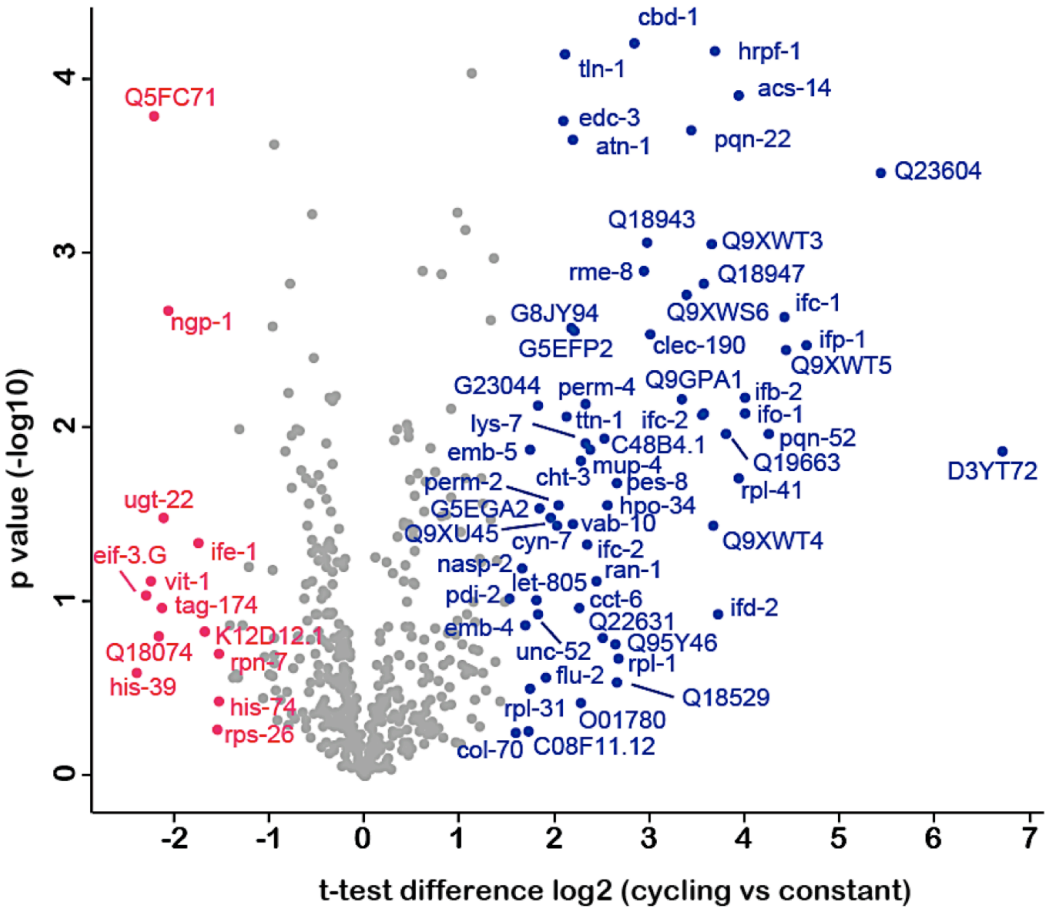

Fig. 6-8 Volcano plot displaying the t-test result of three replicate proteomes (label free intensities) analysis of protein aggregates from Q35::YFP worms held in cycling and constant conditions. X-axis shows fold-change of the intensities between the conditions and the Y-axis the p value of the t-test. Proteins statistically more abundant in one of the conditions are colored, pink in constant and blue in cycling condition.

Therefore, we suggest that expression of proteins that suppress poly-glutamine aggregation and components of the proteostasis network depends on zeitgeber structures. Zeitgebers therefore may play a role in polyQ aggregation (rates and/or amounts) during the lifetime of Q35::YFP transgenic worms.

6.2. Motility Analysis of Q35::YFP, α-synuclein::YFP Worms in Zeitgeber Conditions

Expression of Q35::YFP and α-synuclein::YFP in muscle cells of *C. elegans* has shown motility defects in aging worms (Morley et al., 2002; van Ham et al., 2010). In this study, we measured the number of body bends by age from Day 0 to Day 8 adults of Q35::YFP and α-synuclein::YFP worms held in both constant temperatures and temperature cycles. PolyQ::YFP is soluble in muscle cells until worms reach Day 2 adulthood, then they start to show aggregation by multiple measures. We previously observed slower aggregate formation in worms at temperature cycles (Figs. 6-6, 7), and now we investigated how these temperature cycles affect the motility of Q35 and α-synuclein transgenic worms. Our results from three independent experiments show that the motility decreases with age in both worm strains held in both zeitgeber conditions (Fig. 6-9).

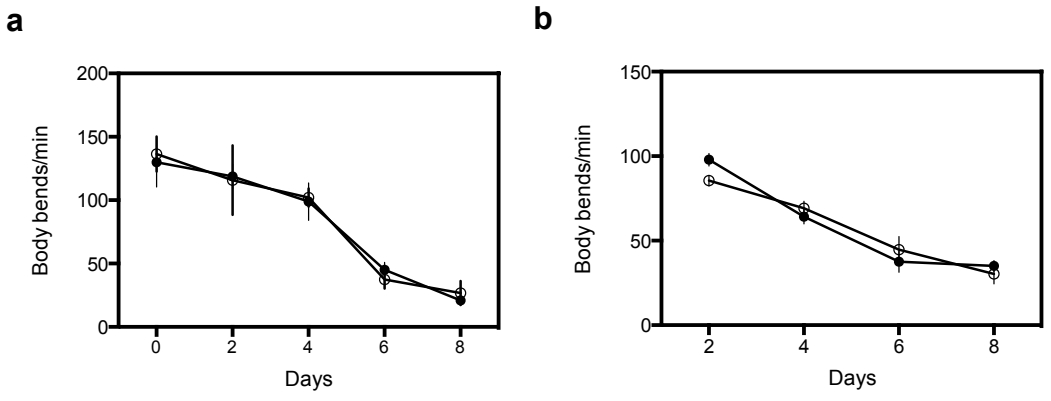

Fig. 6-9: Motility analysis of Q35::YFP worms in contrasting zeitgeber conditions. The number of body bends per minute of a synchronized population of worms from three independent experiments. Body bends were counted for ≥ 10 worms from each experiment. Open circles represent constant temperature (16.5 °C) and Closed circles represent cyclic (13 °C for 12 h and 20 °C for 12 h) conditions. The number of body bends in Q35::YFP worms were significantly decreased with age *(Mann-Whitney U-Test, $p<0.01$)* in both zeitgeber conditions.

The largest decline in the number of body bends was observed at day 6 in Q35 worms, but there was no significant change in motility between zeitgeber conditions in both polyQ and α-synuclein strains. We concluded that the motility assay shows less sensitive than biochemistry or microsopy methods.

6.3. Expression Analysis of *C. elegans* Heat Shock Proteins and *unc-54* in Zeitgeber Conditions

Due to the delayed aggregation of poly-glutamine in temperature cycles, we were interested in the regulation of heat shock proteins (HSPs) in different zeitgeber conditions. There are certain classes of heat shock proteins can prevent the protein aggregation by direct interaction with unfolded substrates, small heat shock proteins are one among them (Haslbeck and Vierling, 2015). In humans, mutations of small heat shock proteins causes cataracts, myopathies and neuropathies (Bakthisaran et al., 2015). Therefore, in the present study, we focused on impact of entraining conditions on small heat shock proteins. As their name implies, heat shock conditions have been used to study regulation of small heat shock protein genes. We employed a temperature range (13 ºC to 20 ºC) normally experienced by the nematodes in their natural habitat and thus do not represent heat- or cold-shock conditions. Schibler's lab showed that binding of HSF-1 to heat shock elements in mammals is rhythmic at physiological temperature cycles (Reinke et al., 2008). Therefore, the regulation of the small heat shock proteins in *C. elegans* was investigated with our entrained conditions. RNA expression of small heat shock proteins *(hsp-16.1, hsp-16.2, hsp-43, hsp-12.6), hsp-4 (Hsp70 homolog)* and *unc-54* in adult animals was determined over a period of 48 hours in either constant conditions (16.5 °C) or in temperature cycles of 12 h at 13 °C and 12 h at 20 °C. Expression levels of these genes are normalized to *act-4* and *ama-1* levels.

6.3.1. Rhythmic mRNA Expression of *hsp-16's* (*hsp-16.1* and *hsp-16.2)* Regulated by Temperature Cycles

We measured the expression of *hsp-16.1* and *hsp-16.2* over 48 hours in order to investigate their regulation in constant conditions and temperature cycles. *hsp-16.1 and hsp-16.2* expression is induced by heat shock (Jones et al., 1989) and suppress the protein aggregation and toxicity (Leroux et al., 1997; Fonte et al., 2008). We measured the levels of RNA in zeitgeber conditions over time and observed an increase in the abundance of *hsp-16s* in the warm phase of the temperature cycle, and that the expression of *hsp-16s* was significantly rhythmic over the period of 24 h for 2 days in a temperature cycle (Figs. 6-10 a, c). In constant conditions, the signal showed no significant changes over the 48 hours of the experiment (Figs. 6-10 b, d). These observations suggest that RNA levels of *hsp-16s* are regulated by temperature cycles in the absence of heat stress.

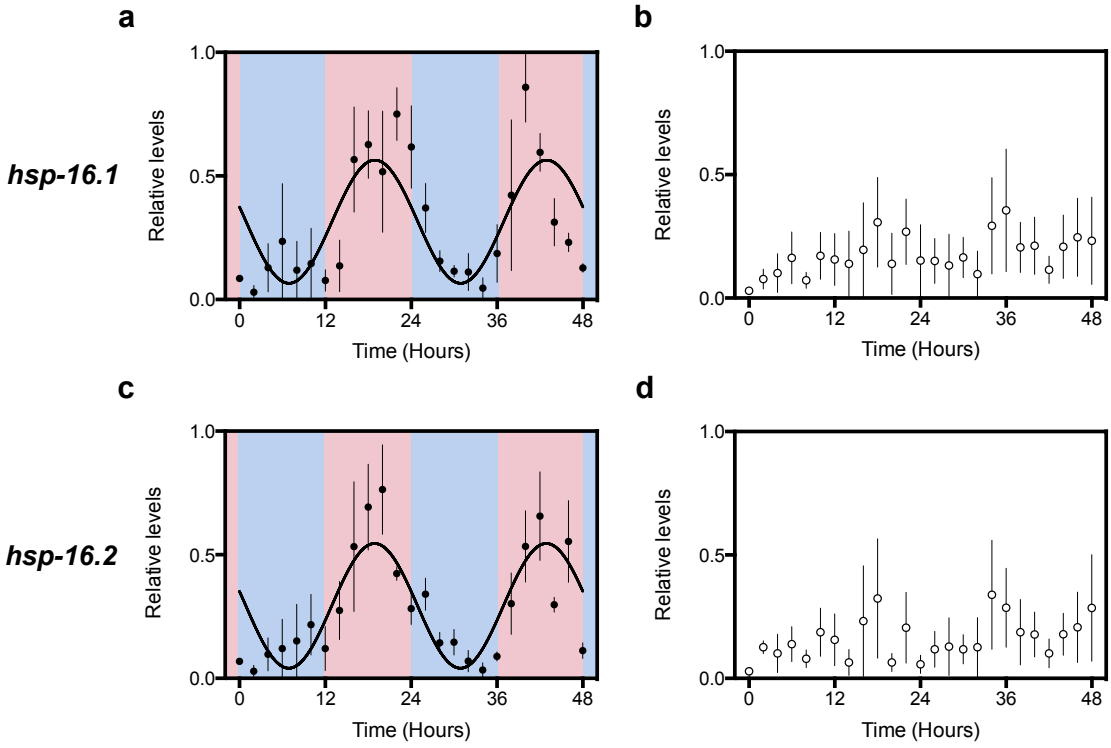

Fig. 6-10: mRNA expression of *hsp-16.1* and *hsp-16.2* over two days in different zeitgeber conditions. Each data point represents the average ± SEM of three independent experiments. RNA levels of *hsp-16.1* and *hsp-16.2* were normalized to *act-4* and *ama-1*. a, c) RNA levels of hsp16 s in temperature cycles. Blue panels represent cold temperature (13 °C) and pink panels represent warm temperature (20 °C). A sinusoidal curve was fitted to the data using

circwave (*p<0.001* for *hsp-16.1* and *hsp-16.2*). mRNA expression is rhythmic in temperature cycles RNA abundance is changed significantly (*ANOVA, p<0.001* for *hsp-16.1*; *p<0.001* for *hsp-16.2*); b, d) mRNA levels of *hsp 16 s* in constant temperature of 16.5 °C. mRNA expression is not rhythmic and data cannot be significantly correlated to a sinusoidal curve using circwave (*p=0.32* for *hsp-16.1*; *p=0.28* for *hsp-16.2*).

6.3.2. Rhythmic mRNA Expression of *hsp-43* Regulated by Temperature Cycles

We also studied the impact of temperature cycles on heat shock proteins that are not regulated by heat shock and are constitutively expressed throughout development (Ding and Candido, 2000c). We chose *hsp-43*, and tested its expression levels in both cyclic and constant temperatures. Interestingly, our preliminary results showed that RNA levels are low in the cold phase compared to the warm phase of the temperature cycle. To test rhythmicity, a sinusoidal curve was fitted to the data of constant and cyclic conditions. We observed a rhythmic expression in temperature cycles (Fig. 6-11a) but not in constant conditions (Fig. 6-11b). Experimental replicates are required to support this observation, but our preliminary results suggest that the expression of *hsp-43*, which is not regulated by heat shock, is regulated by temperature cycles.

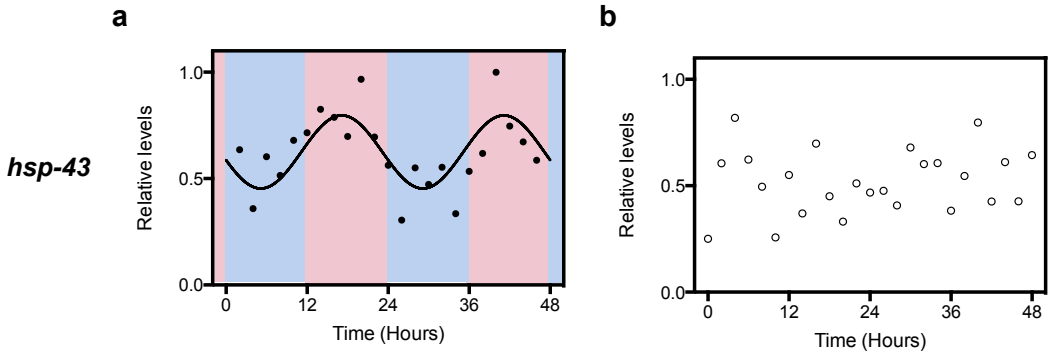

Fig. 4-11: Expression of *hsp-43* mRNA in the different zeitgeber conditions. Open and close circles represents data points constant and temperature cycles respectively. a) RNA expression of *hsp-43* in temperature cycles. The blue and pink panels are representing cold (13 °C for 12 h) and warm (20 °C for 12 h) phases, respectively. RNA levels are high during the warm phase compared to the cold phase. Data was fitted with a sinusoidal curve using circwave *(p<0.001)*; b) Expression of *hsp-43* in constant temperature 16.5 °C. Expression levels are not rhythmic and the data did not fit to a sinusoidal curve *(p=0.77)*.

6.3.3. Rhythmic mRNA Expression of *hsp-4* Regulated by Temperature Cycles

The heat shock protein *hsp-4* acts as an endoplasmic reticulum (ER) chaperone and is regulated by ER stress and heat shock. We measured expression of *hsp-4* in constant and cycling conditions and observed that *hsp-4* mRNA levels increased during the warm phase of the temperature cycle. Using circwave, a sinusoidal curve was fitted to the data of RNA expression in temperature cycles (Fig. 6-12a) but could not be used in constant temperature (Fig. 6-12b). Our preliminary results suggest that expression of *hsp-4* is rhythmic and regulated by temperature cycles. However, induced expression of *hsp-4* was observed only at several time points in the warm phase of temperature cycle. Experimental replicates are necessary to confirm these results and to test the statistical significance.

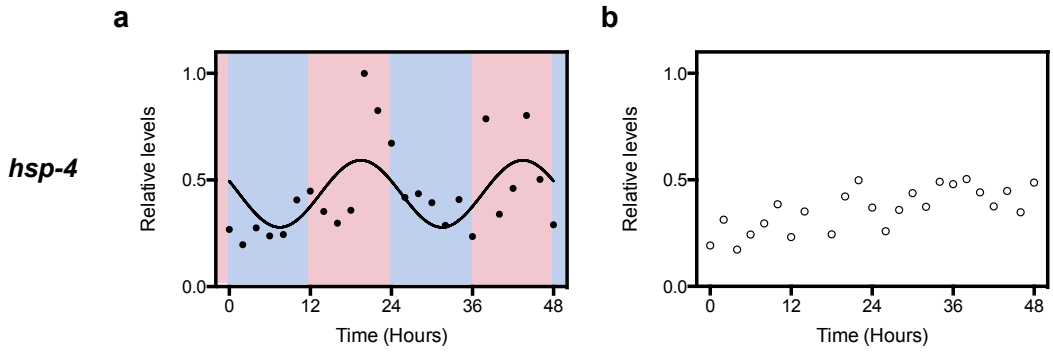

Fig. 6-12: mRNA levels of *hsp-4* in zeitgeber conditions. *hsp-4* RNA expression is normalized to *act-4* and *ama-1*. Open and closed circles are data points of constant and cyclic conditions respectively. a) Expression of *hsp-4* RNA in temperature cycles. Blue and pink panels represent cold (13 °C for 12 h) and warm phase (20 °C for 12 h) respectively. Expression of *hsp-4* RNA is increased at several time points of the warm phase but not in the cold phase. A sinusoidal fit to the data using circwave is significant *(p=0.03)*; b) RNA levels of *hsp-4* in constant temperature (16.5 ºC). Expression levels do not change over time and data could not be fitted with a sinusoidal curve *(p=0.24)*.

6.3.4. mRNA Expression of *hsp-12.6* is not Regulated by Temperature Cycles

We chose *hsp-12.6* in order to investigate the impact of temperature cycles on a heat shock protein that does not respond to heat shock and is not involved in suppression

of protein aggregation (Krause, 2013; Leroux et al., 1997a). We observed an increase in *hsp-12.6* RNA levels in the warm phase of (ZT12-24) compared to the cold phase (ZT2-10) of the first temperature cycle. However, the expression levels did not change in the cold to warm transition phase of 2nd temperature cycle. The expression levels of *hsp-12.6* did not change significantly over time, either in temperature cycles or in constant temperatures (Figs. 6-13 a, b). A sinusoidal fit of the RNA levels in temperature cycles was slightly significant, with a p-value of 0.04. Statistical testing with *ANOVA* failed to show significant changes in expression levels over time. Data from constant conditions could not be fitted to a sinusoidal curve. Our results suggest that zetigeber cycles do not influence on the expression levels of *hsp-12.6*.

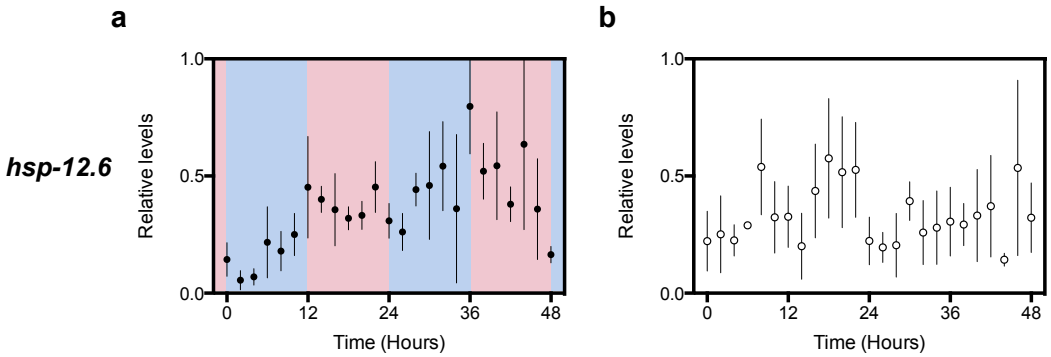

Fig. 6-13: RNA analysis of *hsp-12.6* in zeitgeber conditions. Closed and Open circles represent the average ± SEM of three independent experiments from constant and temperature cycles. RNA levels of hsp-12.6 were normalized to *act-4* and *ama-1*. a) RNA levels of hsp-12.6 in temperature cycles. The blue panel indicates cold temperature (13 °C) and pink panel represent the warm phase (20 °C). RNA expression does not change significantly over time in temperature cycles *(ANOVA, p=0.31)* and the data was fitted by to a sinusoidal curve using circwave with just significant value *(p=0.04)*; b) Expression levels of RNA over time in constant condition of 16.5 °C are not significantly changed *(ANOVA, p=0.93)* and data could not be fitted with sinusoidal curve using circwave *(p=0.57)*.

6.3.5. *unc-54* mRNA Expression is not Regulated by Temperature Cycles

In the transgenic *C. elegans* models of protein aggregation disease from Section 6.1, the expression of the poly Q stretches and of α-synuclein fused to YFP is driven by the promoter of *unc-54* (Morley et al., 2002; van Ham et al., 2010). Because we used these strains to investigate the accumulation of YFP in different zeitgeber conditions, we wanted to confirm that the expression of *unc-54* was not regulated by zeitgeber

cycles. Therefore, we analyzed RNA abundance of *unc-54* in cyclic and constant temperatures. Expression of *unc-54* RNA levels did not change significantly over time, in both constant and cyclic conditions (Figs. 6-14 a, b). To test the rhythmicity, we checked the correlation between a sinusoidal curve and the experimental data using circwave. There was no significant correlation in either of the zeitgeber conditions.

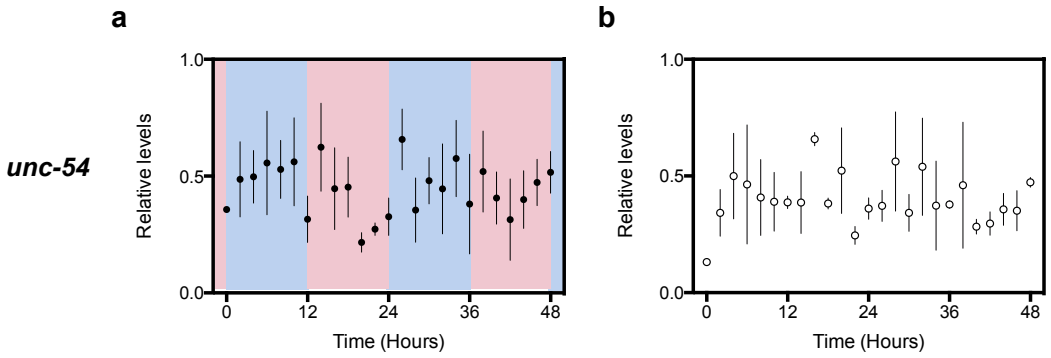

Fig. 6-14: Expression analysis of *unc-54* mRNA in zeitgeber conditions. RNA levels ± SEM of three independent experiments are represented by closed and open circles. RNA levels are normalized to *act-4* and *ama-1* in both conditions. a) RNA levels in temperature cycles with zeitgeber time. Blue and pink panels represent the cold (13 °C for 12 h) and warm phases (20 °C for 12 h) of the temperature cycle for 2 days. Expression levels of *unc-54* RNA are not significantly changed with time *(ANOVA, p=0.91)*. A Sine wave could be fitted with circwave *(p=0.16)*; b) RNA levels of unc-54 in constant temperature with time. mRNA expression of *unc-54* in the worms held at constant temperature (16.5 °C). RNA expression is not changed significantly with zeitgeber time *(ANOVA, p=0.94)* and sinusoidal curve could be fitted using circwave *(p=0.60)*.

Expression levels of *unc-54* are not regulated by temperature cycles, which suggests that the differential expression of YFP in different zeitgeber condition is not a factor, a conclusion based on the fact that *unc-54* did not affect polyQ expression and aggregation in the *C. elegans* Huntington models used in the current study.

6.3.6. Protein levels of HSP16.1::GFP is Rhythmic and Regulated by Temperature Cycles

We analyzed the impact of zeitgeber conditions on RNA levels of *hsp-16 s* in section 6.3.1 and observed that temperature cycles regulate the rhythmic expression of *hsp-16s*. We performed further experiments using a GFP translational reporter of

HSP-16.1 in order to understand the impact of zeitgeber cycles on protein expression of HSP-16.1.

Proteins levels of HSP-16.1::GFP transgenic worms in zeitgeber conditions (5.9.1.2) were measured by western blot and detected with α-GFP antibody. In temperature cycles, the GFP signal of HSP16.1::GFP worms was reduced between ZT6 and 12 of the cold phase and in ZT14 of the warm phase. An increased signal was observed from ZT16 to 24 during the warm phase and between ZT2 and 4 of the cold phase. After normalization to actin, HSP-16.1::GFP expression significantly changes with time in temperature cycles. The expression in temperature cycles is rhythmic and significantly increased, to a maximum of 2 fold during the warm phase compared to the cold phase (Figs. 6-16 a, b). After normalization of the GFP signal with loading control we observed that the expression levels of HSP16.1::GFP are not significantly different over time (Figs 6-16 a, b) in constant condition. Expression analysis of HSP-16.1::GFP in zeitgeber conditions suggests that temperature cycles regulate the expression of HSP-16.1 in the absence of heat stress.

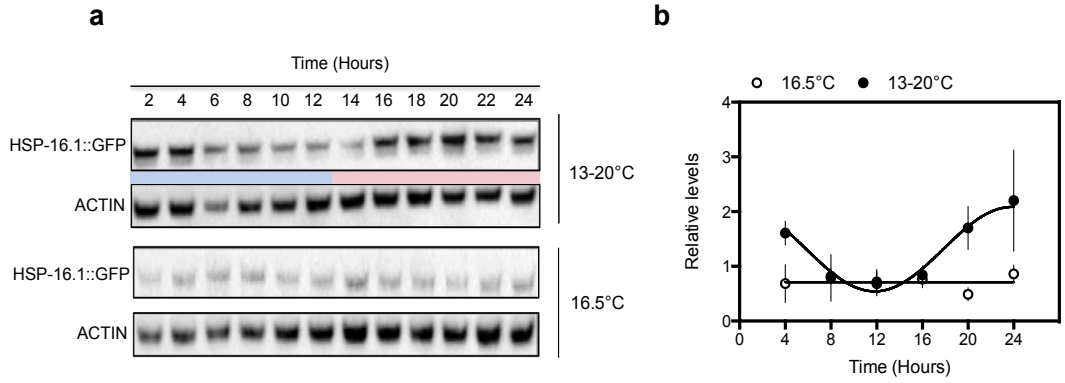

Fig. 6-16: Analysis of HSP-16.1::GFP protein expression in adult *C. elegans* held in 24-hour zeitgeber conditions. a) The top panel shows the visualization of HSP-16.1::GFP and ACTIN probed with α-GFP and α-actin from the protein samples harvested from the worms held in temperature cycle (13 °C for 12 h and 20 °C for 12 h). Lower panel shows HSP-16.1::GFP and ACTIN in western blot from the protein samples harvested from constant temperature conditions (16.5 °C). After probing with α-GFP, the same blot was probed with α-actin as a loading control; b) Quantification of HSP16.1::GFP from constant and cycling temperatures. The closed and open circles represent the average protein expression ±SEM of three independent experiments of temperature cycle and constant temperature respectively. An abundance of HSP16.1::GFP expression is significantly different from cold phase to warm phase in temperature cycles *(ANOVA, $p<0.01$)* but not in constant temperature. Significantly, a sinusoidal curve was fitted to the data points of temperature cycles using Circwave *($p<0.001$)* but not to constant temperature.

6.4. Analysis of Developmental Timing in *C. elegans* poly-glutamine Models

To study the effect of polyQ on *C. elegans* development, we used a novel method based on bioluminescence (Olmedo et al., 2015). The developmental process was analyzed from the starved L1's to young adults of poly-glutamine models. We used strains that expressed the luciferase protein under the promoter of *sur-5* (AM 141(Q40); PE254) and (AM 134 (Q0); PE254), and we analyzed the development at constant temperatures (20 °C and 16.5 °C) and temperature cycle (13 °C for 12 h and 20 °C for 12 h).

6.4.1. Analysis of Development Time of Q0 and Q40 Worms at General Lab Conditions

The bioluminescence signal was measured from Q0 and Q40 worms at 20 °C (general lab conditions) from starved L1 to young adult. The overall luminescence signal was lower in Q40 worms than in Q0 throughout the development process (Figs. 6-17 a, b).

The developmental program of Q40 worms was delayed for an average of 28.3 h compared to Q0 worms (Fig. 6-17g). The average time of development in Q0 and Q40 worms was 50.11 h and 78.41 h, respectively. The length of each larval stage from L1 to L4 is significantly longer in Q40 worms compared to Q0 (Figs. 6-17 c, e). Duration of L3 larval stage is prolonged (increased 2 fold) in Q40 worms compared to Q0 (Fig. 6-17e). Molting periods were also reported as significantly longer in Q40 worms compared to Q0 (Figs. 6-17 d, f). The results suggest that the increased glutamine repeats in transgenic worms delay the developmental process in *C. elegans*.

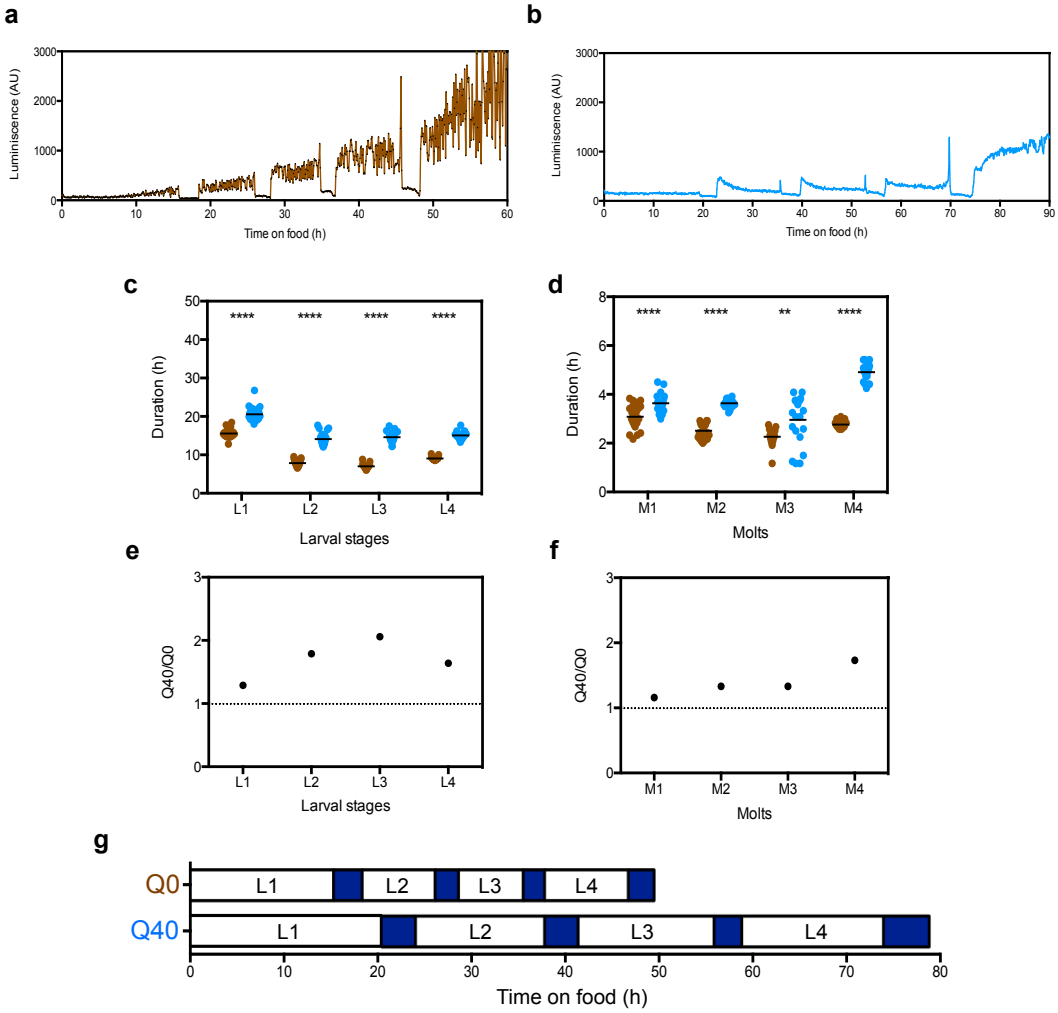

Fig. 6-17: Analysis of development in *C. elegans* polyQ model at 20 °C. Brown represents Q0 and light blue represents Q40. a, b) Bioluminescence of single (AM134 (Q0); PE254) and (AM141(Q40); PE254) worm with time on food; c) Duration of larval stages (L1-L4). Each dot represents a single worm. Larval stages (L1-L4) of Q40 are significantly different from Q0 (*Student t-test,* ****$p<0.001$, N ≥20 worms); d) Duration of molts (M1-M4). The molting period of Q40 worms is significantly longer than that of Q0 worms *(Student t-test,* ****$p<0.001$, **$p<0.05$*)*. e) Ratio between the duration of Q40 and Q0 larval stages; f) Ratio of Q40 and Q0 Molts duration; g) Quantitative analysis of development showing the average of ≥ 20 worms of Q0 and Q40. Molting periods are represented in blue.

6.4.2. Analysis of Development Time of Q0 and Q40 Worms at 16.5 °C

We further analyzed Q0 and Q40 worms at a constant temperature of 16.5 °C. In this condition, the duration of development from starved L1 to M4 was an average of 71.87 h for Q0 and 108.59 h for Q40 worms (Fig. 4-18g), suggesting that Q40 was

delayed in development for 36.72 h compared to Q0. Each larval stage was significantly longer in Q40 compared to Q0 worms (Figs. 4-18 a, b, c). Development of L3 larval stage is prolonged in Q40 worms compared to Q0 (Fig. 4-18e).

The period of all molts except the first molt (M1) was significantly longer in Q40 worms (Figs. 4-18 a, b, d). Duration M4 (molt) was prolonged in Q40 worms. Additionally, the developmental time of both Q0 and Q40 worms was delayed at this condition compared to the worms grown at 20°C. Because we know that developmental time is regulated by temperature, we conclude that glutamine repeats in transgenic polyQ models of *C. elegans* delay the developmental program.

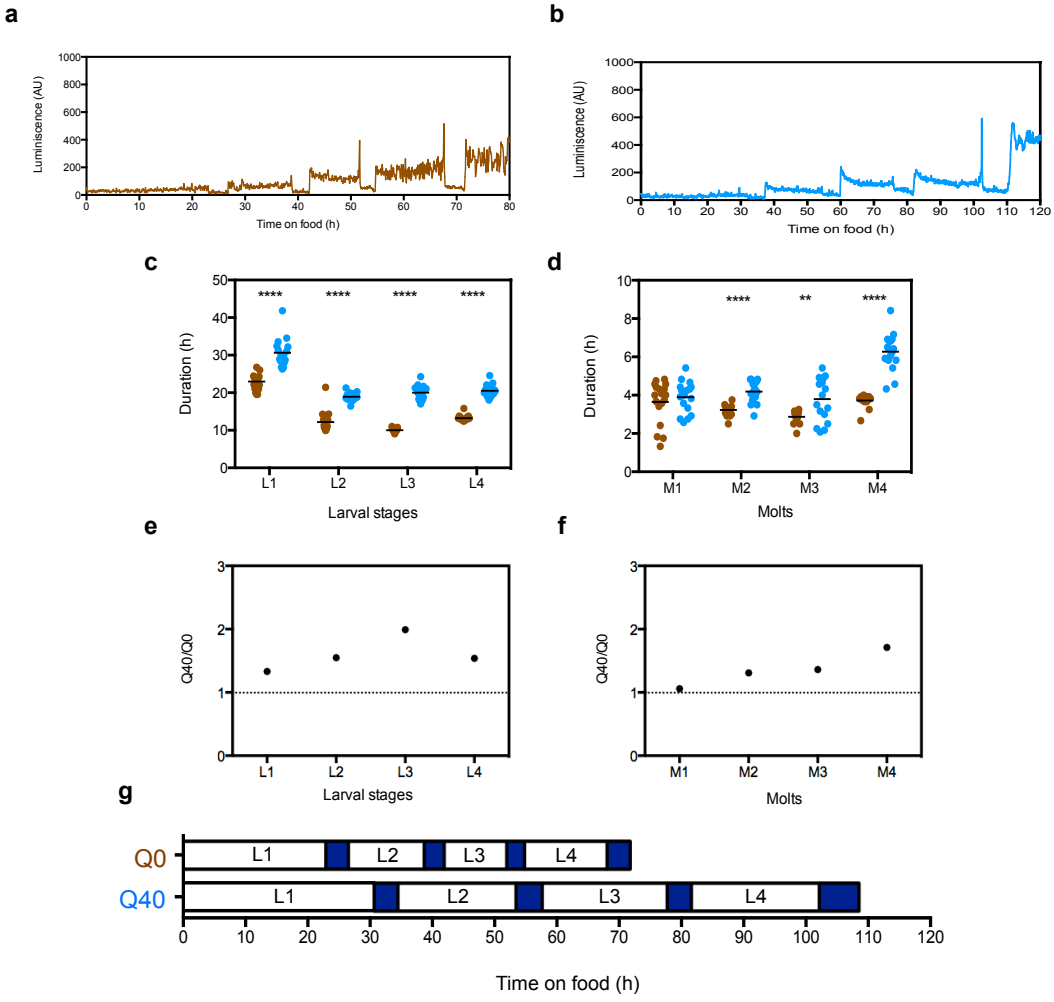

Fig. 6-18: Development analysis of *C. elegans* polyQ models at 16.5 °C. Q0 and Q40 worms are represented with brown and light blue, respectively. a, b) Bioluminescence signal of single Q0 and Q40 worm expressing luciferase under the promoter of sur-5; c) Quantitative analysis of larval duration (L1-L4). The larval stages were significantly longer in Q40 than

Q0 worms *(student t-test, ****p<0.001)*; d) Quantitative analysis of molts duration (M1-M4). Molting duration is significantly longer in M2, M3 and M4 of Q40 but not in M1 *(student t-test, p<****0.001, **p<0.05)*; e) Ratio between the duration of Q40 and Q0 larval stages; f) Ratio of Q40 and Q0 Molts duration; g) Average duration of development in ≥ 20 worms of Q0 and Q40. Molting is represented with blue.

6.4.3. Analysis of Development Time of Q0 and Q40 Worms at 13-20 °C

To understand the developmental process in polyQ models at temperature cycles, bioluminescence signal was measured in both Q0 and Q40 models held in temperature cycle.

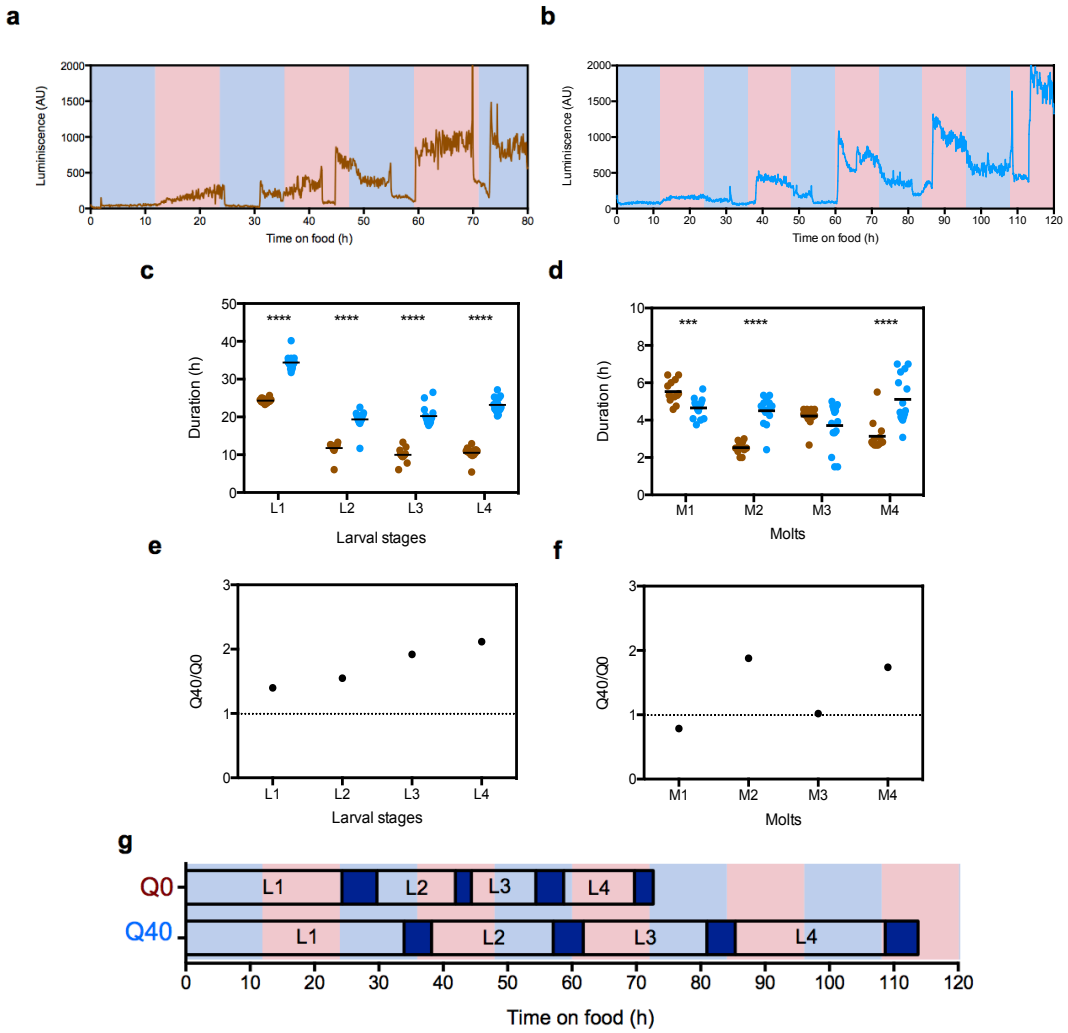

Fig. 6-19: Analysis of development in PolyQ models of *C. elegans* held in temperature cycles. The blue and pink panels represent cold (13 °C) and warm (20 °C) temperatures The brown and blue points represent Q0 and Q40 worms, respectively; a, b) Luciferase signal of single Q0 and Q40 worms; c) Duration of larval stages of Q0 and Q40 worms. All larval

stages are significantly long in Q40 then Q0 worms *(Student t-test, ****p<0.001);* d) Duration of molts in Q0 and Q40 worms. M1, M2 and M4 molts are significantly different *(student t-test, p<****0.001, ***p<0.01)*, but not as significant M3 between Q0 and Q40 worms; e) Ratio between the duration of Q40 and Q0 larval stages; f) Ratio of Q40 and Q0 Molts duration; g) Developmental timing of both strains. Molting is represented in blue. Development is delayed in Q40 compared to Q0.

Thus, the results suggest that the duration of Q40 development is delayed 41.15 h in average compared to Q0 worms. The duration of each larval stage in Q40 is significantly longer than in Q0 worms (Figs. 6-19 a, b, c). Duration of fourth larval stage is prolonged in Q40 worms compared to Q0 (Fig. 6-19e). Interestingly, we also observed that the first and third molts of Q0 worms were significantly longer than second and fourth molt, which may be due to the onset of molting in particular phase of temperature cycle (Figs. 6-19 a, b, d). Duration of second molt was prolonged in Q40 worms (Fig. 6-19f).

The luminescence signal increased during the warm phase compared to the cold phase in both Q0 and Q40 worms. We observed that the duration of development is of 72.71 h in average in Q0 and 113.86 h in Q40 worms (Fig. 6-19e). The developmental analysis of polyQ models at temperature cycles suggests that developmental timing is affected by temperature and by the number of poly-glutamine repeats.

7. Discussion

The circadian system is a pervasive temporal program. The properties of a circadian clock include temperature compensation and a free running circa 24h rhythm that is – in the natural state - entrained. Circadian entrainment synchronizes the biological clock to 24-hour zeitgeber cycles. Zeitgebers include light and dark, warm and cold temperature, etc. In humans, entrainment conditions have changed in recent history – we live in a weak light environment. This tends to result in entrainment to a later phase, a condition that can lead to a mismatch between internal and social time (Roenneberg et al., 2013). This mismatch is most commonly associated with regular work schedules, but may also include shift work. Several diseases are associated with shift work, and with disrupted circadian rhythms, such as cardiovascular diseases, cancer, and metabolic diseases (Ferrell and Chiang, 2015; Musiek, 2015). To date, few studies have reported on the importance of circadian entrainment in modulating symptoms of existing diseases. Although one study has reported that entrainment with high amplitude light dark cycles improved cognitive function in dementia patients (Riemersma-van der Lek et al., 2008), the impact of circadian entrainment on molecular pathology in several diseases including dementia-associated disorders is unclear. In this study, we focused on understanding the impact of circadian entrainment on molecular mechanisms of poly-glutamine aggregation diseases.

Protein aggregation is a hallmark of several diseases, including neurodegenerative diseases, type 2 diabetes and cancer, all of which are also, through different experimental paradigms, associated with a disrupted circadian clock (Hastings and Goedert, 2013; Knowles et al., 2014; Kurose et al., 2014; Musiek, 2015; Savvidis and Koutsilieris, 2012; Valastyan and Lindquist, 2014). In a cell, protein aggregation is regulated by the proteostasis network, which includes protein synthesis, folding, trafficking, aggregation, degradation and autophagy. The co-ordination between these components is essential in order to maintain protein homeostasis (Douglas and Dillin, 2010). The efficiency of the proteostasis network declines with age and disease, subsequently effecting cellular function and possibly leading to cell death (Hipp et al., 2014). Current literature suggests that the circadian clock regulates protein synthesis, degradation and autophagy (Cornelius et al., 1985; Lipton et al., 2015). In addition, recent evidence suggests that induction of heat shock proteins is associated with

circadian entrainment. In mammals, light-dark cycles synchronize SCN, which regulates several physiological processes including body temperature. Body temperature entrains the peripheral oscillators through HSF-1 mediated transcription (Buhr et al., 2010). HSF-1 is a transcription factor, which regulates the expression of heat shock proteins and binding of HSF-1 to heat shock elements is rhythmic (Reinke et al., 2008). Therefore, we hypothesized that circadian entrainment impacts the expression of chaperones or heat shock proteins, which subsequently impacts the protein folding process (Fig. 7-1).

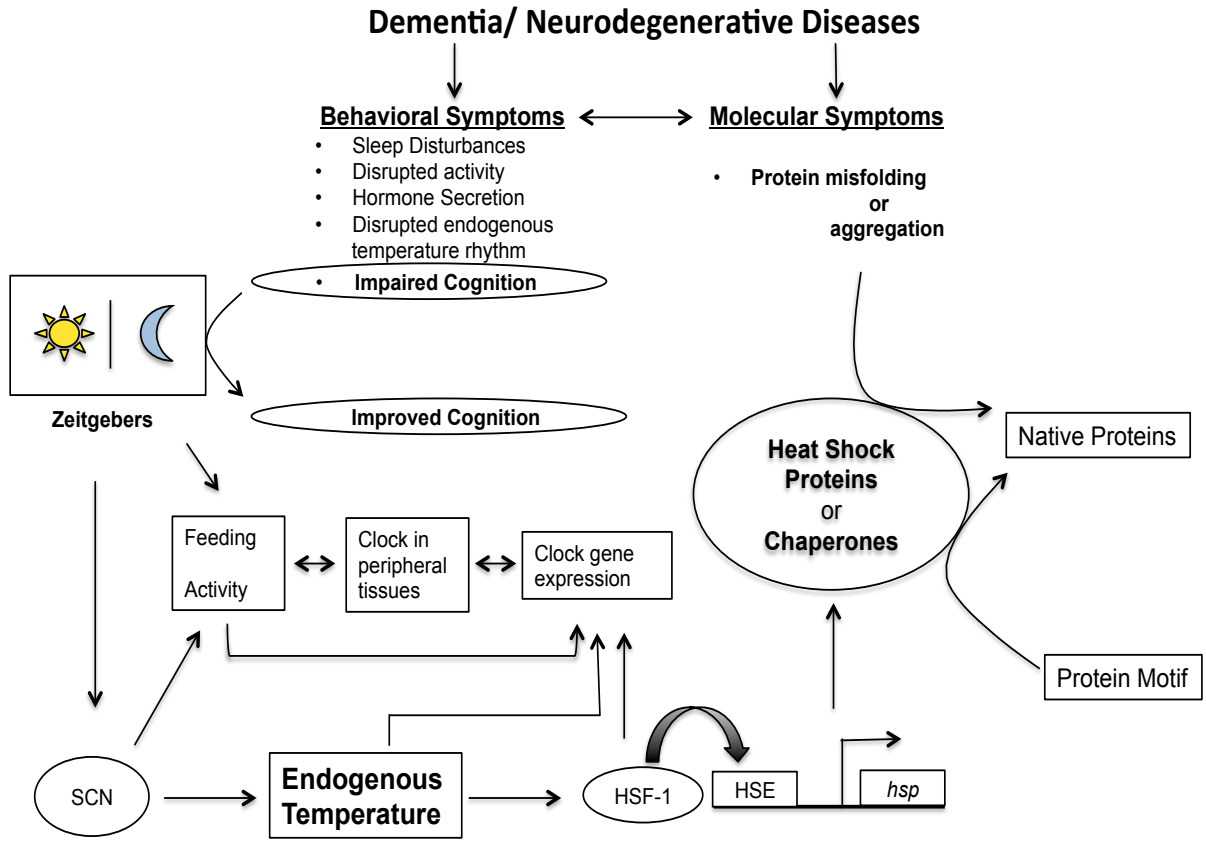

Fig. 7-1: Cartoon of a model for the role of zeitgebers in protein aggregation-associated disorders. Zeitgebers (light-dark cycles) synchronize the biological clock to the external environmental cycles and regulate several behavioural and physiological processes include feeding, endogenous temperature etc. Endogenous temperature may entrain/regulate daily expression of a set of genes via HSF-1. These heat shock proteins suppress protein misfolding or aggregation (molecular symptoms) in neurodegenerative diseases. Imposing zeitgebers improved cognitive performance, which suggest that molecular and behavioral symptoms might impact on each other through zeitgebers.

7.1. Establishing a Novel Biochemistry Method for Quantification of poly-glutamine (polyQ) Aggregation

Aggregation can result from an abnormal expansion of poly-glutamine repeats, which occur due to mutation of specific gene loci associated with Huntington's Disease, Machado-Joseph's, Kennedy's, etc. (Fan et al., 2014). To study polyQ aggregation, fluorescently tagged polyQ transgenic models were generated for *C. elegans*, zebrafish, *Drosophila*, mice, etc. (Calamini et al., 2013). These models were used to visualize molecular and behavioral hallmarks of polyQ diseases such as aggregation, motility defects etc (Brignull et al., 2006; Morley et al., 2002). In our study, *C. elegans* was used as a model for studying the impact of zeitgber (temperature) cycles on polyQ aggregation formation. Many studies have used fluorescence microscopy to capture the polyQ::YFP aggregates in *C. elegans* and then counted the number of fluorescent aggregates (Morley et al., 2002; van Ham et al., 2010; Shemesh et al., 2013). In an effort to make this method more objective (manual counting is not highly accurate) we quantified fluorescence aggregates using ImageJ. We then validated the ImageJ results by manual counting (see section 6.1.2.1).

In order to characterize the progression of aggregate formation both quantitatively and qualitatively, we turned to protein gel electrophoresis. The ideal protocol should yield characteristic patterns of bands as the animal aged, that we could use to compare progression of aggregation between conditions. We attempted to quantify the native Q35::YFP aggregation using published biochemical methods, such as blue native poly acrylamide gel electrophoresis (BN-PAGE) and native agarose gel electrophoresis (NAGE).

Protein lysates of Q35::YFP and α-synuclein::YFP were resolved in BN-PAGE (Nucifora et al., 2012), and the protein bands were resolved to different molecular weights. However, these bands could not be definitively identified due to the lack of suitable molecular weight markers for non-denaturing gels (Fig. 6-1). Thus, soluble and insoluble protein species could not be identified and analysed using BN-PAGE.

I attempted to resolve protein lysates using NAGE (van Ham et al., 2010) in order to quantify Q35::YFP aggregates. After separating protein lysates in the NAGE, we identified some protein species inside the gel, and other proteins species were found in the wells (Fig. 6-2). Due to the lack of suitable molecular weight markers and loading controls, these protein species could not be precisely quantified and identified. Furthermore, we cannot identify the characteristic protein band pattern with the protein lysates of aging worms using these methods. Therefore, we suggest that soluble and insoluble aggregates of native proteins cannot be measured using BN-PAGE and NAGE.

Because the native gels were unsuited to quantify the protein aggregates, we decided to use a semi-denaturing approach (Shemesh et al., 2013) for quantification of high molecular weight Q35::YFP aggregates by semi-denaturing detergent agarose gel electrophoresis (SDD-AGE). Using this method, each protein sample split and treated with and without heat treatment. The heated protein sample, considered a fully denatured protein, apparently forms monomers, while the non-heated protein sample is semi-denatured, and stays as high molecular weight proteins (Kryndushkin et al., 2003). Heated and non-heated protein lysates from Q35::YFP worms were resolved into SDD-AGE, followed by western blot. A high molecular weight protein band was identified in non-heat treated samples and a low molecular weight band in heat-treated samples (Fig. 6-3). Due to the lack of suitable protein markers and loading controls, especially the aggregated proteins could not be precisely quantified. We concluded that SDD-AGE is not a robust method for comparing soluble and insoluble proteins.

Recent literature suggests that soluble Q35::YFP can be resolved in a 10% polyacrylamide SDS gel, but that insoluble aggregates cannot because they are retained in the wells (Silva et al., 2011). We used Bio-rad 4-15% Criterion^{TM} TGX Stain-Free^{TM} gradient SDS-PAGE gel to resolve the Q35::YFP protein lysates. The soluble Q35::YFP monomers in the gradient gel were resolved inside the gel, but the insoluble aggregates were not (Fig. 6-4). This observation compares to the results published by Morimoto's lab (Silva et al., 2011). Interestingly, the amount of soluble proteins quantified from the gradient gel suggests that soluble proteins are more abundant in zeitgeber cycles than in constant conditions. However, because total

protein lysates were used for SDS-PAGE, we suspected that soluble Q35::YFP may have been contaminated with SDS-solubilized aggregate species. We concluded that this method cannot be used for quantifying the insoluble and soluble Q35::YFP.

Following several unsuccessful attempts with published methods (as described above), we developed a novel method for quantifying Q35::YFP using ultracentrifugation followed by gradient NuPAGE (Penna and Cahalan, 2007) and western blotting (Burnette, 1981). In developing our method, we relied in part on methods from published papers of the Hartl and Morimoto labs (Silva et al., 2011; Walther et al., 2015). In our method, native proteins of soluble and insoluble species (aggregates) were separated using ultracentrifugation. After ultracentrifugation, we dissolved insoluble pellets in 5% (v/v) SDS sample buffer (Laemmli, 1970) and resolved the proteins in a NuPAGE 4-12% Bis-Tris gel in MES running buffer and performed western blot. High SDS concentrations contribute to solubilizing SDS-soluble fractions of the aggregates, which are more toxic than SDS-resistant aggregates (Hoffner and Djian, 2014; Tonoki et al., 2011). This novel protocol helped us to characterise the (putatively) toxic SDS-soluble composition of poly-glutamine aggregates. In parallel, we quantified soluble proteins (those found in the supernatant) using NuPAGE 4-12% Bis-Tris gel in MES running buffer followed by western blot. For these types of gels (essentially, SDS-PAGE) there are suitable molecular markers and normalization tools, allowing quantification of the insoluble and soluble Q35::YFP using this method.

7.2. 24-hour Temperature Cycles Reduce the poly-glutamine (polyQ) Aggregation

Deficient or overwhelmed proteostasis will eventually impact on protein folding mechanisms, causing protein misfolding and leading to protein aggregation (Labbadia and Morimoto, 2015), a phenomenon commonly observed in the aging process and in disease (Knowles et al., 2014; Labbadia and Morimoto, 2015). In this study, we focused on polyQ aggregation, which is commonly found in polyQ expansion disorders, including Huntington's Disease (Fan et al., 2014). Disrupted circadian rhythms, including core-body temperature rhythms, have been identified in

mammalian Huntington's disease models (Kudo et al., 2011b; Musiek, 2015). However, it has been reported that food and light entrainment restored the peripheral oscillations and cognitive functions in dementia associated diseases (Maywood et al., 2010; Riemersma-van der Lek et al., 2008). Formally, one could ask which came first in certain human diseases, a disrupted circadian rhythm or the neurodgeneration (Hastings and Goedert, 2013; Musiek, 2015). At least entrainment with light is predicted to have an impact on the amplitude of the temperature cycle (Baehr et al., 2000). Endogenous temperature rhythms and the induction of heat shock proteins are associated with the light–dark cycles (Kornmann et al., 2007; Reinke et al., 2008). By extension, a higher amplitude light-dark cycle may lead to higher amplitude HSF-1 activity. Since the heat shock proteins are essential for the protein folding process (Fig. 7-1), we hypothesis that entrainment may impact the molecular pathology (protein misfolding or aggregation) of these diseases. Since the temperature is associated with the prevention of aggregates (Morimoto, 2011; Wu et al., 2010), we proposed that polyQ aggregation could be reduced by normal, physiological temperature entrainment. *C. elegans* is found both in the soil and above ground, where, in both environments, it is exposed to temperature cycles. Our lab used temperature cycles to reveal a circadian clock in the nematode (Olmedo et al., 2012). In addition, *C. elegans* is a powerful model system for protein aggregation diseases, having been used for mutant screens to reveal suppressors and generally for the cell biology of aggregate formation (Li and Le, 2013).

In our study, the *C. elegans* Q35::YFP model was used to investigate the impact of a temperature cycle on polyQ aggregation. The expression of polyQ in this model was driven by the muscle specific promoter, *unc-54* (Morley et al., 2002). Our basic protocol called for comparison of constant temperature and temperature cycles for progression of aggregate formation. As a first, control experiment, we checked the impact of temperature cycles on the mRNA expression of *unc-54* gene and found no difference in the expression levels of *unc-54* between temperature cycles and constant temperature (Fig. 6-14). This control experiment suggests that constant and cyclic temperatures can be used for aggregation studies without directly impacting production of the transgene.

The next question focused on measuring the number of Q35::YFP fluorescent aggregates with microscopy according to age in constant and temperature cycles. We found that aggregates increase with age. The observations correlate with published studies of Q35::YFP aggregation in *C. elegans* (Morley et al., 2002; Shemesh et al., 2013). However, the numbers of aggregates were different between constant and temperature cycles. In cyclic conditions, number of aggregates was lower at day 2, 4 and 8 compared to constant conditions (Fig. 6-5).

We then used our biochemical method (described above) to compare the amount of soluble and insoluble proteins of Q35::YFP in constant vs. cyclic conditions. Here, we found that the formation of SDS-soluble aggregates is lower at day 6 and 8 adult worms in cyclic conditions as compared to constant conditions (Fig. 6-6). Since the SDS-soluble aggregates are considered as highly toxic species (Tonoki et al., 2011) in Huntington's disease, we suggest that exposing patients with polyQ disorders to entrainment conditions can reduce the toxicity of disease. However, it remains unclear why poly-glutamine aggregation is decreased in cyclic conditions.

Although we found a change in the amount of aggregates depending on zeitgeber conditions, we were surprised at the (small) size of this effect. We therefore wondered if there were qualitative differences in the aggregates. This is an important aspect, as recent reports from the Hartl, Mann and Morimoto labs indicate that enrichment of chaperones in aggregates can be protective (Walther et al., 2015). In this study, we investigated the aggregate composition in constant and temperature cycles using proteomics tools (mass spectrometry). Our data show that several known poly-glutamine suppressors (RME-8, RAN-1, CCT-6, and RPL-1) and proteostastic components such as CYN-7 and RPL-41 (Kazemi-Esfarjani and Benzer, 2000; Nollen et al., 2004; Page et al., 1996; Silva et al., 2011; Zhang et al., 2010) are enriched in the aggregates in worms held in temperature cycles as compared to constant conditions (Fig. 6-8). We suggest, therefore, that a lower polyQ aggregation in temperature cycles may be a result of the increase in abundance and efficiency of proteostasis components (Chaperones, ubiquitin proteome system, etc.) or to a decrease in aggregate suppressors in constant conditions.

Precisely how the abundance and efficiency of proteostasis components increases in entrainment conditions is not known. Several studies have shown that protein synthesis, autophagy and degradation are clock regulated (Cornelius et al., 1985; Lipton et al., 2015), but how the protein folding machinery is regulated in entrainment conditions is poorly understood. In the following section 7.3, we will discuss the details of heat shock protein expression in entrained conditions.

In addition to aggregate quantification, we analyzed the motility of Q35::YFP worms with age in zeitgeber conditions. An increase in amount of aggregation effects the declining motility of Q35::YFP, α-synuclein::YFP worms with age (Morley et al., 2002; van Ham et al., 2010). Therefore, we tested the impact of zeitgeber conditons on motility of Q35::YFP, α-synuclein::YFP worms. Our observations were similar to the published papers that motility is decreasing with age. However, we did not observe significant differences between the conditions until Day8 worms. Therefore, we summarize that motility assay shows less sensitive than biochemistry or microscopy methods. We also speculate that aggregate suppression may impact on life span of animals held in different zeitgeber conditions.

7.3. 24-hour Temperature Cycles Induce the Rhythmic Expression of Some Heat Shock Proteins

Chaperones or heat shock proteins are the key regulators of protein folding. We hypothesized that a possible mechanism for the reduction of toxic species in the aggregates in entrainment conditions would be that the temperature cycles induce the expression of heat shock proteins. Schibler's lab has reported the rhythmic mRNA expression of Hsp70, Hsp90 and Hsp105 homologs in entrainment conditions (Kornmann et al., 2007). These heat shock proteins are classified as ATP dependent chaperones. This class is unable to interact with unfolded substrates (misfolded proteins or aberrant aggregates) without ATP independent chaperones such as small heat shock proteins or Hsp40's (Brehme et al., 2014; Haslbeck and Vierling, 2015). The basic function of small heat shock proteins is binding to unfolded substrate to prevent protein aggregation (Bakthisaran et al., 2015). The expression of several mammalian heat shock genes (HSPB1, HSPB2, HSPB3, HSPB6, HSPB7, HSPB8)

found to be rhythmic in free running conditions of several microarray datasets. Among them, HSPB1 found to be rhythmic in several tissues such as aorta, colon, lung, cerebellum, kidney, pituitary and liver. HSPB2 is rhythmic in distal colon, HSPB3 is rhythmic in distal colon and heart, HSPB6 is rhythmic in SCN, HSPB7 is rhythmic in lung and HSPB8 is rhythmic in brown adipose, lung and liver. (Hoogerwerf et al., 2008; Hughes et al., 2009; Panda et al., 2002; Rudic et al., 2004; Rudic et al., 2005). In the present study, we focused on the impact of physiological temperature cycles on expression of genes for small heat shock proteins in *C. elegans.* We selected heat shock proteins that have chaperone properties, such as HSP-16.1 and HSP-16.2. As a control, we chose HSP-12.6, a small heat shock protein that lacks a chaperone function (Leroux et al., 1997a; Leroux et al., 1997b).

mRNA and protein of *hsp-16*s was detected using Northern blots and fluorescent imaging, but only is worms exposed to stressors, mainly heat shock. In constant 20°C lab conditions, *hsp-16* is not detectable by Northern blot (Ding and Candido, 2000a; Jones et al., 1989; Leroux et al., 1997b; Stringham et al., 1992). In contrast, we easliy detected the mRNA expression of *hsp-16.1* and *hsp-16.2* at constant 16.5°C (without heat shock exposure or other stress conditions; Figs. 6-10 b, d) using quantitative RT-PCR. Obviously, the increased sensitivity of the method (qPCR vs. Northern blot) allowed detection of this gene expression in constant (physiological temprature) conditions. Furthermore, we also measured the protein levels of HSP-16.1 using a fluorescence reporter. The expression of HSP-16.1::GFP was detected in the worms held at a constant temperature of 16.5°C (Figs. 6-16 b, c), suggesting that the mRNA and protein expression of *hsp-16s* can occur independent of stress conditions. Recently published data from Hartl's lab showed the presence of HSP16's in the insoluble fractions of aging worms grown at lab conditions without stress conditions (Walther et al., 2015). This finding supports our observations that the basal levels of *hsp-16 s* can be found in the cell even in the absence of thermal stress.

Based on previous studies, we know that the expression levels of *hsp-16 s* are modulated by heat shock (Stringham et al., 1992). Our experiments call for temperature entrainment cycles in the physiological range. We asked if these would support expression of the small heat shock protein genes. Specifically, we used

zeitgeber conditions as described above for the poly-glutamine aggregation studies. In this study, we observed that mRNA expression of the genes *hsp-16.1* and *hsp-16.2* is rhythmic in the worms held in temperature cycles (Figs. 6-10 a, c) but not in constant conditions. We observed a two-fold increase in the abundance of *hsp-16 genes mRNA* in the warm phase as compared to the cold phase of the temperature cycle and the expression levels are significantly rhythmic over the period of 24 h for 2 days in a temperature cycle. Following measurement of the relative expression between constant and cyclic conditions, our data showed that mRNA levels of *hsp-16.1* and *hsp-16.2* are more abundant in temperature cycles as compared to constant temperature (Fig. 6-10). we further analyzed the protein expression of fluorescently tagged HSP 16.1 in zeitgeber conditions. We observed the protein expression of HSP-16.1::GFP is significantly rhythmic in temperature cycles (Figs. 6-16 a, c) but not in constant conditions, and an increase in the abundance of HSP-16.1::GFP in temperature cycles as compared to constant conditions. We suggest therefore that entrainment conditions within the physiological range are sufficient to increase the expression levels of *hsp-16 genes.* Interestingly, a study from the Link lab has reported that the overexpression of HSP-16.2 suppresses the β-amyloid aggregation and toxicity in *C. elegans* Alzheimer's model (Fonte et al., 2008). Based on this observation and on our data, we suggest that entrainment conditions can increase the abundance of several proteins, including HSP-16.1 in the cell, which might reduce the aberrant protein aggregation and toxicity.

We also measured the expression of the small heat shock protein *hsp-12.6*, which cannot suppress the aggregation and is unaltered by stress (Leroux et al., 1997a). The mRNA expression of *hsp-12.6* is not rhythmic either in temperature cycle or constant conditions (Fig. 6-13). This observation suggests that the heat shock proteins, which lack chaperone function, might be not rhythmic in entrainment conditions.

In addition, we studied the impact of entrainment conditions on a small heat shock protein, HSP-43, whose function is not well defined (Ding and Candido, 2000c). Recent studies have indicated that HSP-43 is associated with natural aggregates, in cases where the HSP-12 family was not (Walther et al., 2015). We speculated that HSP-43 might have a chaperone property similar to HSP-16s. We therefore measured

mRNA expression of *hsp-43* in constant and temperature cycles and found that the mRNA expression is rhythmic and its abundance increased in temperature cycles relative to constant conditions (Fig. 6-11). This result represents a single experiment, thus replicate experiments are required to further support this conclusion.

The mammalian homologs of Hsp70, Hsp90 and Hsp105 are rhythmic in 24h light-dark cycles (Kornmann et al., 2007). We studied the impact of 24h temperature cycle on *hsp-4* in *C. elegans,* a homolog of Hsp70 in mammals (Heschl and Baillie, 1989). With temperature entrainment, the mRNA expression of *hsp-4* is rhythmic and abundant. In constant temperature, the Hsp70 homolog is not rhythmic. This suggests that this gene is regulated by circadian clock entrainment in mammals and *C. elegans*. There is no evidence that light-dark cycles directly regulate heat shock protein expression. Since the *C. elegans* is an ectothermic animal, we suggest that temperature cycles can directly regulate the heat shock protein expression. In mammals, however, light-dark cycles regulate endogenous temperature rhythms through the circadian oscillator, and the endogenous temperature rhythms are, in turn, associated with induction of heat shock proteins (Reinke et al., 2008). We propose that the rhythmic expression of Hsp70 homologs is more closely associated with temperature entrainment than with light entrainment, a speculation that can be applied for all rhythmic heat shock proteins under entrainment conditions.

7.4. Delayed Developmental Timing in *C. elegans* polyQ Model

The *C. elegans* life cycle has four discrete larval stages (L1, L2, L3 and L4) separated by molts (M1, M2, M3 and M4) and followed by the adult stage. The speed of development in *C. elegans* can be controlled by several environmental factors, primarily food and temperature conditions (Cassada and Russell, 1975). Recently, a high-throughput method showed that developmental timing is delayed in the mutants of *daf-2*, *lin-42*, etc. (Monsalve et al., 2011; Ruaud et al., 2011). We have also shown that metabolic stress can delay development (M. Olmedo, M. Geibel, unpublished data).

Given that neurodegenerative processes invoke metabolic stress, we asked if development would be impacted in our transgenic animals. Consequently, we studied the developmental timing in poly-glutamine expressed transgenic worms (Q40::YFP). As a control, we used control (Q0::YFP) worms. These worms were crossed with a LUC::GFP strain (PE254), and the developmental timing was measured at constant 20 °C and also 16.5 °C and further in a temperature cycle (13 °C for 12 h and 20 °C for 12 h) using published methods (Olmedo et al., 2015). Interestingly, the duration of larval development was lengthened at all larval stages in poly-glutamine expressing worms as compared to controls. This observation was consistent in all temperature conditions (Figs. 6-17e, 18e, 19e). In addition, the duration of molting stages M1 to M4 was extended in the Q40 worms held at constant conditions (Figs. 6-17e, 18e). However, the longer molting was observed only in M2 and M4 stages in the poly-glutamine worms held in temperature cycle, but not with M1 and M3 (Fig. 6-19e). We further analyzed the delay of the entire developmental program using the data acquired from larval development and molting. This data suggest that the average developmental delay of Q40 worms at 20 °C is about 28 h; at 16.5 °C it is about 36 h; and in the temperature cycle the lengthening is about 41 h. The reason for such developmental delay of poly-glutamine expressed worms is unclear, although one may speculate that the delay could be due to an increase in misfolding or aggregation in the poly-glutamine model. However, because there are several pathways associated with the developmental process, the explanation might be more complicated. Given that polyQ glutamine expansion is apparently causative for several polyQ disorders including Huntington's disease (Fan et al., 2014),we also speculate that transgenic expression of other genes associated with neurodegenerative diseases may have an impact on development and aging in *C. elegans.*

The implications for this observation are far-ranging. Several studies have reported the comparison of aging associated phenotypes between Q0 and Q40 worms (Adamla and Ignatova, 2015; Beam et al., 2012; Morley et al., 2002; Nollen et al., 2004). Our results imply that aging can be delayed in Q40 worms compared to Q0. Given that animals will reach adulthood at least a day later, this would have to be taken into account when calculating the age of the animal.

8. References

Adamla, F., and Ignatova, Z. (2015). Somatic expression of unc-54 and vha-6 mRNAs declines but not pan-neuronal rgef-1 and unc-119 expression in aging Caenorhabditis elegans. Sci Rep *5*, 10692.

Aevermann, B.D., and Waters, E.R. (2008). A comparative genomic analysis of the small heat shock proteins in Caenorhabditis elegans and briggsae. Genetica *133*, 307-319.

Akerfelt, M., Trouillet, D., Mezger, V., and Sistonen, L. (2007). Heat shock factors at a crossroad between stress and development. Ann N Y Acad Sci *1113*, 15-27.

Amm, I., Sommer, T., and Wolf, D.H. (2014). Protein quality control and elimination of protein waste: the role of the ubiquitin-proteasome system. Biochim Biophys Acta *1843*, 182-196.

Aschoff, J. (1960). Exogenous and endogenous components in circadian rhythms. Cold Spring Harb Symp Quant Biol *25*, 11-28.

Aschoff, J. (1965). Circadian Rhythms in Man. Science *148*, 1427-1432.

Aschoff, J. (1981). A survey on biological rhythms (US: Springer).

Aton, S.J., Colwell, C.S., Harmar, A.J., Waschek, J., and Herzog, E.D. (2005). Vasoactive intestinal polypeptide mediates circadian rhythmicity and synchrony in mammalian clock neurons. Nat Neurosci *8*, 476-483.

Aziz, N.A., Anguelova, G.V., Marinus, J., Lammers, G.J., and Roos, R.A. (2010). Sleep and circadian rhythm alterations correlate with depression and cognitive impairment in Huntington's disease. Parkinsonism Relat Disord *16*, 345-350.

Baehr, E.K., Revelle, W., and Eastman, C.I. (2000). Individual differences in the phase and amplitude of the human circadian temperature rhythm: with an emphasis on morningness-eveningness. J Sleep Res *9*, 117-127.

Baker, C.L., Loros, J.J., and Dunlap, J.C. (2012). The circadian clock of Neurospora crassa. FEMS Microbiol Rev *36*, 95-110.

Bakthisaran, R., Tangirala, R., and Rao Ch, M. (2015). Small heat shock proteins: Role in cellular functions and pathology. Biochim Biophys Acta *1854*, 291-319.

Baler, R., Dahl, G., and Voellmy, R. (1993). Activation of human heat shock genes is accompanied by oligomerization, modification, and rapid translocation of heat shock transcription factor HSF1. Mol Cell Biol *13*, 2486-2496.

Beam, M., Silva, M.C., and Morimoto, R.I. (2012). Dynamic imaging by fluorescence correlation spectroscopy identifies diverse populations of polyglutamine oligomers formed in vivo. J Biol Chem *287*, 26136-26145.

Bettencourt, C., and Lima, M. (2011). Machado-Joseph Disease: from first descriptions to new perspectives. Orphanet J Rare Dis *6*, 35.

Bradford, M.M. (1976). A rapid and sensitive method for the quantitation of microgram quantities of protein utilizing the principle of protein-dye binding. Anal Biochem *72*, 248-254.

Brady, J.P., Garland, D., Duglas-Tabor, Y., Robison, W.G., Jr., Groome, A., and Wawrousek, E.F. (1997). Targeted disruption of the mouse alpha A-crystallin gene induces cataract and cytoplasmic inclusion bodies containing the small heat shock protein alpha B-crystallin. Proc Natl Acad Sci U S A *94*, 884-889.

Breen, D.P., Vuono, R., Nawarathna, U., Fisher, K., Shneerson, J.M., Reddy, A.B., and Barker, R.A. (2014). Sleep and circadian rhythm regulation in early Parkinson disease. JAMA Neurol *71*, 589-595.

Brehme, M., Voisine, C., Rolland, T., Wachi, S., Soper, J.H., Zhu, Y., Orton, K., Villella, A., Garza, D., Vidal, M.*, et al.* (2014). A chaperome subnetwork safeguards proteostasis in aging and neurodegenerative disease. Cell Rep *9*, 1135-1150.

Brignull, H.R., Moore, F.E., Tang, S.J., and Morimoto, R.I. (2006). Polyglutamine proteins at the pathogenic threshold display neuron-specific aggregation in a pan-neuronal Caenorhabditis elegans model. J Neurosci *26*, 7597-7606.

Brockwell, D.J., and Radford, S.E. (2007). Intermediates: ubiquitous species on folding energy landscapes? Curr Opin Struct Biol *17*, 30-37.

Brown, S.A., and Azzi, A. (2013). Peripheral circadian oscillators in mammals. Handb Exp Pharmacol, 45-66.

Brown, S.A., Zumbrunn, G., Fleury-Olela, F., Preitner, N., and Schibler, U. (2002). Rhythms of mammalian body temperature can sustain peripheral circadian clocks. Curr Biol *12*, 1574-1583.

Bryngelson, J.D., Onuchic, J.N., Socci, N.D., and Wolynes, P.G. (1995). Funnels, pathways, and the energy landscape of protein folding: a synthesis. Proteins *21*, 167-195.

Buhr, E.D., and Takahashi, J.S. (2013). Molecular components of the Mammalian circadian clock. Handb Exp Pharmacol, 3-27.

Buhr, E.D., Yoo, S.H., and Takahashi, J.S. (2010). Temperature as a universal resetting cue for mammalian circadian oscillators. Science *330*, 379-385.

Bunning, E. (1935). Zur Kenntnis der endogenen Tagesrhythmik bei Insekten und Pflanzen. *53*, 594-623.

Bunning, E. (1967). The physiology clock (The Heidelberg Science Library).

Burnette, W.N. (1981). "Western blotting": electrophoretic transfer of proteins from sodium dodecyl sulfate--polyacrylamide gels to unmodified nitrocellulose and

radiographic detection with antibody and radioiodinated protein A. Anal Biochem *112*, 195-203.

Cadavez, L., Montane, J., Alcarraz-Vizan, G., Visa, M., Vidal-Fabrega, L., Servitja, J.M., and Novials, A. (2014). Chaperones ameliorate beta cell dysfunction associated with human islet amyloid polypeptide overexpression. PLoS One *9*, e101797.

Calamini, B., Lo, D.C., and Kaltenbach, L.S. (2013). Experimental models for identifying modifiers of polyglutamine-induced aggregation and neurodegeneration. Neurotherapeutics *10*, 400-415.

Cassada, R.C., and Russell, R.L. (1975). The dauerlarva, a post-embryonic developmental variant of the nematode Caenorhabditis elegans. Dev Biol *46*, 326-342.

Chiang, W.C., Ching, T.T., Lee, H.C., Mousigian, C., and Hsu, A.L. (2012). HSF-1 regulators DDL-1/2 link insulin-like signaling to heat-shock responses and modulation of longevity. Cell *148*, 322-334.

Cho, J.Y., and Sternberg, P.W. (2014). Multilevel modulation of a sensory motor circuit during C. elegans sleep and arousal. Cell *156*, 249-260.

Coogan, A.N., Schutova, B., Husung, S., Furczyk, K., Baune, B.T., Kropp, P., Hassler, F., and Thome, J. (2013). The circadian system in Alzheimer's disease: disturbances, mechanisms, and opportunities. Biol Psychiatry *74*, 333-339.

Cornelius, G., Schroeder-Lorenz, A., and Rensing, L. (1985). Circadian-clock control of protein synthesis and degradation in Gonyaulax polyedra. Planta *166*, 365-370.

Datskevich, P.N., Nefedova, V.V., Sudnitsyna, M.V., and Gusev, N.B. (2012). Mutations of small heat shock proteins and human congenital diseases. Biochemistry (Mosc) *77*, 1500-1514.

de Candolle, A.P. (1835). Pflanzen-Physiologie, oder Darstellung der Lebenskräfte und Lebensverrichtungen der Gewächse (Stuttgart u. Tübingen), pp. 639-640.

de Marian, J.J. (1729). Observation botanique. Histoire de l'Academie Royale des Sciences.

Dexter, D.T., and Jenner, P. (2013). Parkinson disease: from pathology to molecular disease mechanisms. Free Radic Biol Med *62*, 132-144.

Diaz-Villanueva, J.F., Diaz-Molina, R., and Garcia-Gonzalez, V. (2015). Protein Folding and Mechanisms of Proteostasis. Int J Mol Sci *16*, 17193-17230.

Dill, K.A., and Chan, H.S. (1997). From Levinthal to pathways to funnels. Nat Struct Biol *4*, 10-19.

Ding, L., and Candido, E.P. (2000a). Association of several small heat-shock proteins with reproductive tissues in the nematode Caenorhabditis elegans. Biochem J *351*, 13-17.

Ding, L., and Candido, E.P. (2000b). HSP25, a small heat shock protein associated with dense bodies and M-lines of body wall muscle in Caenorhabditis elegans. J Biol Chem *275*, 9510-9517.

Ding, L., and Candido, E.P. (2000c). HSP43, a small heat-shock protein localized to specific cells of the vulva and spermatheca in the nematode Caenorhabditis elegans. Biochem J *349*, 409-412.

Dobson, C.M. (2003). Protein folding and misfolding. Nature *426*, 884-890.

Dong, G., and Golden, S.S. (2008). How a cyanobacterium tells time. Curr Opin Microbiol *11*, 541-546.

Douglas, P.M., and Dillin, A. (2010). Protein homeostasis and aging in neurodegeneration. J Cell Biol *190*, 719-729.

Dowson-Day, M.J., and Millar, A.J. (1999). Circadian dysfunction causes aberrant hypocotyl elongation patterns in Arabidopsis. Plant J *17*, 63-71.

Duncan, M.J., Smith, J.T., Franklin, K.M., Beckett, T.L., Murphy, M.P., St Clair, D.K., Donohue, K.D., Striz, M., and O'Hara, B.F. (2012). Effects of aging and genotype on circadian rhythms, sleep, and clock gene expression in APPxPS1 knock-in mice, a model for Alzheimer's disease. Exp Neurol *236*, 249-258.

Dutrochet, H. (1835). Mémoires pour servir à l' Histoire des végétaux et des animaux. 287.

Eelderink-Chen, Z., Mazzotta, G., Sturre, M., Bosman, J., Roenneberg, T., and Merrow, M. (2010). A circadian clock in Saccharomyces cerevisiae. Proc Natl Acad Sci U S A *107*, 2043-2047.

Eisenmann, D.M. (2005). WormBook. In WormBook, T.C.e.R. Community, ed. (doi/10.1895/wormbook.1.7.1, http://www.wormbook.org.).

Eskin, A. (1979). Identification and physiology of circadian pacemakers. Introduction. Fed Proc *38*, 2570-2572.

Fan, H.C., Ho, L.I., Chi, C.S., Chen, S.J., Peng, G.S., Chan, T.M., Lin, S.Z., and Harn, H.J. (2014). Polyglutamine (PolyQ) diseases: genetics to treatments. Cell Transplant *23*, 441-458.

Ferrell, J.M., and Chiang, J.Y. (2015). Circadian rhythms in liver metabolism and disease. Acta Pharm Sin B *5*, 113-122.

Fersht, A.R. (1997). Nucleation mechanisms in protein folding. Curr Opin Struct Biol *7*, 3-9.

Fiala, G.J., Schamel, W.W., and Blumenthal, B. (2011). Blue native polyacrylamide gel electrophoresis (BN-PAGE) for analysis of multiprotein complexes from cellular lysates. J Vis Exp.

Fleckenstein, T., Kastenmuller, A., Stein, M.L., Peters, C., Daake, M., Krause, M., Weinfurtner, D., Haslbeck, M., Weinkauf, S., Groll, M.*, et al.* (2015). The Chaperone Activity of the Developmental Small Heat Shock Protein Sip1 Is Regulated by pH-Dependent Conformational Changes. Mol Cell *58*, 1067-1078.

Fonte, V., Kipp, D.R., Yerg, J., 3rd, Merin, D., Forrestal, M., Wagner, E., Roberts, C.M., and Link, C.D. (2008). Suppression of in vivo beta-amyloid peptide toxicity by overexpression of the HSP-16.2 small chaperone protein. J Biol Chem *283*, 784-791.

Froehlich, A.C., Chen, C.H., Belden, W.J., Madeti, C., Roenneberg, T., Merrow, M., Loros, J.J., and Dunlap, J.C. (2010). Genetic and molecular characterization of a cryptochrome from the filamentous fungus Neurospora crassa. Eukaryot Cell *9*, 738-750.

Fujimoto, M., Hayashida, N., Katoh, T., Oshima, K., Shinkawa, T., Prakasam, R., Tan, K., Inouye, S., Takii, R., and Nakai, A. (2010). A novel mouse HSF3 has the potential to activate nonclassical heat-shock genes during heat shock. Mol Biol Cell *21*, 106-116.

Gekakis, N., Staknis, D., Nguyen, H.B., Davis, F.C., Wilsbacher, L.D., King, D.P., Takahashi, J.S., and Weitz, C.J. (1998). Role of the CLOCK protein in the mammalian circadian mechanism. Science *280*, 1564-1569.

Gidalevitz, T., Ben-Zvi, A., Ho, K.H., Brignull, H.R., and Morimoto, R.I. (2006). Progressive disruption of cellular protein folding in models of polyglutamine diseases. Science *311*, 1471-1474.

Go, N. (1984). The consistency principle in protein structure and pathways of folding. Adv Biophys *18*, 149-164.

Golombek, D.A., and Rosenstein, R.E. (2010). Physiology of circadian entrainment. Physiol Rev *90*, 1063-1102.

Hardin, P.E. (2011). Molecular genetic analysis of circadian timekeeping in Drosophila. Adv Genet *74*, 141-173.

Hartl, F.U., Bracher, A., and Hayer-Hartl, M. (2011). Molecular chaperones in protein folding and proteostasis. Nature *475*, 324-332.

Haslbeck, M., and Vierling, E. (2015). A first line of stress defense: small heat shock proteins and their function in protein homeostasis. J Mol Biol *427*, 1537-1548.

Hastings, J.W., Astrachan, L., and Sweeney, B.M. (1961). A persistent daily rhythm in photosynthesis. J Gen Physiol *45*, 69-76.

Hastings, M.H., and Goedert, M. (2013). Circadian clocks and neurodegenerative diseases: time to aggregate? Curr Opin Neurobiol *23*, 880-887.

Herczenik, E., and Gebbink, M.F. (2008). Molecular and cellular aspects of protein misfolding and disease. FASEB J *22*, 2115-2133.

Herzog, E.D., Aton, S.J., Numano, R., Sakaki, Y., and Tei, H. (2004). Temporal precision in the mammalian circadian system: a reliable clock from less reliable neurons. J Biol Rhythms *19*, 35-46.

Heschl, M.F., and Baillie, D.L. (1989). Characterization of the hsp70 multigene family of Caenorhabditis elegans. DNA *8*, 233-243.

Hipp, M.S., Park, S.H., and Hartl, F.U. (2014). Proteostasis impairment in protein-misfolding and -aggregation diseases. Trends Cell Biol *24*, 506-514.

Hoffner, G., and Djian, P. (2014). Monomeric, oligomeric and polymeric proteins in huntington disease and other diseases of polyglutamine expansion. Brain Sci *4*, 91-122.

Hofmeister, W. (1867). Die Lehre von der Pflanzenzelle (Leipzig).

Holmberg, M., Duyckaerts, C., Durr, A., Cancel, G., Gourfinkel-An, I., Damier, P., Faucheux, B., Trottier, Y., Hirsch, E.C., Agid, Y*., et al.* (1998). Spinocerebellar ataxia type 7 (SCA7): a neurodegenerative disorder with neuronal intranuclear inclusions. Hum Mol Genet *7*, 913-918.

Hoogerwerf, W.A., Sinha, M., Conesa, A., Luxon, B.A., Shahinian, V.B., Cornelissen, G., Halberg, F., Bostwick, J., Timm, J., and Cassone, V.M. (2008). Transcriptional profiling of mRNA expression in the mouse distal colon. Gastroenterology *135*, 2019-2029.

Hu, K., Van Someren, E.J., Shea, S.A., and Scheer, F.A. (2009). Reduction of scale invariance of activity fluctuations with aging and Alzheimer's disease: Involvement of the circadian pacemaker. Proc Natl Acad Sci U S A *106*, 2490-2494.

Hughes, M.E., DiTacchio, L., Hayes, K.R., Vollmers, C., Pulivarthy, S., Baggs, J.E., Panda, S., and Hogenesch, J.B. (2009). Harmonics of circadian gene transcription in mammals. PLoS Genet *5*, e1000442.

Hull, R.L., Andrikopoulos, S., Verchere, C.B., Vidal, J., Wang, F., Cnop, M., Prigeon, R.L., and Kahn, S.E. (2003). Increased dietary fat promotes islet amyloid formation and beta-cell secretory dysfunction in a transgenic mouse model of islet amyloid. Diabetes *52*, 372-379.

Hurd, M.W., Debruyne, J., Straume, M., and Cahill, G.M. (1998). Circadian rhythms of locomotor activity in zebrafish. Physiol Behav *65*, 465-472.

Huynh, D.P., Del Bigio, M.R., Ho, D.H., and Pulst, S.M. (1999). Expression of ataxin-2 in brains from normal individuals and patients with Alzheimer's disease and spinocerebellar ataxia 2. Ann Neurol *45*, 232-241.

Jankovic, J.T., E. (2007). Parkinson’s disease and movement disorders (Philadelphia: Lippincott Williams and Wilkins).

Johnson, J.R., Rajamanoharan, D., McCue, H.V., Rankin, K., and Barclay, J.W. (2016). Small Heat Shock Proteins Are Novel Common Determinants of Alcohol and Nicotine Sensitivity in Caenorhabditis elegans. Genetics *202*, 1013-1027.

Jones, D., Dixon, D.K., Graham, R.W., and Candido, E.P. (1989). Differential regulation of closely related members of the hsp16 gene family in Caenorhabditis elegans. DNA *8*, 481-490.

Jones, D., Stringham, E.G., Babich, S.L., and Candido, E.P. (1996). Transgenic strains of the nematode C. elegans in biomonitoring and toxicology: effects of captan and related compounds on the stress response. Toxicology *109*, 119-127.

Kalmus, H. (1935). Periodizität und autochronie (ideochronie) als zeitregelnde eigenschaffen der organismen. Biologia generalis *11*, 93-114.

Kappe, G., Franck, E., Verschuure, P., Boelens, W.C., Leunissen, J.A., and de Jong, W.W. (2003). The human genome encodes 10 alpha-crystallin-related small heat shock proteins: HspB1-10. Cell Stress Chaperones *8*, 53-61.

Karplus, M., and Weaver, D.L. (1976). Protein-folding dynamics. Nature *260*, 404-406.

Kazemi-Esfarjani, P., and Benzer, S. (2000). Genetic suppression of polyglutamine toxicity in Drosophila. Science *287*, 1837-1840.

Kiesel, A. (1894). Untersuchungen zur physiologie des facettierten auges.

Kim, R. (2011). Native agarose gel electrophoresis of multiprotein complexes. Cold Spring Harb Protoc *2011*, 884-887.

Kippert, F., Saunders, D.S., and Blaxter, M.L. (2002). Caenorhabditis elegans has a circadian clock. Curr Biol *12*, R47-49.

Knowles, T.P., Vendruscolo, M., and Dobson, C.M. (2014). The amyloid state and its association with protein misfolding diseases. Nat Rev Mol Cell Biol *15*, 384-396.

Ko, C.H., and Takahashi, J.S. (2006). Molecular components of the mammalian circadian clock. Hum Mol Genet *15 Spec No 2*, R271-277.

Koide, R., Onodera, O., Ikeuchi, T., Kondo, R., Tanaka, H., Tokiguchi, S., Tomoda, A., Miike, T., Isa, F., Beppu, H.*, et al.* (1997). Atrophy of the cerebellum and brainstem in dentatorubral pallidoluysian atrophy. Influence of CAG repeat size on MRI findings. Neurology *49*, 1605-1612.

Kondo, T., and Ishiura, M. (2000). The circadian clock of cyanobacteria. Bioessays *22*, 10-15.

Konopka, R.J., and Benzer, S. (1971). Clock mutants of Drosophila melanogaster. Proc Natl Acad Sci U S A *68*, 2112-2116.

Kopp, M., Meissl, H., and Korf, H.W. (1997). The pituitary adenylate cyclase-activating polypeptide-induced phosphorylation of the transcription factor CREB (cAMP response element binding protein) in the rat suprachiasmatic nucleus is inhibited by melatonin. Neurosci Lett *227*, 145-148.

Kornmann, B., Schaad, O., Bujard, H., Takahashi, J.S., and Schibler, U. (2007). System-driven and oscillator-dependent circadian transcription in mice with a conditionally active liver clock. PLoS Biol *5*, e34.

Kourtis, N., Nikoletopoulou, V., and Tavernarakis, N. (2012). Small heat-shock proteins protect from heat-stroke-associated neurodegeneration. Nature *490*, 213-218.

Krause, M. (2013). Structural and functional characterization of small Heat shock proteins of the nematode Caenorhabditis elegans

Kryndushkin, D.S., Alexandrov, I.M., Ter-Avanesyan, M.D., and Kushnirov, V.V. (2003). Yeast [PSI+] prion aggregates are formed by small Sup35 polymers fragmented by Hsp104. J Biol Chem *278*, 49636-49643.

Kudo, T., Loh, D.H., Truong, D., Wu, Y., and Colwell, C.S. (2011a). Circadian dysfunction in a mouse model of Parkinson's disease. Exp Neurol *232*, 66-75.

Kudo, T., Schroeder, A., Loh, D.H., Kuljis, D., Jordan, M.C., Roos, K.P., and Colwell, C.S. (2011b). Dysfunctions in circadian behavior and physiology in mouse models of Huntington's disease. Exp Neurol *228*, 80-90.

Kume, K., Zylka, M.J., Sriram, S., Shearman, L.P., Weaver, D.R., Jin, X., Maywood, E.S., Hastings, M.H., and Reppert, S.M. (1999). mCRY1 and mCRY2 are essential components of the negative limb of the circadian clock feedback loop. Cell *98*, 193-205.

Kurose, T., T, H., Yabe, D., and Seino, Y. (2014). The role of chronobiology and circadian rhythms in type 2 diabetes mellitus: implications for management of diabetes. ChronoPhysiology and Therapy *4*, 41-49.

La Spada, A.R., and Taylor, J.P. (2003). Polyglutamines placed into context. Neuron *38*, 681-684.

Labbadia, J., and Morimoto, R.I. (2015). The biology of proteostasis in aging and disease. Annu Rev Biochem *84*, 435-464.

Laemmli, U.K. (1970). Cleavage of structural proteins during the assembly of the head of bacteriophage T4. Nature *227*, 680-685.

Lai, C.H., Chou, C.Y., Ch'ang, L.Y., Liu, C.S., and Lin, W. (2000). Identification of novel human genes evolutionarily conserved in Caenorhabditis elegans by comparative proteomics. Genome Res *10*, 703-713.

Lee, K., Loros, J.J., and Dunlap, J.C. (2000). Interconnected feedback loops in the Neurospora circadian system. Science *289*, 107-110.

Lehman, M.N., Silver, R., Gladstone, W.R., Kahn, R.M., Gibson, M., and Bittman, E.L. (1987). Circadian rhythmicity restored by neural transplant. Immunocytochemical characterization of the graft and its integration with the host brain. J Neurosci *7*, 1626-1638.

Leroux, M.R., Ma, B.J., Batelier, G., Melki, R., and Candido, E.P. (1997a). Unique structural features of a novel class of small heat shock proteins. J Biol Chem *272*, 12847-12853.

Leroux, M.R., Melki, R., Gordon, B., Batelier, G., and Candido, E.P. (1997b). Structure-function studies on small heat shock protein oligomeric assembly and interaction with unfolded polypeptides. J Biol Chem *272*, 24646-24656.

Levinthal, C. (1968). Are There Pathways for Protein Folding. J Chim Phys Pcb *65*, 44-45.

Levinthal, C., Signer, E.R., and Fetherolf, K. (1962). Reactivation and hybridization of reduced alkaline phosphatase. Proc Natl Acad Sci U S A *48*, 1230-1237.

Li, J., and Le, W. (2013). Modeling neurodegenerative diseases in Caenorhabditis elegans. Exp Neurol *250*, 94-103.

Linder, B., Jin, Z., Freedman, J.H., and Rubin, C.S. (1996). Molecular characterization of a novel, developmentally regulated small embryonic chaperone from Caenorhabditis elegans. J Biol Chem *271*, 30158-30166.

Lipton, J.O., Yuan, E.D., Boyle, L.M., Ebrahimi-Fakhari, D., Kwiatkowski, E., Nathan, A., Guttler, T., Davis, F., Asara, J.M., and Sahin, M. (2015). The Circadian Protein BMAL1 Regulates Translation in Response to S6K1-Mediated Phosphorylation. Cell *161*, 1138-1151.

Livak, K.J., and Schmittgen, T.D. (2001). Analysis of relative gene expression data using real-time quantitative PCR and the 2(-Delta Delta C(T)) Method. Methods *25*, 402-408.

MacDonald, M.E., Barnes, G., Srinidhi, J., Duyao, M.P., Ambrose, C.M., Myers, R.H., Gray, J., Conneally, P.M., Young, A., Penney, J.*, et al.* (1993). Gametic but not somatic instability of CAG repeat length in Huntington's disease. J Med Genet *30*, 982-986.

Markaki, M., and Tavernarakis, N. (2010). Modeling human diseases in Caenorhabditis elegans. Biotechnol J *5*, 1261-1276.

Matilla-Duenas, A., Goold, R., and Giunti, P. (2008). Clinical, genetic, molecular, and pathophysiological insights into spinocerebellar ataxia type 1. Cerebellum *7*, 106-114.

Maywood, E.S., Fraenkel, E., McAllister, C.J., Wood, N., Reddy, A.B., Hastings, M.H., and Morton, A.J. (2010). Disruption of peripheral circadian timekeeping in a mouse model of Huntington's disease and its restoration by temporally scheduled feeding. J Neurosci *30*, 10199-10204.

McNaught, K.S., Jackson, T., JnoBaptiste, R., Kapustin, A., and Olanow, C.W. (2006). Proteasomal dysfunction in sporadic Parkinson's disease. Neurology *66*, S37-49.

McWatters, H.G., and Devlin, P.F. (2011). Timing in plants--a rhythmic arrangement. FEBS Lett *585*, 1474-1484.

Mendillo, M.L., Santagata, S., Koeva, M., Bell, G.W., Hu, R., Tamimi, R.M., Fraenkel, E., Ince, T.A., Whitesell, L., and Lindquist, S. (2012). HSF1 drives a transcriptional program distinct from heat shock to support highly malignant human cancers. Cell *150*, 549-562.

Merck, K.B., Horwitz, J., Kersten, M., Overkamp, P., Gaestel, M., Bloemendal, H., and de Jong, W.W. (1993). Comparison of the homologous carboxy-terminal domain and tail of alpha-crystallin and small heat shock protein. Mol Biol Rep *18*, 209-215.

Merrow, M., Franchi, L., Dragovic, Z., Gorl, M., Johnson, J., Brunner, M., Macino, G., and Roenneberg, T. (2001). Circadian regulation of the light input pathway in Neurospora crassa. EMBO J *20*, 307-315.

Merrow, M., Spoelstra, K., and Roenneberg, T. (2005). The circadian cycle: daily rhythms from behaviour to genes. EMBO Rep *6*, 930-935.

Migliori, M.L., Simonetta, S.H., Romanowski, A., and Golombek, D.A. (2011). Circadian rhythms in metabolic variables in Caenorhabditis elegans. Physiol Behav *103*, 315-320.

Miki, T., Matsumoto, T., Zhao, Z., and Lee, C.C. (2013). p53 regulates Period2 expression and the circadian clock. Nat Commun *4*, 2444.

Millar, A.J. (2004). Input signals to the plant circadian clock. J Exp Bot *55*, 277-283.

Mohawk, J.A., Green, C.B., and Takahashi, J.S. (2012). Central and peripheral circadian clocks in mammals. Annu Rev Neurosci *35*, 445-462.

Monsalve, G.C., Van Buskirk, C., and Frand, A.R. (2011). LIN-42/PERIOD controls cyclical and developmental progression of C. elegans molts. Curr Biol *21*, 2033-2045.

Morimoto, R.I. (2011). The heat shock response: systems biology of proteotoxic stress in aging and disease. Cold Spring Harb Symp Quant Biol *76*, 91-99.

Morley, J.F., Brignull, H.R., Weyers, J.J., and Morimoto, R.I. (2002). The threshold for polyglutamine-expansion protein aggregation and cellular toxicity is dynamic and influenced by aging in Caenorhabditis elegans. Proc Natl Acad Sci U S A *99*, 10417-10422.

Morton, A.J., Wood, N.I., Hastings, M.H., Hurelbrink, C., Barker, R.A., and Maywood, E.S. (2005). Disintegration of the sleep-wake cycle and circadian timing in Huntington's disease. J Neurosci *25*, 157-163.

Morton, E.A., and Lamitina, T. (2013). Caenorhabditis elegans HSF-1 is an essential nuclear protein that forms stress granule-like structures following heat shock. Aging Cell *12*, 112-120.

Musiek, E.S. (2015). Circadian clock disruption in neurodegenerative diseases: cause and effect? Front Pharmacol *6*, 29.

Muzerengi, S., Contrafatto, D., and Chaudhuri, K.R. (2007). Non-motor symptoms: identification and management. Parkinsonism Relat Disord *13 Suppl 3*, S450-456.

Niwa, F., Kuriyama, N., Nakagawa, M., and Imanishi, J. (2011). Circadian rhythm of rest activity and autonomic nervous system activity at different stages in Parkinson's disease. Auton Neurosci *165*, 195-200.

Nollen, E.A., Garcia, S.M., van Haaften, G., Kim, S., Chavez, A., Morimoto, R.I., and Plasterk, R.H. (2004). Genome-wide RNA interference screen identifies previously undescribed regulators of polyglutamine aggregation. Proc Natl Acad Sci U S A *101*, 6403-6408.

Nucifora, L.G., Burke, K.A., Feng, X., Arbez, N., Zhu, S., Miller, J., Yang, G., Ratovitski, T., Delannoy, M., Muchowski, P.J.*, et al.* (2012). Identification of novel potentially toxic oligomers formed in vitro from mammalian-derived expanded huntingtin exon-1 protein. J Biol Chem *287*, 16017-16028.

Olmedo, M., Geibel, M., Artal-Sanz, M., and Merrow, M. (2015). A High-Throughput Method for the Analysis of Larval Developmental Phenotypes in Caenorhabditis elegans. Genetics *201*, 443-448.

Olmedo, M., O'Neill, J.S., Edgar, R.S., Valekunja, U.K., Reddy, A.B., and Merrow, M. (2012). Circadian regulation of olfaction and an evolutionarily conserved, nontranscriptional marker in Caenorhabditis elegans. Proc Natl Acad Sci U S A *109*, 20479-20484.

Page, A.P., MacNiven, K., and Hengartner, M.O. (1996). Cloning and biochemical characterization of the cyclophilin homologues from the free-living nematode Caenorhabditis elegans. Biochem J *317 (Pt 1)*, 179-185.

Pallier, P.N., Maywood, E.S., Zheng, Z., Chesham, J.E., Inyushkin, A.N., Dyball, R., Hastings, M.H., and Morton, A.J. (2007). Pharmacological imposition of sleep slows cognitive decline and reverses dysregulation of circadian gene expression in a transgenic mouse model of Huntington's disease. J Neurosci *27*, 7869-7878.

Panda, S., Antoch, M.P., Miller, B.H., Su, A.I., Schook, A.B., Straume, M., Schultz, P.G., Kay, S.A., Takahashi, J.S., and Hogenesch, J.B. (2002). Coordinated transcription of key pathways in the mouse by the circadian clock. Cell *109*, 307-320.

Paulose, J.K., Wright, J.M., Patel, A.G., and Cassone, V.M. (2016). Human Gut Bacteria Are Sensitive to Melatonin and Express Endogenous Circadian Rhythmicity. PLoS One *11*, e0146643.

Peng, J., Elias, J.E., Thoreen, C.C., Licklider, L.J., and Gygi, S.P. (2003). Evaluation of multidimensional chromatography coupled with tandem mass spectrometry (LC/LC-MS/MS) for large-scale protein analysis: the yeast proteome. J Proteome Res *2*, 43-50.

Penna, A., and Cahalan, M. (2007). Western Blotting using the Invitrogen NuPage Novex Bis Tris minigels. J Vis Exp, 264.

Pierangeli, G., Cortelli, P., Provini, F., Plazzi, G., and Lugaresi, E. (1997). Circadian Rhythm of Body Core Temperature in Neurodegenerative Diseases (Milan: Springer).

Pittendrigh, C.S. (1960). Circadian rhythms and the circadian organization of living systems. Cold Spring Harb Symp Quant Biol *25*, 159-184.

Pittendrigh, C.S., Bruce, V.G., Rosensweig, N.S., and Rubin, M.L. (1959). Growth patterns in Neurospora: a biological clock in Neurospora. Nature *184*, 169-170.

Powers, E.T., Morimoto, R.I., Dillin, A., Kelly, J.W., and Balch, W.E. (2009). Biological and chemical approaches to diseases of proteostasis deficiency. Annu Rev Biochem *78*, 959-991.

Ptitsyn, O.B. (1973). [Stages in the mechanism of self-organization of protein molecules]. Dokl Akad Nauk SSSR *210*, 1213-1215.

Qin, Y., Wang, H., and Chang, Z. (2007). HSP12. 1, A small heat shock protein in C. elegans, has chaperone-like activity. Progress in biochemistry and biophysics *34*, 620.

Raizen, D.M., Zimmerman, J.E., Maycock, M.H., Ta, U.D., You, Y.J., Sundaram, M.V., and Pack, A.I. (2008). Lethargus is a Caenorhabditis elegans sleep-like state. Nature *451*, 569-572.

Ramos-Lobo, A.M., Buonfiglio, D.C., and Cipolla-Neto, J. (2015). Streptozotocin-induced diabetes disrupts the body temperature daily rhythm in rats. Diabetol Metab Syndr *7*, 39.

Reinke, H., Saini, C., Fleury-Olela, F., Dibner, C., Benjamin, I.J., and Schibler, U. (2008). Differential display of DNA-binding proteins reveals heat-shock factor 1 as a circadian transcription factor. Genes Dev *22*, 331-345.

Richter, C.P. (1922). A behavioristic study of the activity of the rat. Comparative Psychology Monographs *1*, 1-15.

Riemersma-van der Lek, R.F., Swaab, D.F., Twisk, J., Hol, E.M., Hoogendijk, W.J., and Van Someren, E.J. (2008). Effect of bright light and melatonin on cognitive and noncognitive function in elderly residents of group care facilities: a randomized controlled trial. JAMA *299*, 2642-2655.

Roenneberg, T., Daan, S., and Merrow, M. (2003). The art of entrainment. J Biol Rhythms *18*, 183-194.

Roenneberg, T., Kantermann, T., Juda, M., Vetter, C., and Allebrandt, K.V. (2013). Light and the human circadian clock. Handb Exp Pharmacol, 311-331.

Roenneberg, T., and Merrow, M. (1998). Molecular circadian oscillators: an alternative hypothesis. J Biol Rhythms *13*, 167-179.

Roenneberg, T., and Merrow, M. (2000). Circadian clocks: Omnes viae Romam ducunt. Curr Biol *10*, R742-745.

Roenneberg, T., and Merrow, M. (2005). Circadian clocks - the fall and rise of physiology. Nat Rev Mol Cell Biol *6*, 965-971.

Roenneberg, T., and Morse, D. (1993). Two circadian oscillators in one cell. Nature *362*, 362-364.

Ruaud, A.F., Katic, I., and Bessereau, J.L. (2011). Insulin/Insulin-like growth factor signaling controls non-Dauer developmental speed in the nematode Caenorhabditis elegans. Genetics *187*, 337-343.

Rudic, R.D., McNamara, P., Curtis, A.M., Boston, R.C., Panda, S., Hogenesch, J.B., and Fitzgerald, G.A. (2004). BMAL1 and CLOCK, two essential components of the circadian clock, are involved in glucose homeostasis. PLoS Biol *2*, e377.

Rudic, R.D., McNamara, P., Reilly, D., Grosser, T., Curtis, A.M., Price, T.S., Panda, S., Hogenesch, J.B., and FitzGerald, G.A. (2005). Bioinformatic analysis of circadian gene oscillation in mouse aorta. Circulation *112*, 2716-2724.

Sachs (1857). Uber das bewegungsorgan und die periodischen bewegungen der blätter von Phaseolus und Oxalis. Bot Z *15*, 793-802; 809-815.

Saigusa, T., Ishizaki, S., Watabiki, S., Ishii, N., Tanakadate, A., Tamai, Y., and Hasegawa, K. (2002). Circadian behavioural rhythm in Caenorhabditis elegans. Curr Biol *12*, R46-47.

Sammut, M., Cook, S.J., Nguyen, K.C., Felton, T., Hall, D.H., Emmons, S.W., Poole, R.J., and Barrios, A. (2015). Glia-derived neurons are required for sex-specific learning in C. elegans. Nature *526*, 385-390.

Santagata, S., Hu, R., Lin, N.U., Mendillo, M.L., Collins, L.C., Hankinson, S.E., Schnitt, S.J., Whitesell, L., Tamimi, R.M., Lindquist, S.*, et al.* (2011). High levels of nuclear heat-shock factor 1 (HSF1) are associated with poor prognosis in breast cancer. Proc Natl Acad Sci U S A *108*, 18378-18383.

Sato, T., Miura, M., Yamada, M., Yoshida, T., Wood, J.D., Yazawa, I., Masuda, M., Suzuki, T., Shin, R.M., Yau, H.J.*, et al.* (2009). Severe neurological phenotypes of Q129 DRPLA transgenic mice serendipitously created by en masse expansion of CAG repeats in Q76 DRPLA mice. Hum Mol Genet *18*, 723-736.

Savvidis, C., and Koutsilieris, M. (2012). Circadian rhythm disruption in cancer biology. Mol Med *18*, 1249-1260.

Schibler, U., Ripperger, J., and Brown, S.A. (2003). Peripheral circadian oscillators in mammals: time and food. J Biol Rhythms *18*, 250-260.

Seo, K., Choi, E., Lee, D., Jeong, D.E., Jang, S.K., and Lee, S.J. (2013). Heat shock factor 1 mediates the longevity conferred by inhibition of TOR and insulin/IGF-1 signaling pathways in C. elegans. Aging Cell *12*, 1073-1081.

Shemesh, N., Shai, N., and Ben-Zvi, A. (2013). Germline stem cell arrest inhibits the collapse of somatic proteostasis early in Caenorhabditis elegans adulthood. Aging Cell *12*, 814-822.

Silva, J.L., De Moura Gallo, C.V., Costa, D.C., and Rangel, L.P. (2014). Prion-like aggregation of mutant p53 in cancer. Trends Biochem Sci *39*, 260-267.

Silva, M.C., Fox, S., Beam, M., Thakkar, H., Amaral, M.D., and Morimoto, R.I. (2011). A genetic screening strategy identifies novel regulators of the proteostasis network. PLoS Genet *7*, e1002438.

Simonetta, S.H., Migliori, M.L., Romanowski, A., and Golombek, D.A. (2009). Timing of locomotor activity circadian rhythms in Caenorhabditis elegans. PLoS One *4*, e7571.

Simonetta, S.H., Romanowski, A., Minniti, A.N., Inestrosa, N.C., and Golombek, D.A. (2008). Circadian stress tolerance in adult Caenorhabditis elegans. J Comp Physiol A Neuroethol Sens Neural Behav Physiol *194*, 821-828.

Singh, R.N., and Sulston, J.E. (1978). Some observations on moulting in Caenorhabditis elegans. Nematologica *24*, 63-71.

Singh, V., and Aballay, A. (2006). Heat-shock transcription factor (HSF)-1 pathway required for Caenorhabditis elegans immunity. Proc Natl Acad Sci U S A *103*, 13092-13097.

Skene, D.J., and Swaab, D.F. (2003). Melatonin rhythmicity: effect of age and Alzheimer's disease. Exp Gerontol *38*, 199-206.

Stringham, E.G., Dixon, D.K., Jones, D., and Candido, E.P. (1992). Temporal and spatial expression patterns of the small heat shock (hsp16) genes in transgenic Caenorhabditis elegans. Mol Biol Cell *3*, 221-233.

Tamaru, T., Hattori, M., Honda, K., Benjamin, I., Ozawa, T., and Takamatsu, K. (2011). Synchronization of circadian Per2 rhythms and HSF1-BMAL1:CLOCK interaction in mouse fibroblasts after short-term heat shock pulse. PLoS One *6*, e24521.

Tonoki, A., Kuranaga, E., Ito, N., Nekooki-Machida, Y., Tanaka, M., and Miura, M. (2011). Aging causes distinct characteristics of polyglutamine amyloids in vivo. Genes Cells *16*, 557-564.

Tyedmers, J., Mogk, A., and Bukau, B. (2010). Cellular strategies for controlling protein aggregation. Nat Rev Mol Cell Biol *11*, 777-788.

Valastyan, J.S., and Lindquist, S. (2014). Mechanisms of protein-folding diseases at a glance. Dis Model Mech *7*, 9-14.

van der Linden, A.M., Beverly, M., Kadener, S., Rodriguez, J., Wasserman, S., Rosbash, M., and Sengupta, P. (2010). Genome-wide analysis of light- and temperature-entrained circadian transcripts in Caenorhabditis elegans. PLoS Biol *8*, e1000503.

van Ham, T.J., Holmberg, M.A., van der Goot, A.T., Teuling, E., Garcia-Arencibia, M., Kim, H.E., Du, D., Thijssen, K.L., Wiersma, M., Burggraaff, R.*, et al.* (2010). Identification of MOAG-4/SERF as a regulator of age-related proteotoxicity. Cell *142*, 601-612.

Videnovic, A., and Golombek, D. (2013). Circadian and sleep disorders in Parkinson's disease. Exp Neurol *243*, 45-56.

Vihervaara, A., and Sistonen, L. (2014). HSF1 at a glance. J Cell Sci *127*, 261-266.

Walker, G.A., and Lithgow, G.J. (2003). Lifespan extension in C. elegans by a molecular chaperone dependent upon insulin-like signals. Aging Cell *2*, 131-139.

Walther, D.M., Kasturi, P., Zheng, M., Pinkert, S., Vecchi, G., Ciryam, P., Morimoto, R.I., Dobson, C.M., Vendruscolo, M., Mann, M.*, et al.* (2015). Widespread Proteome Remodeling and Aggregation in Aging C. elegans. Cell *161*, 919-932.

Winklhofer, K.F., Tatzelt, J., and Haass, C. (2008). The two faces of protein misfolding: gain- and loss-of-function in neurodegenerative diseases. EMBO J *27*, 336-349.

Witting, W., Kwa, I.H., Eikelenboom, P., Mirmiran, M., and Swaab, D.F. (1990). Alterations in the circadian rest-activity rhythm in aging and Alzheimer's disease. Biol Psychiatry *27*, 563-572.

Wu, Y., Cao, Z., Klein, W.L., and Luo, Y. (2010). Heat shock treatment reduces beta amyloid toxicity in vivo by diminishing oligomers. Neurobiol Aging *31*, 1055-1058.

Wu, Y.H., Fischer, D.F., Kalsbeek, A., Garidou-Boof, M.L., van der Vliet, J., van Heijningen, C., Liu, R.Y., Zhou, J.N., and Swaab, D.F. (2006). Pineal clock gene oscillation is disturbed in Alzheimer's disease, due to functional disconnection from the "master clock". FASEB J *20*, 1874-1876.

Yoshii, T., Hermann-Luibl, C., and Helfrich-Forster, C. (2016). Circadian light-input pathways in Drosophila. Commun Integr Biol *9*, e1102805.

Zandi, E., Tran, T.N., Chamberlain, W., and Parker, C.S. (1997). Nuclear entry, oligomerization, and DNA binding of the Drosophila heat shock transcription factor are regulated by a unique nuclear localization sequence. Genes Dev *11*, 1299-1314.

Zhang, K., Ezemaduka, A.N., Wang, Z., Hu, H., Shi, X., Liu, C., Lu, X., Fu, X., Chang, Z., and Yin, C.C. (2015). A novel mechanism for small heat shock proteins to function as molecular chaperones. Sci Rep *5*, 8811.

Zhang, S., Binari, R., Zhou, R., and Perrimon, N. (2010). A genomewide RNA interference screen for modifiers of aggregates formation by mutant Huntingtin in Drosophila. Genetics *184*, 1165-1179.

Zhong, G., Bolitho, S., Grunstein, R., Naismith, S.L., and Lewis, S.J. (2013). The relationship between thermoregulation and REM sleep behaviour disorder in Parkinson's disease. PLoS One *8*, e72661.

Zhou, J.N., Hofman, M.A., and Swaab, D.F. (1995). VIP neurons in the human SCN in relation to sex, age, and Alzheimer's disease. Neurobiol Aging *16*, 571-576.

Zhuchenko, O., Bailey, J., Bonnen, P., Ashizawa, T., Stockton, D.W., Amos, C., Dobyns, W.B., Subramony, S.H., Zoghbi, H.Y., and Lee, C.C. (1997). Autosomal

dominant cerebellar ataxia (SCA6) associated with small polyglutamine expansions in the alpha 1A-voltage-dependent calcium channel. Nat Genet *15*, 62-69.

Zwanzig, R., Szabo, A., and Bagchi, B. (1992). Levinthal's paradox. Proc Natl Acad Sci U S A *89*, 20-22.

9. Appendices

9.1 Abbreviations

M	Mole
l	Liter
ml	Milliliter
µl	Microliter
mM	Millimolar
°C	Celsius
µM	Micromolar
h	Hour
polyQ	Poly-glutamine
SCN	Suprachiasmatic nucleus
HSP	Heat Shock Protein
HSF	Heat Shock Factor
YFP	Yellow Fluorescent Protein
LUC	Luciferase
GFP	Green Fluorescent Protein
WC	White Color
iPRGCs	Intrinsically Photosensitive Retinal Ganglion Cells
BMAL	Aryl Hydrocarbon Receptor Nuclear Translocator-Like Protein
PER	Period Protein
NPAS2	Neuronal PAS Domain Protein 2
CRY	Cryptochrome Protein
TOC	Timing of CAB Expression Protein
LHY	Late Elongated Hypocotyl Protein
CCA	Circadian Clock Associated Protein
CLK	Clock Protein
CYC	Cycle Protein
TIM	Timeless Protein
VVD	Vivid Protein
FRQ	Frequency Protein

HSE	Heat Shock Elements
ATP	Adenosine Triphosphate
mRNA	Messenger RNA
SIP	Stress Induced Protein
UPR	Ubiquitin Proteome Response
HSR	Heat Shock Response
SEM	Standar Error Mean
SDS	Sodium Dodecyl Sulfate
AGE	Agarose Gel Electrophoresis
PAGE	Polyacrylamide Gel Electrophoresis
MES	2-(N-morpholino)ethanesulfonic acid
LC-MS	Liquid Chromatography–Mass Spectrometry

10. Acknowledgments

Finally, it is time to thank my research family at Munich. First and foremost, I would like to express my deepest gratitude to my “Doktor-Mutter” Martha Merrow, who cared for me as a mother, taught me as a teacher, encouraged me as a friend, and supported me as a mentor. I am indebted to her for her support in my career development as a circadian biologist. Without her guidance and support this dissertation would not have been possible. Our stimulating discussions and exchange of ideas are extremely helpful to nurture my scientific and analytical skills.

I would like to thank an amazing co-supervisor in my career Maria Olmedo, who was there with me during my early steps in the lab. She was one of the most important people in my career, who taught me the scientific skills and gave valuable suggestions for my research project. I enjoyed working with her, discussing about protocols, results and improving my thesis.

My special thanks to Prof. Till Roenneberg for his valuable scientific advice and encouragement. I hope his words come true that I will become a famous scientist.

I thank Cornelia Madeti and Mirjam Geibel for being good friends. I enjoyed our lunchtime discussions and the valuable feedback on my research. Thank you so much for introducing me to burritos. Conny you did a wonderful job in translating the summary of my thesis to German.

I extend my thanks to lovely Zheng Chen for being there with me for every good and odd movement in this journey.

Special thanks to Tanja Popp, Astrid Bauer and Angela Meckl for their extremely helpful technical support.

I am so thankful to our wonderful secretary Susanne Piccone, who encouraged and supported me in several ways. Thanks a lot for the help with all kind of papers, forms and other organizational things!

My special thanks to Mr. James Merrow, for his kind help on editing my thesis.

My great friend Manfred Gödel, you are wonderful and thank you so much for sharing your knowledge. I will never forget your help for the time when I moved into the new flat.

I would like to thank my colleagues Helmut Klausner, David Lenssen, Charisa de Bekker, Eva Winnebeck, Caroline, Alexander Benz, Petra, Deniz Dögan, Tjeerd and Latha for your friendship and a scientific and warm atmosphere. Thank you so much Karin Meissner and Luisa Klau Pilz for valuable suggestion on statistics.

I would like to thank Charo Robles for doing proteomics experiments and data analysis.

Thank you so much to Prof. Ulrich Hartl, Prof. Peter Becker, Prof. Mathias Mann, Prof. Barbara Conradt, Dr. Eric lambie, Dr. Cristina Lagido and Dr. Prasad Kasturi for sharing the reagents and equipment.

I am so lucky to have a friend like Anisha Begum Shaik, who was always, be with my bad or good times. Thank you so much for your support.

Finally, I am so thankful to my parents for their extreme love, support, and encouragement. I am so grateful to you.

11. Curriculum Vitae

Name	**Bala Subrahmanya Chakravarthy Koritala**
Date of Birth	
Place of Birth	
Nationality	
E-mail	

Education:

2013- 2016	**Ph.D. Dissertation** **Supervisors:** Prof. Martha Merrow Dr. Maria Olmedo Medical Faculty, Ludwig Maximilians University, Munich, Germany.
2012-2014	**Master of Science in Biology** Ludwig Maximilians University, Munich, Germany.
2009-2011	**Master of Technology in Biotechnology** AMITY University, NOIDA, India.
2005-2009	**Bachelor of Technology in Industrial Biotechnology** Faculty of Engineering Bharath University, Chennai, India.

Research training:

Jun 2014	**Summer School: Sleep and Circadian Neuroscience** University of Oxford, Oxford, United kingdom

Talks at Conference

22nd May 2016	**Endogenous Temperature Cycles Impact The Formation of Pathological Aggregates** Location: Society for Research on Biological Rhythms-2016, Palm Harbor, Florida, United States of America.
25th Feb 2016	**Role of Zeitgebers in Molecular Mechanisms of Neurodegenerative Disease** Location: Hotch-Kiss Brain Institute, University of Calgary, Calgary, Canada.
10th Sep 2015	**The Circadian Clock Regulation in Models of Neurodegenerative Disease** Location: German Society of Medical Psychology Munich, Germany.
14th July 2015	**Chaperone Expression and Insoluble Proteins are Modified by Zeitgeber Cycles** Location: German Clock Club-2015, Munich, Germany.

Teaching Experience

2013-2016	**Teaching at Uni-Tag in Every Semester** **Lecture:** Aging and Neurodegenerative diseases. Ludwig Maximilians University, Munich, Germany.
Apr 2013	Participated in Teaching of "**WahlpflichtKurs-Chronobiology"** to Medical Students at LMU.

Topic: Ciracdian clock and Protein aggregation

June 2015- Sep 2015 Coached Erasmus Student (Deniz Dögan)

May 2016- Jun 2016 Coached Student Assistant (Tjeerd van der Galiën)

Honors/ Awards

2016 **Merit Award** from Society of Research on Biological Rhythms-2016, Palm Harbor, Florida, United States of America.

2008 **Appreciation Award** from International Crops Research Institute for the Semi-Arid Tropics (ICRISAT), Global Headquarters, Patancheru, INDIA.

2006 **Merit Certificate** for Presentation on "Environmental Trends" in Science and Humanities Association CHIRPY-06 at Bharath Institute of Higher Education and Research, Bharath University, Chennai, INDIA.